www.turkishimmunology.org

e-ISSN 2147-8325

April 2026

TURKISH JOURNAL OF IMMUNOLOGY

14
Volume
1
Issue

The official scientific and periodical publication of the Turkish Society of Immunology.

gamunex®-C %10 IV/SC

insan immünoglobulini

Her IVIG aynı değildir.[1]

Kaprilat/Kromatografi ile Yüksek Saflıkta Üretim[3]

Ozmolalitesi Fizyolojik Değerlere Yakındır[2]

Şeker İçermez

Grifols Inc. Kalitesiyle Üretim[1]

Düşük İnfüzyon Hacmi[3]

Eser Miktarda Sodyum ve Düşük IgA İçeriği[2,3]

Glisin ile Stabilize Formülasyon[3]

%10 Konsantrasyonda, İnfüzyona Hazır Likit Form[3]

Detaylı bilgi ve KÜB için:

GMX-DRG-2026-04

Referanslar: **1.**Gamunex-C masterfile **2.**Gelfand EW. Differences between IGIV products; impact on clinical outcome. Int Immunopharmacol. 2006; 6(4):592-599 **3.**Gamunex-C KÜB

GRIFOLS

Dem İlaç

TURKISH JOURNAL OF
IMMUNOLOGY

EISSN 2667-646X

APRIL 2026
VOLUME 14 / ISSUE 1

TÜRK İMMÜNOLOJİ DERNEĞİ

Owner
Owned by on behalf of the Turkish Society of Immunology:
Prof. İhsan Gürsel

.doc

Publication and Design
DOC Design and Informatics Co. Ltd.
E-mail: info@dotdoc.com.tr
Web page: www.dotdoc.com.tr

Publishing Coordinator
Gizem Pakdil

Design Lead
Ali Pekşen

Software
Asım Demirağ

Informatics
Nuh Naci Kişnişci

Typesetting
A Manikanndaprabhu

TURKISH JOURNAL OF
IMMUNOLOGY

EISSN 2667-646X

APRIL 2026
VOLUME 14 / ISSUE 1

EDITORIAL BOARD

TURKISH JOURNAL OF
IMMUNOLOGY

EISSN 2667-646X

APRIL 2026
VOLUME 14 / ISSUE 1

ADVISORY BOARD

TURKISH JOURNAL OF
IMMUNOLOGY

EISSN 2667-646X

APRIL 2026
VOLUME 14 / ISSUE 1

TURKISH JOURNAL OF
IMMUNOLOGY

EISSN 2667-646X

APRIL 2026
VOLUME 14 / ISSUE 1

CONTENT

TURKISH JOURNAL OF
IMMUNOLOGY

EISSN 2667-646X

APRIL 2026
VOLUME 14 / ISSUE 1

COVER IMAGE

Aziz Sancar

Image Credit:
Design by **.doc**

Integration in Immunology: From DNA Repair to Immune Regulation

Dear Colleagues,

Immunology is no longer confined to the study of defense—it is now recognized as an integrated system linking genome integrity, cellular stress, and disease. The first issue of the year reflects this evolving perspective and marks an important milestone for the *Turkish Journal of Immunology* (TJI).

We are particularly honored to welcome Prof. Aziz Sancar to our editorial board. His contribution to this issue through a dedicated editorial is both inspiring and symbolic, underscoring the importance of fundamental science in shaping our understanding of complex biological systems. His presence strengthens our commitment to scientific excellence and intellectual rigor. In his perspective on the NER–STING axis, Sancar revisits nucleotide excision repair as a fundamental mechanism of genome maintenance and extends its biological significance into innate immunity, highlighting how excised DNA fragments may contribute to immune signaling through the cGAS–STING pathway.

We are also delighted to have the support and active involvement of members of the European Federation of Immunological Societies (EFIS) on our editorial board. Their engagement represents an important step toward further internationalization of the journal and reinforces our aim to position TJI as a recognized and respected voice within the global immunology community.

An original study from Türkiye investigates soluble immune checkpoint proteins in systemic lupus erythematosus and Sjögren's syndrome, focusing on key regulatory molecules such as TIM-3, LAG-3, and Galectin-9. The findings demonstrate significantly elevated levels of these soluble checkpoints in SLE patients and reveal correlations with disease activity, highlighting their potential as biomarkers of immune dysregulation. These results underscore that immune checkpoint pathways extend beyond oncology and play a critical role in the regulation of autoimmunity.

An other original study from Türkiye compares two magnetic cell separation systems for $CD14^+$ cell enrichment. The column-based method showed higher cell recovery and stronger CD14 mRNA enrichment, although both systems produced functionally comparable cells. These findings emphasize that method selection can significantly influence experimental outcomes in downstream analyses.

At the level of innate antiviral immunity, a collaborative study from China, Pakistan, and the United States provides mechanistic insight into the regulation of type I interferon responses. The study demonstrates that asparagine endopeptidase regulates the cGAS–STING pathway through modulation of apoptotic caspases, thereby maintaining basal interferon levels while preventing excessive immunopathology. Together with

Correspondence
Günnur Deniz

E-mail
gdeniz@istanbul.edu.tr

Published
April 30, 2026

Suggested Citation
Deniz G. Integration in immunology: from DNA repair to immune regulation. Turk J Immunol. 2026;14(1):1–2.

DOI
10.36519/tji.2026.1152

Sancar's perspective, these findings reinforce the central theme —immune balance— highlighting that the immune system must be tightly regulated to be both effective and safe.

Complementing these findings, a review article from Iran examines the impact of respiratory viral coinfections, emphasizing how simultaneous or sequential infections can reshape host immune responses, influence disease severity, and reprogram immune dynamics. These observations highlight that immune responses are not directed against a single pathogen in isolation but are shaped by complex and context-dependent interactions.

Finally, an original study from Iraq explores the relationship between inflammatory responses and autoimmune mechanisms in gout, demonstrating that this traditionally metabolic disease is also closely linked to immune activation. The findings suggest that inflammatory and autoimmune pathways intersect more broadly than previously appreciated, supporting the need to reconsider classical disease classifications from an immunological perspective.

Taken together, the contributions in this issue converge on a unifying concept: the immune system is not static—it adapts, integrates signals from diverse biological processes, and responds dynamically to both internal and external challenges.

We sincerely thank all authors, reviewers, and editorial board members for their dedication and valuable contributions. Their efforts are essential in maintaining the scientific quality and integrity of the journal.

As we begin this new year, we remain committed to enhancing the visibility, impact, and international reach of TJI. We look forward to continuing this journey together.

With warm regards,

Prof. Günnur Deniz
On behalf of the Editorial Board
Turkish Journal of Immunology

The NER–STING Axis: When DNA Repair Becomes Immune Signaling: A Perspective for the Turkish Journal of Immunology

Aziz Sancar[1]

[1]University of North Carolina School of Medicine, Department of Biochemistry and Biophysics, Chapel Hill, USA

When I began studying how cells repair ultraviolet (UV)-induced DNA damage, the objective was precise and mechanistic: to understand how damaged DNA is recognized and corrected at the molecular level. Through detailed biochemical analyses, nucleotide excision repair (NER) was defined as the pathway that removes bulky DNA lesions as short oligonucleotides of approximately 27–29 nucleotides in length. Subsequent genome-wide analyses of excision products revealed that these fragments can range from approximately 24–32 nucleotides, with the majority clustering around 26–27 nucleotides. This mechanistic understanding established NER as a central guardian of genomic stability (1).

For many years, the biological implications of NER were considered primarily within the framework of mutation prevention and cancer biology. The excised DNA fragments were viewed as transient intermediates–necessary products of lesion removal that were subsequently degraded after fulfilling their role in repair. The immune system was not part of this discussion.

However, as scientific fields evolve, so does the interpretation of earlier discoveries.

In recent years, increasing attention has been directed toward the relationship between DNA damage responses and innate immune signaling. The cyclic GMP–AMP synthase (cGAS)–stimulator of interferon genes (STING) pathway, now recognized as a principal sensor of cytosolic DNA, activates TBK1, induces IRF3 phosphorylation, and drives type I interferon production (2). While initially characterized as a defense mechanism against viral DNA, this pathway also responds to endogenous DNA species under specific conditions (3).

Ultraviolet radiation provides a useful model for exploring this intersection. UV light induces cyclobutane pyrimidine dimers and 6–4 photoproducts in DNA. Through the coordinated action of damage recognition factors, helicases, and endonucleases,

Correspondence
Aziz Sancar

E-mail
aziz_sancar@med.unc.edu

Published
April 30, 2026

Suggested Citation
Sancar A. The NER–STING axis: When DNA repair becomes immune signaling: A Perspective for the Turkish Journal of Immunology. Turk J Immunol. 2026;14(1):3–5.

DOI
10.36519/tji.2026.1101

the damaged DNA segment is excised as an approximately 26–27 nt single-stranded DNA (ssDNA) oligonucleotide. Under normal circumstances, these excision products are efficiently processed. Yet cellular stress, altered regulatory pathways, or disruptions in downstream handling may allow these excised ssDNA fragments to access the cytoplasm, where they have the potential to engage innate immune sensors (Figure 1) (4).

The study by Kemp et al. (5) in 2015 offered important insight into this connection. Their findings demonstrated that UV irradiation potentiates STING-dependent signaling through deregulation of UNC-51–like kinase 1 (ULK1), a kinase associated with autophagy. This observation suggested that the cellular response to UV damage extends beyond DNA lesion repair and includes modulation of immune signaling pathways.

These findings do not alter the fundamental mechanics of NER. Rather, they expand its biological context. Genome stability and immune surveillance, long studied as distinct systems, may in fact represent integrated components of cellular defense. From an evolutionary perspective, this integration is logical. Cells must defend not only against pathogens but also against environmental and endogenous threats that compromise genomic integrity.

The implications of the NER–STING interface extend across multiple areas of immunology.

In sterile inflammation, endogenous DNA fragments generated during stress may contribute to interferon responses even in the absence of infection. In tissues chronically exposed to ultraviolet light, repair-associated DNA species could influence local immune signaling.

In autoimmunity, excessive type I interferon activity is a hallmark of several diseases. While apoptotic debris and mitochondrial DNA have been proposed as sources of immunostimulatory DNA, repair-derived ssDNA fragments may warrant further investigation as contributors to interferon amplification (6).

In cancer biology, DNA-damaging therapies enhance tumor immunogenicity not only by increasing mutation burden but also by activating cytosolic DNA sensing pathways. Accumulation of DNA fragments in the cytoplasm triggers the cGAS–STING axis, leading to type I interferon production and the promotion of anti-tumor immune responses (7). In this context, DNA repair–derived oligonucleotides, originally characterized through nucleotide excision repair studies (1), may represent an additional endogenous source of immunostimulatory DNA. Thus, DNA repair and innate immune activation emerge as interconnected components of the cellular stress response.

Aging represents another dimension in which these systems intersect. Accumulation of DNA damage over time

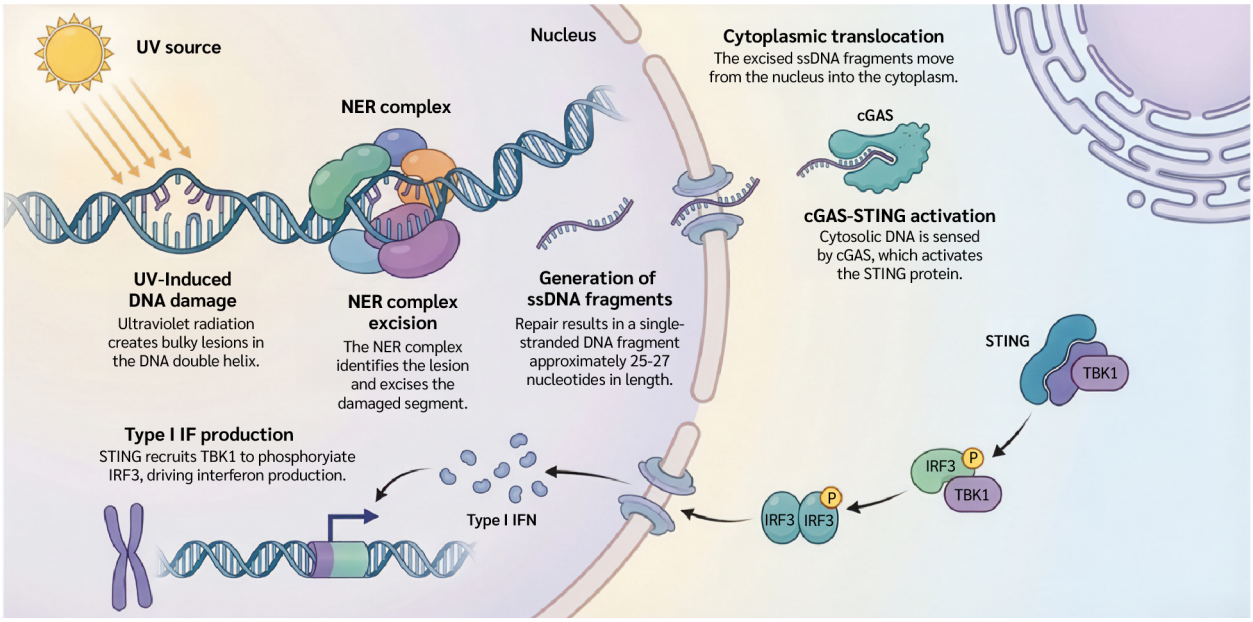

Figure 1. The NER–STING axis: Connecting DNA repair to innate immunity.

may lead to persistent low-level activation of innate immune pathways, contributing to chronic inflammatory states. Understanding how repair intermediates are processed or contained may therefore have broader relevance for immune regulation across the lifespan.

These developments illustrate a broader principle in science: mechanistic discoveries often acquire additional biological meaning as new technologies and conceptual frameworks emerge. When nucleotide excision repair was first characterized, its significance lay in preventing mutagenesis and preserving genomic fidelity. Today, it occupies a place within a larger network that links DNA damage responses to innate immune signaling.

The cell does not divide its defense systems into the categories that we assign in academic disciplines. Genome maintenance and immune vigilance are coordinated elements of a unified protective strategy. The emerging NER–STING axis underscores this integration and invites continued interdisciplinary investigation.

The story of nucleotide excision repair began with ultraviolet light and damaged DNA. It now extends into the biology of innate immunity. This expansion does not redefine the pathway; rather, it reveals its broader relevance within cellular defense architecture. As our understanding deepens, the connection between genome integrity and immune regulation will likely become even more refined.

Fundamental research, pursued with precision and persistence, can illuminate relationships that were not initially anticipated. The evolving dialogue between DNA repair and immunology represents one such example.

Future studies should clarify how nucleotide excision repair–derived ssDNA fragments are processed and whether they can access the cytoplasm under specific cellular conditions. Understanding how these repair intermediates intersect with innate immune sensing pathways may reveal new links between genome maintenance, inflammation, and disease. Elucidating this interface could open new perspectives in cancer immunology and immune regulation.

Ultimately, the emerging NER–STING axis reminds us that mechanisms originally evolved to preserve genome integrity may also serve as unexpected bridges between DNA repair and innate immune defense.

References

1 Sancar A. Excision repair in mammalian cells. J Biol Chem. 1995;270(27):15915–8. [CrossRef]

2 Chen Q, Sun L, Chen ZJ. Regulation and function of the cGAS–STING pathway of cytosolic DNA sensing. Nat Immunol. 2016;17(10):1142–9. [CrossRef]

3 Ablasser A, Chen ZJ. cGAS in action: Expanding roles in immunity and inflammation. Science. 2019;363(6431):eaat8657. [CrossRef]

4 Crowl JT, Gray EE, Pestal K, Volkman HE, Stetson DB. Intracellular nucleic acid detection in autoimmunity. Nat Rev Immunol. 2017;17(4):264–75. [CrossRef]

5 Kemp MG, Lindsey-Boltz LA, Sancar A. UV light potentiates STING-dependent innate immune signaling through deregulation of ULK1 (Unc51-like kinase 1). J Biol Chem. 2015;290(19):12184–94. [CrossRef]

6 Harding SM, Benci JL, Irianto J, et al. Mitotic progression following DNA damage enables pattern recognition within micronuclei. Nature. 2017;548(7668):466–70. [CrossRef]

7 Deng L, Liang H, Xu M, Yang X, Burnette B, Arina A, et al. STING-dependent cytosolic DNA sensing promotes radiation-induced type I interferon-dependent antitumor immunity in immunogenic tumors. Immunity. 2014;41(5):843–52. [CrossRef]

REVIEW ARTICLE

Turkish Journal of Immunology, 14(1):6–14

Respiratory Viral Coinfections: Impacts on Virus Replication and Host Immune Response

Fariba Shokri[1], Abas Gheisoori[1], Abas Maleki[2], Shima Izadi Dakhrabadi[3], Azra Kenarkoohi[4], Shahab Falahi[5], Ali Nazari[1], Jalil Feizi[4], Zeinab Karimi[6]

[1]Ilam University of Medical Sciences, School of Medicine, Department of Internal Medicine, Ilam, Iran; [2]Ilam University of Medical Sciences, Clinical Microbiology Research Center, Ilam, Iran; [3]Tehran University of Medical Sciences, School of Public Health, PhD of Medical Virology, Tehran, Iran; [4]Ilam University of Medical Sciences, School of Allied Medical Sciences, Department of Laboratory Sciences, Ilam, Iran; [5]Ilam University of Medical Sciences, Zoonotic Diseases Research Center, Ilam, Iran; [6]Ilam University of Medical Sciences, Tuberculosis and Lung Diseases Research Center, Ilam, Iran

Abstract

Viral coinfections can affect viral pathogenicity, immune responses, and disease symptoms. Coinfection may occur among viruses that target the same cells, and it is more common in respiratory viruses due to their co-circulation within the population. Respiratory virus co-circulation is a major driver of coinfection and refers to the simultaneous presence and transmission of multiple respiratory viruses among humans. Coinfection with respiratory viruses, such as influenza and SARS-CoV-2, may cause more severe symptoms, complicate treatment, and increase the burden on healthcare systems. Viral coinfection often modifies immune responses to a secondary infection. Therefore, understanding the effects of respiratory viral coinfections may play an important role in reducing mortality and improving strategies for controlling viral infections. In this review, we integrate experimental and clinical findings to clarify how the sequence of infection and innate immune activation determines the outcomes of respiratory viral coinfections.

Keywords: Respiratory viral infection, coinfections, immune responses, SARS-CoV-2

Correspondence
Zeinab Karimi

E-mail
karimi-z@medilam.ac.ir

Received
February 11, 2026

Accepted
April 21, 2026

Published
April 30, 2026

Suggested Citation
Shokri F, Gheisoori A, Maleki A, Izadi Dakhrabadi S, Kenarkoohi A, Falahi S, et al. Respiratory viral coinfections: Impacts on virus replication and host immune response. Turk J Immunol. 2026;14(1):6–14.

DOI
10.36519/tji.2026.1032

Introduction

Coinfection is common among respiratory viral infections and can result in severe symptoms in affected patients (19). The global prevalence of viral coinfection is still unknown; however, interest in this topic has increased in recent years. Studies have estimated a coinfection rate of 5.01% among patients with coronavirus disease

2019 (COVID-19), with higher prevalence reported in children (9.39%) (2). One cohort study reported a coinfection rate of 97.2% in pediatric cases (3). Although coinfection has a wide range of prevalence, most studies indicate that coinfection rates are higher in children.

There are several types of viral coinfections, including homologous coinfection, which refers to the simultaneous infection of two different viruses from the same viral family; heterotypic coinfection, which results from the simultaneous infection of two viruses within the same viral species; and heterologous coinfection, which results from the simultaneous infection of two different viruses from different families (4). Respiratory virus co-circulation is one of the important reasons for coinfection. Co-circulation refers to the concurrent circulation and transmission of multiple respiratory viruses within the human population (4). Coinfection is usually observed during winter and cold months and is defined as infection with two or more viruses simultaneously or a secondary viral infection occurring shortly after a previous infection (4). Viral coinfection can influence viral pathogenicity, immune responses, and disease symptom (5).

In particular, coinfection with respiratory viruses such as influenza and COVID-19 can lead to more severe symptoms, complicate treatment, and place a greater burden on healthcare staff (6). Coinfection is particularly important in respiratory viral infections because these viruses can easily cause epidemics or pandemics, as demonstrated by the severe acute respiratory syndrome coronavirus 2 (SARS-CoV-2) pandemic. Coinfections may lead to more extensive damage to the respiratory tract epithelium and lung alveoli. This damage leads to increased release of damage-associated molecular patterns (DAMPs), such as adenosine triphosphate (ATP) and mitochondrial DNA. These molecules themselves are powerful stimulators of inflammasome activation and interleukin-1 (IL-1) production (7). Inflammation is mediated by pro-inflammatory cytokines, including IL-1, IL-6, tumor necrosis factor (TNF), and IL-8. IL-1 is the most studied cytokine with properties relevant to several inflammatory diseases, including viral infections (8). Viral coinfection usually alters immune responses and sometimes influences the course of the second infection. As summarized in Table 1, interferon-mediated viral interference and order-dependent immune modulation are emerging as key mechanisms governing respiratory viral coinfections (9). Some studies have shown that coinfection in COVID-19 patients is associated with increased disease severity and mortality, decreased lymphocyte counts, and reduced numbers of cluster of differentiation 4-positive ($CD4^+$) T cells, $CD8^+$ T cells, and B cells (10). In this review, we synthesize current evidence regarding respiratory viral coinfections and examine their effects on viral replication and immune responses.

Influenza and SARS-CoV-2 Coinfection

Studies have shown that the influenza A virus is more frequently associated with SARS-CoV-2 coinfection than influenza virus type B (6). In hamsters and mice, influenza virus infection increases levels of IL-6, TNF-α, IL-1α, and interferon-β (IFN-β). Infection with SARS-CoV-2 leads to increased levels of IL-1α, IL-6, and IFN-β, although these levels are lower than those observed in a single infection with influenza A virus. Influenza infection after SARS-CoV-2 causes increased levels of TNF-α, IL-1α, IL-6, and IFN-β (Figure 1) (12).

Studies investigating influenza and SARS-CoV-2 coinfection in hACE2 transgenic mice have shown increased disease severity, viral persistence in the lungs, pneumonia, and lung injury. One study evaluated innate immune responses in influenza and SARS-CoV-2 coinfection in human respiratory tissue explants and human airway and alveolar epithelial cells. Coinfections resulted in a significant upregulation of innate immune responses to SARS-CoV-2 compared with single infections and led to more severe host damage (18).

Coinfection of influenza and SARS-CoV-2 has been shown to induce lymphopenia, which ultimately impairs

Highlights

- Coinfection outcomes are driven by the sequence of infection and innate immune activation.
- Type I/III interferons establish antiviral states that can suppress secondary viral replication under certain conditions.
- IL-1-mediated inflammation amplifies lung injury and may represent a therapeutic target.
- Respiratory viruses can compete, cooperate, or hybridize, shaping viral evolution and severity.
- Mechanistic mapping clarifies contradictory clinical observations across coinfections.

Table 1. Respiratory viral coinfection and outcomes.

Virus pair	Primary mechanism	Immune response changes	Virus replication / Dynamics	Disease outcome / Severity	References
IAV and RSV	Interferon-mediated viral interference	IAV induces strong type I interferon and pro-inflammatory cytokine responses; RSV elicits weaker cytokine induction	IAV suppresses RSV replication; prior RSV infection reduces IAV-associated immunopathology	Reduced probability of coinfection; lower morbidity when RSV precedes IAV	Jocelyne Piret, 2022 (11) Babawale and Guerrero-Plata, 2024 (12)
HRV and IAV	IFN-induced antiviral state	HRV induces ISGs via type I/III interferon signaling in airway epithelial cells	Prior HRV infection inhibits IAV replication for several days	Attenuated influenza severity when HRV precedes IAV	Jocelyne Piret, 2022 (11) Du et al., 2022 (4); (5)
RSV & hMPV	IFN-dependent suppression	RSV-induced interferon responses inhibit hMPV-associated cytokine signaling	RSV suppresses hMPV replication; inhibition is reversed in IFN-deficient conditions	Similar clinical presentation; RSV often dominates coinfection	Jocelyne Piret, 2022; (11) Babawale and Guerrero-Plata, 2024 (12)
IAV and SARS-CoV-2	Order-dependent immune modulation	IAV first: modest cytokine induction; SARS-CoV-2 first: rapid increase in TNF-α, IL-1α, IL-6, IFN-β	Viral replication and pathology depend on infection sequence	SARS-CoV-2 first leads to increased severity; IAV first often results in milder disease	Babawale and Guerrero-Plata, 2024 (12)
RSV and SARS-CoV-2	Innate immune priming via IFN signaling	RSV induces type I IFNs, TNF-α, IL-6, and ISGs (e.g., ISG15, IRF3)	RSV infection before or concurrent with SARS-CoV-2 reduces SARS-CoV-2 replication; SARS-CoV-2 first suppresses RSV replication	Prior RSV infection protects against severe SARS-CoV-2 disease; reverse order increases severity	Morris et al., 2023 (13)
RSV and HRV	Cytokine amplification	Coinfection increases expression of IFN-λ1 and CXCL10 compared with monoinfections	Viral replication effects not clearly defined	Enhanced immune signaling; clinical impact unclear	Nipaporn Sankuntaw, 2024 (14)
HPIV and adenovirus	Mixed Th1/Th2 immune activation	HPIV induces IFN-α, IL-2, IL-6, TNF-α; adenovirus contributes to overlapping cytokine responses	Direct effects on viral replication not reported	Clinical outcomes of coinfection not well characterized	Dermot Linden, 2019 (15)
Multiple respiratory viruses (modeling studies)	Resource competition and innate immunity	Innate immune activation and competition for host cellular resources shape interactions	Faster-replicating viruses (e.g., HRV) suppress slower viruses; IAV reduces RSV production; RSV delays IAV clearance	Disease severity varies depending on viral kinetics and immune activation	Pinky and Dobrovolny, 2016; (16) Pinky et al., 2023 (17)

IAV: Influenza A virus, **RSV:** Respiratory syncytial virus, **HRV:** Human rhinovirus, **hMPV:** Human metapneumovirus, **IFN:** Interferon, **ISGs:** Interferon-stimulated genes, **SARS-CoV-2:** Severe acute respiratory syndrome coronavirus 2, **TNF-α:** Tumor necrosis factor alpha, **IL:** Interleukin, **IFN-β:** Interferon beta, **IFNs:** Interferons, **ISG15:** Interferon-stimulated gene 15, **IRF3:** Interferon regulatory factor 3, **IFN-λ1:** Interferon lambda 1, **CXCL10:** C-X-C motif chemokine ligand 10, **HPIV:** Human parainfluenza virus, **Th1:** T helper type 1, **Th2:** T helper type 2, **IFN-α:** Interferon alpha.

adaptive immune responses and reduces levels of neutralizing antibodies and T-cell responses (19). Influenza virus infection before SARS-CoV-2 has been reported to suppress SARS-CoV-2 replication (20).

Coinfection with these viruses stimulates activation of inflammatory immune responses, increases immunopathology, and contributes to lung damage and acute respiratory distress syndrome (ARDS) (21). However, another study found that pre-infection with influenza enhanced SARS-CoV-2 replication, viral load, and lung damage (22).

Immune responses to the first infection (influenza virus in this case) can affect inflammatory responses to SARS-CoV-2 and play an auxiliary role in viral infectivity. It is possible that immune responses to the first infection facilitate receptor access for the second virus. On the other hand, a viral infection has a confounding effect on another one. The results obtained in various studies are inconsistent; however, sequential influenza and SARS-CoV-2 infections influence each other's progression.

Influenza and Respiratory Syncytial Virus Coinfection

In mice, respiratory syncytial virus (RSV) infection has been shown to lead to protection against subsequent influenza infection (12). Influenza infection prior to RSV caused airway dysfunction and weight loss, whereas RSV infection prior to influenza was associated with lower mortality and morbidity. Levels of TNF, IL-6, and interferon-γ (IFN-γ) were elevated in coinfection groups compared with RSV control groups. Tumor necrosis factor and IL-6 levels were decreased in coinfection groups compared with influenza control groups. This study also showed that the protective effect of RSV caused a decrease in influenza immunopathology, which may be due to increased levels of IFN-γ after RSV infection (23). Another study showed the protective effect of influenza against RSV infection lasting up to 1–5 months after recovery (24).

Additionally, a study confirmed that influenza suppresses RSV replication by achieving a higher growth rate compared with RSV (16). In mice, RSV infection can protect

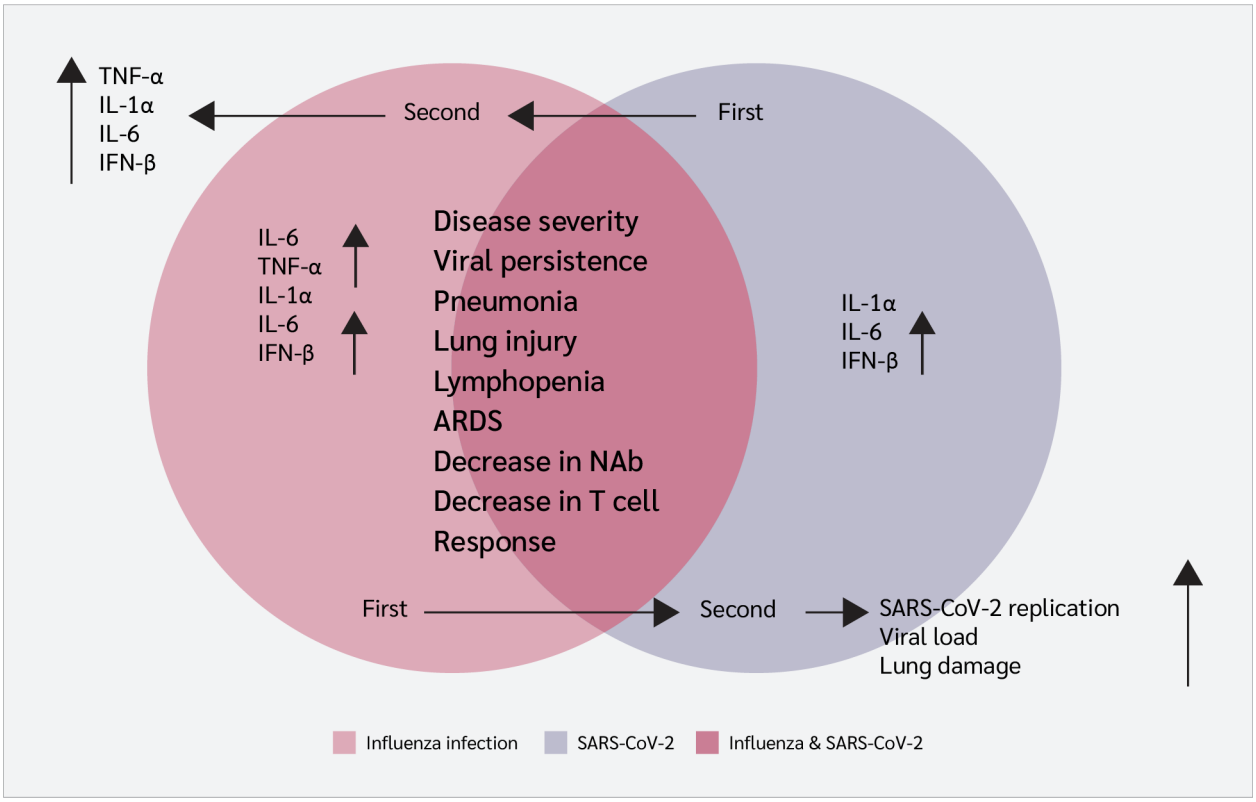

Figure 1. Influenza and SARS-CoV-2 coinfection.
TNF: Tumor necrosis factor, **IL-1:** Interleukin-1, **IL-6:** Interleukin-6, **IFN:** Interferon, **ARDS:** Acute respiratory distress syndrome, **NAB:** Neutralizing antibody.

against influenza infection and reduce inflammatory responses during influenza virus infection (12).

In this context, competitive conditions inhibit RSV replication. The possibility of using this feature to inhibit the replication of dangerous viruses by leveraging high-replication, low-risk viruses should be investigated.

A study found that RSV and influenza coinfection can lead to the formation of hybrid viruses. These hybrid viral particles can express several proteins from both parental viruses (25). The ability to integrate and produce new viruses during coinfection may lead to the emergence of dangerous viruses with the potential for global pandemics. Given the potential to produce new infectious viral particles with high replication capacity and pathogenicity, especially in respiratory viruses, this hypothesis should be carefully examined.

Influenza Coinfection with Adenovirus and Rhinovirus

Influenza and adenovirus coinfection has been shown to increase levels of inflammatory cytokines such as IL-6 and IL-1α in the A549 lung cell line (26).

Studies have shown that rhinovirus infection reduces influenza virus replication during subsequent infection. Interferon responses stimulated by rhinovirus infection in airway epithelial cells play a protective role against influenza infection (27). Another study revealed the protective effect of rhinovirus against subsequent influenza infection in human bronchial epithelial cells (HBECs) and human nasal epithelial cells (HNECs) (28).

Influenza A (H1N1) infection in airway cells was found to suppress rhinovirus replication, whereas rhinovirus did not change H1N1 replication in airway epithelial cells (29).

Influenza and Parainfluenza Coinfection

A study showed that primary infection with parainfluenza viruses enhances influenza virus replication in respiratory epithelial cells (30). Human parainfluenza virus type 2 has a booster effect on cell fusion in epithelial cells. Parainfluenza virus induced cell fusion and increased access to sialic acid for influenza hemagglutinin (HA) antigen, thereby increasing influenza virus infectivity (30).

SARS-CoV-2 and RSV Coinfection

Respiratory syncytial virus and SARS-CoV-2 coinfection, particularly when RSV infection precedes SARS-CoV-2, has been associated with decreased disease severity and reduced SARS-CoV-2 replication in BALB/c mice models (13). SARS-CoV-2 coinfection has also been shown to enhance RSV replication.

Conversely, when RSV infection occurs after SARS-CoV-2 infection, reduced RSV replication and protection have been observed (13). Previous RSV infection appeared to have a protective effect against subsequent SARS-CoV-2 infection in BALB/c mice (31). This effect may be due to persistent interferon responses after RSV infection.

SARS-CoV-2 and Adenovirus Coinfection

In vitro studies on SARS-CoV-2 and adenovirus have shown that these viruses do not affect each other's replication in Vero E6 cells. However, hamsters coinfected with these viruses exhibited more severe lung damage and clinical symptoms.

Inflammatory immune responses, including interferon, IL-6, CC motif chemokine ligand 17 (CCL17), and transforming growth factor-β (TGF-β), remained elevated for a prolonged period after infection in coinfected animals compared with those with single infections. Notably, IL-6 levels were markedly increased in coinfected animals, which may explain the severe symptoms and lung damage in this condition (32).

In another study, levels of IL-6, IL-1, and interferon-α (IFN-α) were significantly elevated in A549 cells coinfected with SARS-CoV-2 and adenovirus compared with adenovirus mono-infection 3 days after infection (26).

SARS-CoV-2 and Rhinovirus Coinfection

A study indicated that SARS-CoV-2 replication decreases after rhinovirus infection. However, when SARS-CoV-2 infection occurs first, rhinovirus replication does not change (28).

SARS-CoV-2, RSV, and Pneumoviridae Virus Coinfection

Studies have shown that prior human metapneumovirus (hMPV) infection increases lung susceptibility to SARS-CoV-2 infection (33). Respiratory syncytial virus infection has been shown to inhibit hMPV replication, with interferon responses playing a central role.

It is difficult to distinguish between RSV and hMPV

infection or coinfection because both viruses present similarly, including severe bronchiolitis. Studies have shown that hMPV viral load is higher in mono-infection than in coinfection with RSV, although this pattern is not observed in RSV mono-infection. Interferon responses against RSV may reduce hMPV replication (12,34).

Immune Responses

Immune responses triggered by an initial infection can shape the host's response to a subsequent infectious challenge. In respiratory infections, especially those caused by respiratory viruses, interferons are among the earliest immune signals produced and place host cells into an antiviral state while inducing the expression of pro-inflammatory genes (35,36).

These changes in gene expression influence multiple aspects of the local environment, including mucus production, extracellular and intracellular conditions, and immune cell activity. As a result, understanding the impact of a primary infection on immunity to a secondary infection requires consideration of several interconnected factors, such as alterations in viral receptor expression, viral entry and replication, viral gene expression, competition for host cellular resources, enhancement of inflammatory responses, and mechanisms that regulate or limit immune activation (Figure 2).

Additionally, IL-1 production is important because it is considered a key mediator of immunity and inflammation (37,38). For example, during influenza virus infection, IL-1 induces trypsin upregulation (39), and trypsin is necessary for viral fusion during influenza virus entry (40). These findings suggest that IL-1 may facilitate influenza infectivity; accordingly, viral infections that elevate IL-1 levels could enhance influenza virus entry and fusion.

Interleukin-1 enhances the recruitment of neutrophils and macrophages to the lungs, and these cells increase tissue damage by releasing enzymes and free radicals, potentially leading to more severe ARDS (41). Interleukin-1 also increases vascular permeability, leading to edema (fluid accumulation) in lung tissue, which further impairs gas exchange. (35)

Therefore, interleukin-1β (IL-1β) is an attractive potential therapeutic target for intervention in severe cases of these coinfections (42). Nevertheless, we have only briefly mentioned the impact of immune responses, such as IL-1, in this context. The effects of these cytokines in coinfections with different viruses should be further studied, and such studies may help identify new therapeutic targets.

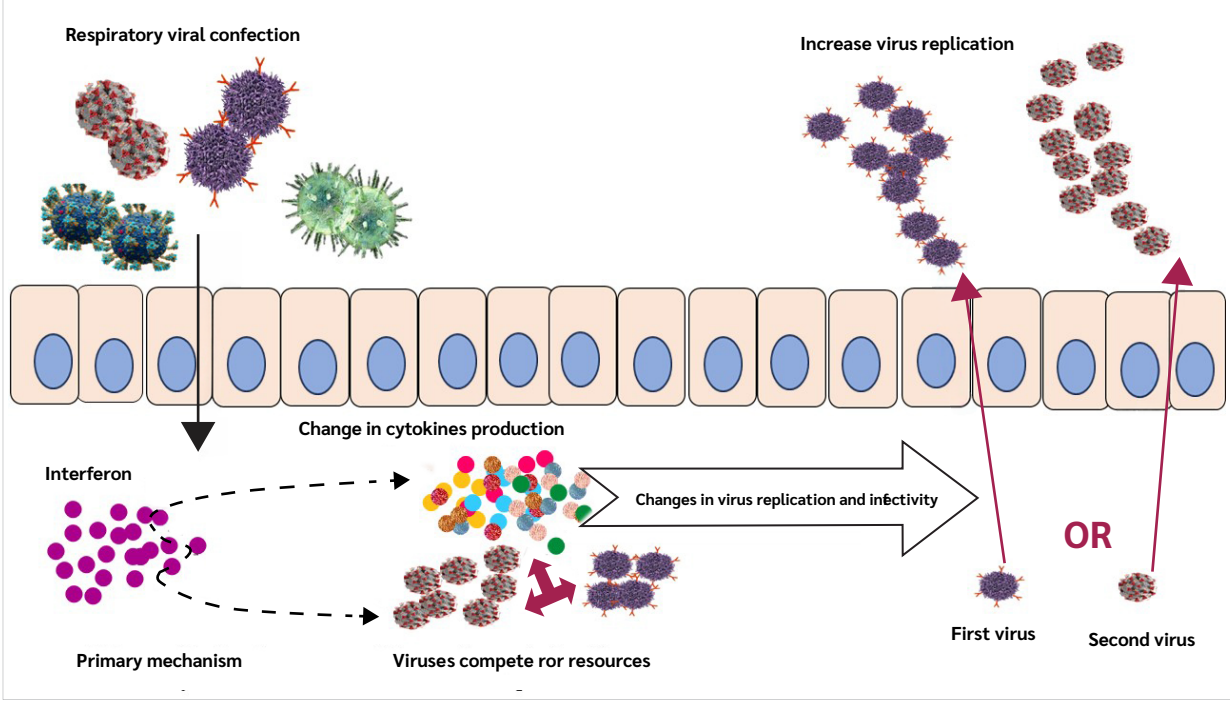

Figure 2. Mechanisms of respiratory viral coinfection.

Immune responses during respiratory viral infections represent a double-edged sword. While they help clear the virus, they sometimes go too far and end up damaging tissue instead. For instance, overproduction of inflammatory cytokines like IFN-γ has been linked to chronic obstructive pulmonary disease (COPD), ARDS, and even fatal pneumonia (43).

In one study, ferrets were first infected with RSV and then with influenza A virus (IAV) 3 days later. The findings demonstrated that IAV slowed down RSV replication, whereas RSV seemed to delay the clearance of IAV-infected cells (17).

When multiple viruses infect the same host, their interactions can vary—they may enhance one another, interfere with each other, or have no noticeable effect at all. These interactions vary depending on which viruses are involved, highlighting the importance of understanding what is happening at the molecular level (12). A deeper characterization of virus-virus and virus-host interactions is therefore essential not only for predicting disease outcomes but also for developing better treatments that reduce tissue damage while still clearing the infection.

Conclusion

Respiratory viral coinfection represents a significant challenge in respiratory infectious diseases. Such coinfections can affect immune responses and result in the emergence of new viruses. The immune response and disease severity may vary when the immune system faces several viral infections simultaneously.

This condition may facilitate the generation of new viral strains that are sometimes more infectious. Coinfection can also affect viral replication. However, differences in experimental models, infection sequence, viral dose, and host species likely explain the contradictory outcomes observed across studies.

For some viruses, prior infection or coinfection can act like a vaccine, reducing viral replication. Many hypotheses have been proposed regarding coinfection, including its role in the emergence of new viruses, changes in viral infectivity, and disease symptoms. The hypothesis of using one virus as a vaccine against another, through modulation of immune responses, also warrants further investigation.

Considering these aspects, coinfection is particularly relevant during viral pandemics and in immunocompromised patients. Therefore, investigating the impact of viral coinfections can be considered a goal to prevent further mortality and to help restrain viral infections.

Future Directions

- Future research should focus on the molecular pathways of virus-virus and virus-host interactions and understanding these mechanisms at the single-cell level in human tissues.
- Large-scale, longitudinal cohort studies are needed to translate experimental findings into clinically relevant insights for human populations.
- Investigations should explore whether attenuated viral vectors or engineered stimuli of specific innate immune pathways (e.g., controlled induction of IFN-λ) can be developed as prophylactic or early intervention strategies to mitigate subsequent severe infections.
- Surveillance programs and experimental studies should assess the risk of coinfection as a catalyst for the emergence of viruses with altered transmissibility, pathogenicity, or antigenic profiles.

Ethical Approval: Not applicable

Informed Consent: Not applicable

Peer-review: Externally peer-reviewed

Author Contributions: Concept – Z.K., F.S., A.G., S.F.; Design – A.M., S.I.D., A.K.; Supervision – A.K., S.F., Z.K.; Literature Review – A.N., J.F., A.M., F.S., S.I.D.; Writer – Z.K., A.G., F.S., A.M.; Critical Reviews – A.K., S.F., S.I.D., A.N., J.F.; Other – A.G., A.N., J.F.

Conflict of Interest: The authors declare no conflict of interest.

Financial Disclosure: The authors declared that this study has no financial support.

Acknowledgment: The authors thank the anonymous reviewers for their insightful comments and constructive suggestions, which improved the quality of the manuscript. The authors also thank the editorial team of the *Turkish Journal of Immunology* for their professional support and assistance throughout the publication process.

AI Statement: Not applicable

References

1 Georgakopoulou VE. Insights from respiratory virus co-infections. World J Virol. 2024;13(4):98600. [CrossRef]

2 Krumbein H, Kümmel LS, Fragkou PC, Thölken C, Hünerbein BL, Reiter R, et al. Respiratory viral co-infections in patients with COVID-19 and associated outcomes: A systematic review and meta-analysis. Rev Med Virol. 2023;33(1):e2365. [CrossRef]

3 Fu C, Huang Q, Zhao J, Mo L, Tang W, Lu J, et al. Clinical characteristics and co-infection analysis of influenza a virus in pediatric respiratory infections: a study based on tNGS technology. Eur J Clin Microbiol Infect Dis. 2025;44(7):1695–704. [CrossRef]

4 Trepat K, Gibeaud A, Trouillet-Assant S, Terrier O. Exploring viral respiratory coinfections: Shedding light on pathogen interactions. PLoS Pathog. 2024;20(9):e1012556. [CrossRef]

5 Du Y, Wang C, Zhang Y. Viral coinfections. Viruses. 2022;14(12):2645.

6 Golpour M, Jalali H, Alizadeh-Navaei R, Talarposhti MR, Mousavi T, Ghara AAN. Co-infection of SARS-CoV-2 and influenza A/B among patients with COVID-19: a systematic review and meta-analysis. BMC Infect Dis. 2025;25(1):145. [CrossRef]

7 Alpkvist H. Damage-associated molecular patterns and pathogen-associated molecular patterns in severe bacterial infections [doctoral thesis]. Stockholm (SE): Karolinska Institutet; 2024.

8 Conti P, Ronconi G, Caraffa A, Gallenga CE, Ross R, Frydas I, et al. Induction of pro-inflammatory cytokines (IL-1 and IL-6) and lung inflammation by Coronavirus-19 (COVID-19 or SARS-CoV-2): anti-inflammatory strategies. J Biol Regul Homeost Agents. 2020;34(2):327–31. [CrossRef]

9 Kumar N, Sharma S, Barua S, Tripathi BN, Rouse BT. Virological and immunological outcomes of coinfections. Clin Microbiol Rev. 2018;31(4):e00111–17. [CrossRef]

10 Zhang G, Zhang J, Gao Q, Zhao Y, Lai Y. Clinical and immunologic features of co-infection in COVID-19 patients, along with potential traditional Chinese medicine treatments. Front Immunol. 2024;15:1357638. [CrossRef]

11 Piret J, Boivin G. Viral interference between respiratory viruses. Emerg Infect Dis. 2022;28(2):273–81. [CrossRef]

12 Babawale PI, Guerrero-Plata A. Respiratory viral coinfections: insights into epidemiology, immune response, pathology, and clinical outcomes. Pathogens. 2024;13(4):316. [CrossRef]

13 Morris DR, Qu Y, Thomason KS, de Mello AH, Preble R, Menachery VD, et al. The impact of RSV/SARS-CoV-2 co-infection on clinical disease and viral replication: insights from a BALB/c mouse model. bioRxiv [Preprint]. May 24, 2023:2023.05.24.542043. [CrossRef]

14 Sankuntaw N, Punyadee N, Chantratita W, Lulitanond V. Coinfection with respiratory syncytial virus and rhinovirus increases IFN-λ1 and CXCL10 expression in human primary bronchial epithelial cells. New Microbiol. 2024;47(1):60–7.

15 Linden D, Guo-Parke H, Coyle PV, Fairley D, McAuley DF, Taggart CC, et al. Respiratory viral infection: a potential "missing link" in the pathogenesis of COPD. Eur Respir Rev. 2019;28(151):180063. [CrossRef]

16 Pinky L, Dobrovolny HM. Coinfections of the respiratory tract: viral competition for resources. PLoS One. 2016;11(5):e0155589. [CrossRef]

17 Pinky L, DeAguero JR, Remien CH, Smith AM. How interactions during viral-viral coinfection can shape infection kinetics. Viruses. 2023;15(6):1303. [CrossRef]

18 Ho JCW, Ng K, Ching RHH, Peiris M, Nicholls JM, Chan MCW, et al. Dynamic interaction between SARS-CoV-2 and influenza a virus infection in human respiratory tissues and cells. Microorganisms. 2025;13(5):988. [CrossRef]

19 Kim EH, Nguyen TQ, Casel MAB, Rollon R, Kim SM, Kim YI, et al. Coinfection with SARS-CoV-2 and influenza A virus increases disease severity and impairs neutralizing antibody and $CD4^+$ T cell responses. J Virol. 2022;96(6):e0187321. [CrossRef]

20 Oishi K, Horiuchi S, Minkoff JM, tenOever BR. The host response to influenza A virus interferes with SARS-CoV-2 replication during coinfection. J Virol. 2022;96(15):e0076522. [CrossRef]

21 Swets MC, Russell CD, Harrison EM, Docherty AB, Lone N, Girvan M, et al. SARS-CoV-2 co-infection with influenza viruses, respiratory syncytial virus, or adenoviruses. Lancet. 2022;399(10334):1463–4. [CrossRef]

22 Bai L, Zhao Y, Dong J, Liang S, Guo M, Liu X, et al. Coinfection with influenza A virus enhances SARS-CoV-2 infectivity. Cell

Res. 2021;31(4):395–403. [CrossRef]

23 Hartwig SM, Miller AM, Varga SM. Respiratory syncytial virus provides protection against a pubsequent influenza A virus infection. J Immunol. 2022;208(3):720–31. [CrossRef]

24 Kramer SC, Pirikahu S, Casalegno JS, Domenech de Cellès M. Characterizing the interactions between influenza and respiratory syncytial viruses and their implications for epidemic control. Nat Commun. 2024;15(1):10066. [CrossRef]

25 Haney J, Vijayakrishnan S, Streetley J, Dee K, Goldfarb DM, Clarke M, et al. Coinfection by influenza A virus and respiratory syncytial virus produces hybrid virus particles. Nat Microbiol. 2022;7(11):1879–90. [CrossRef]

26 Stincarelli MA, Arvia R, Guidotti B, Giannecchini S. Respiratory virus-specific and time-dependent interference of adenovirus type 2, SARS-CoV-2 and influenza virus H1N1pdm09 during viral dual co-infection and superinfection *in vitro*. Viruses. 2024;16(12):1947. [CrossRef]

27 Wu A, Mihaylova VT, Landry ML, Foxman EF. Interference between rhinovirus and influenza A virus: a clinical data analysis and experimental infection study. Lancet Microbe. 2020;1(6):e254–62. [CrossRef]

28 Essaidi-Laziosi M, Alvarez C, Puhach O, Sattonnet-Roche P, Torriani G, Tapparel C, et al. Sequential infections with rhinovirus and influenza modulate the replicative capacity of SARS-CoV-2 in the upper respiratory tract. Emerg Microbes Infect. 2022;11(1):412–23. [CrossRef]

29 Essaidi-Laziosi M, Geiser J, Huang S, Constant S, Kaiser L, Tapparel C. Interferon-dependent and respiratory virus-specific interference in dual infections of airway epithelia. Sci Rep. 2020;10(1):10246. Erratum in: Sci Rep. 2020;10(1):12523. [CrossRef]

30 Goto H, Ihira H, Morishita K, Tsuchiya M, Ohta K, Yumine N, et al. Enhanced growth of influenza A virus by coinfection with human parainfluenza virus type 2. Med Microbiol Immunol. 2016;205(3):209–18. [CrossRef]

31 Hartwig SM, Odle A, Wong L-YR, Meyerholz DK, Perlman S, Varga SM. Respiratory syncytial virus infection provides protection against severe acute respiratory syndrome coronavirus challenge. J Virol. 2024;98(9):e0066924. [CrossRef]

32 Svyatchenko VA, Ternovoi VA, Lutkovskiy RY, Protopopova EV, Gudymo AS, Danilchenko NV, et al. Human adenovirus and influenza a virus exacerbate SARS-CoV-2 infection in animal models. Microorganisms. 2023;11(1):180. [CrossRef]

33 Hashemi SA, Safamanesh S, Ghasemzadeh-Moghaddam H, Ghafouri M, Mohajerzadeh-Heydari MS, Namdar-Ahmadabad H, et al. Report of death in children with SARS-CoV-2 and human metapneumovirus (hMPV) coinfection: Is hMPV the trigger? J Med Virol. 2021;93(2):579–81. [CrossRef]

34 Talah S, Carbonneau J, Hamelin ME, Gilca R, Boivin G. Viral loads of pneumoviruses: correlation with coinfection rates and disease severity. J Med Virol. 2024;96(11):e70054. [CrossRef]

35 Fahey E, Doyle SL. IL-1 family cytokine regulation of vascular permeability and angiogenesis. Front Immunol. 2019;10:1426. [CrossRef]

36 Ivashkiv LB, Donlin LT. Regulation of type I interferon responses. Nat Rev Immunol. 2014;14(1):36–49. [CrossRef]

37 Makaremi S, Asgarzadeh A, Kianfar H, Mohammadnia A, Asgharizazar V, Safarzadeh E. The role of IL-1 family of cytokines and receptors in pathogenesis of COVID-19. Inflamm Res. 2022;71(7-8):923–47. [CrossRef]

38 Mantovani A, Dinarello CA, Molgora M, Garlanda C. Interleukin-1 and related cytokines in the regulation of inflammation and immunity. Immunity. 2019;50(4):778–95. [CrossRef]

39 Indalao IL, Sawabuchi T, Takahashi E, Kido H. IL-1β is a key cytokine that induces trypsin upregulation in the influenza virus-cytokine-trypsin cycle. Arch Virol. 2017;162(1):201–11. Erratum in: Arch Virol. 2018;163(12):3487. [CrossRef]

40 Li ZN, Lee BJ, Langley WA, Bradley KC, Russell RJ, Steinhauer DA. Length requirements for membrane fusion of influenza virus hemagglutinin peptide linkers to transmembrane or fusion peptide domains. J Virol. 2008;82(13):6337–48. [CrossRef]

41 Dang W, Tao Y, Xu X, Zhao H, Zou L, Li Y. The role of lung macrophages in acute respiratory distress syndrome. Inflamm Res. 2022;71(12):1417–32. [CrossRef]

42 Hosseinian N, Cho Y, Lockey RF, Kolliputi N. The role of the NLRP3 inflammasome in pulmonary diseases. Ther Adv Respir Dis. 2015;9(4):188–97. [CrossRef]

43 Kombe Kombe AJ, Fotoohabadi L, Gerasimova Y, Nanduri R, Lama Tamang P, Kandala M, et al. The role of inflammation in the pathogenesis of viral respiratory infections. Microorganisms. 2024;12(12):2526. [CrossRef]

ORIGINAL RESEARCH

Turkish Journal of Immunology, 14(1):15–23

Asparagine Endopeptidase (AEP) Promotes Type I IFN Expression via the cGAS-STING Pathway by Suppressing the Activity of Apoptotic Caspases

Inam Ullah Khan[1,2], Gabriel Brooks[3], Abdus Saboor Shah[4], Yutao Zhang[5], Fang Guo[1]

[1]Ministry of Education Key Laboratory of System Biomedicine, Shanghai Jiao Tong University, Shanghai, China; [2]Department of Biochemistry, Bannu Medical College, Bannu, Khyber Pakhtunkhwa, Pakistan; [3]Department of Microbiology and Immunology, University of Maryland School of Medicine, Baltimore, MD, USA; [4]Department of Biomedical Sciences, East China Normal University School of Life Sciences, Shanghai, PR China; [5]Peking University School of Life Sciences, Beijing, China

Abstract

Objective: Fine-tuned control of interferon (IFN) induction is crucial for triggering an effective immune response that can resolve infection without causing host pathology. Apoptotic caspases (caspase-3 and caspase-9) negatively regulate virus-induced cytokine production and maintain immune homeostasis against viral infection by cleaving cyclic GMP-AMP synthase (cGAS) and interferon regulatory factor 3 (IRF3) in the cGAS-STING pathway. However, continuous unchecked suppression of interferons by these caspases would compromise innate immunity against infection. Here, we report that caspase-3 and caspase-9 themselves are regulated by asparagine endopeptidase (AEP) to maintain basal IFN levels.

Materials and Methods: We investigated the expression of IFN-β, cGAS, and IRF3, and the activity of caspase-3 and caspase-9, *in vitro* in wild-type (WT) and AEP$^{-/-}$ RAW 264.7 cells in response to vaccinia virus (VACV) infection.

Results: AEP$^{-/-}$ RAW 264.7 cells showed significantly diminished levels of IFN-β, cGAS, and IRF3, and higher caspase-3 and caspase-9 activity *in vitro* in response to VACV infection. AEP-null mice were more susceptible to VACV, and all (n=7) AEP-deficient mice succumbed to VACV on day 4, compared to WT mice, which died on day 7. This was associated with higher viral loads in the lungs (p=0.0042) and the spleen (p=0.001), and with significantly lower IFN-β levels (p=0.0018) in sera from AEP-null mice.

Conclusion: We conclude that AEP suppresses the expression and activity of caspase-3 and caspase-9 and protects cGAS and IRF3 from being completely cleaved by these apoptotic caspases. This mechanism maintains basal type I IFN production.

Keywords: Asparagine endopeptidase, apoptotic caspases, innate antiviral immunity, IFN-β

Correspondence
Fang Guo and Inam Ullah Khan

E-mail
fguo@sjtu.edu.cn and inamktk@gmail.com

Received
October 31, 2025

Accepted
December 26, 2025

Published
April 30, 2026

Suggested Citation
Khan IU, Brooks G, Shah AS, Zhang Y, Guo F. Asparagine endopeptidase (AEP) promotes type I IFN expression via the cGAS-STING pathway by suppressing the activity of apoptotic caspases. Turk J Immunol. 2026;14(1):15-23.

DOI
10.36519/tji.2026.897

Introduction

Type I interferons (IFNs) play a critical role in suppressing the spread of viral infection (1). Viral infection triggers systemic immune responses in host cells, leading to the activation of different transcriptional factors and the production of various cytokines, including type I IFNs. Released IFNs bind to interferon receptors (IFNARs) and induce the expression of numerous interferon-stimulated genes (ISGs), which interrupt almost every stage of the viral life cycle, culminating in the establishment of an antiviral state (2). However, these IFNs stimulate neighboring cells in a self-amplifying loop, thereby enhancing type I IFN production (3). Increased levels of type I IFNs have numerous immunomodulatory functions in both the innate and adaptive immune responses. Thus, increased production of type I IFNs is associated with immunopathology (4). If the immune system is too active, there is a danger of developing autoimmune disease, while a suppressed immune system may lead to infections or cancer (5). Tight control of innate immune activation is therefore crucial for inducing an effective immune response that can resolve the infection without causing host pathology.

Apoptotic caspases, particularly caspase-3 and caspase-9, contribute to the mechanisms that control innate immunity and maintain immune homeostasis against viral infection (6). Ning et al. (2) showed that apoptotic caspases suppress the production of type I IFNs by cleaving cyclic GMP-AMP synthase (cGAS) and interferon regulatory factor 3 (IRF3). Loss of caspase-3 and caspase-9 resulted in elevated type I IFN levels via the cGAS-stimulator of interferon genes (STING) pathway and enhanced innate immune responses to both DNA and RNA viruses (2).

The cGAS-STING pathway is a crucial part of the innate immune system that detects cytosolic DNA and initiates a type I IFN response to defend against infections (7). Activated by the binding of self or non-self double-stranded DNA, cGAS catalyzes the production of 2′3′-cyclic GMP-AMP (cGAMP), which in turn activates STING. Activated STING recruits and activates transcription factors like IRF3 and IRF7, which then enter the nucleus and promote the transcription of genes encoding type I IFNs and other cytokines (8). Cells from cGAS-deficient ($cGAS^{-/-}$) mice were found to be unable to produce type I IFNs and other cytokines in response to DNA transfection or DNA virus challenge (9). Asparagine endopeptidase (AEP), also known as legumain, is a lysosomal cysteine protease from the C13 peptidase family that cleaves protein substrates on the C-terminal side of asparagine (10). It plays an important role in numerous physiological and pathological processes, including immune disorders, cancer, kidney physiology, neurological diseases such as Alzheimer's disease (5,11,12), and immunity to infections (13). Asparagine endopeptidase also processes and activates a range of additional proteins (14). Mice lacking AEP were unable to generate a strong antiviral immune response against the influenza virus (13). Similarly, $AEP^{-/-}$ mice were found unable to kill *Pseudomonas aeruginosa* (13). Thus, there is increasing evidence that AEP plays a role in immunity against infections. However, its role in innate immunity to viral infection is not fully known, and its mechanism remains to be elucidated. We hypothesized that AEP is involved in innate immunity to viruses by promoting IFN-β production via the cGAS-STING pathway, thereby helping sustain the basal level of IFN secretion in cells.

Here, we report that AEP promotes the induction of type I IFN by downregulating the expression of caspase-9. Lower levels of caspase-9, in turn, suppress the activity of caspase-3, which results in increased cGAS levels, leading to basal type I IFN production that would otherwise be completely abolished.

Materials and Methods

Cells, Viral Strain, and Infection

Cell culture, viral infection, and IFN-β measurement in the culture media supernatant were performed as previously described by Khan et al. (15) Murine macrophage-like cell line RAW 264.7 and $AEP^{-/-}$ RAW 264.7 cells were cultured in 36-mm plates in Dulbecco's Modified Eagle's Medium (DMEM) supplemented with 10% fetal bovine serum (FBS) and 2 mM L-glutamine. For *in vitro* infection, cells were infected with vaccinia virus (VACV) Western Reserve (WR) strain at a multiplicity of infection (MOI) of 0.1 for 1 h after overnight incubation at 37°C. After 3 h, the culture medium was replaced with complete DMEM with 10% FBS. For the collection of endogenous proteins and mRNA, cells were grown as above and collected at 8 h post-infection. Cell supernatants were gently centrifuged at 180 g for 3 min, and an enzyme-linked immunosorbent assay (ELISA) for IFN-β was performed on the supernatants using the mouse IFN-β ELISA kit (Thermo Fisher Scientific, Waltham, MA, USA) according to the manufacturer's instructions.

Mice

AEP$^{-/-}$ mice were kindly donated by the Key Laboratory of Cell Proliferation and Differentiation, School of Life Sciences, Peking University, Beijing, China, and were maintained under specific pathogen-free conditions in an environmentally controlled facility at the School of Pharmacy, Shanghai Jiao Tong University, Shanghai, China. Mice were housed at 22°C on a 12 h/12 h light/dark cycle. Food and water were provided *ad libitum*. All experiments were conducted in accordance with the institutional ethical guidelines for animal research and were approved by the Institutional Animal Care and Use Committee (IACUC) of Shanghai Jiao Tong University, Shanghai, China.

Lentivirus-Mediated AEP Overexpression

Lentiviral vectors encoding the AEP coding sequence were constructed by Hanyin Biotechnology Co., Shanghai, China. Recombinant AEP-overexpressing lentivirus and negative control lentivirus were prepared and titrated to 10^9 transduction units (TU)/mL. For AEP overexpression, cells were grown in six-well plates at a density of 2×10^5 cells per well, followed by transfection with the pLV-EF1α-AEP-IRES-Bsd plasmid and 8 μg/mL polybrene the next day. At 72 h after viral infection, AEP expression was examined by Western blotting.

In vivo Viral Challenge

Age- and sex-matched mice were divided into three groups (wild-type [WT], AEP$^{-/-}$, and uninfected), each containing seven mice (n=7). Wild-type and AEP$^{-/-}$ groups were anesthetized with isoflurane and infected intranasally (i.n.) with VACV at $1x10^6$ plaque-forming units (PFU) per mouse in 50 μL of phosphate-buffered saline (PBS) or PBS alone. Airways were washed with 500 μL of PBS. IFN-β protein expression was quantified by quantitative real-time reverse transcription polymerase chain reaction (qRT-PCR) in total RNA extracted from lung tissue using the RNeasy mini kit (Qiagen, Hilden, Germany).

Mouse serum was collected 48 h after infection to measure IFN-β production. For gene expression, analysis or viral load in the tissue, in some experiments, mice were euthanized on day 5 after treatment to harvest the lungs. Lungs were homogenized with an Omni tissue homogenizer (Omni International, Kennesaw, GA, USA) in Opti-MEM I medium containing 25% sucrose (Life Technologies, Carlsbad, CA, USA). IFN-β levels in the lung homogenates were measured by ELISA. Viral titers were determined by standard plaque assay as previously described (16). Bone marrow-derived macrophages (BMDMs) from mice were isolated and cultured as previously described by Bailey et al. (17).

Gene Expression Analysis by Real-Time PCR

TRIzol reagent (Ambion, Austin, TX, USA) was used for RNA extraction for quantitative PCR following the manufacturer's instructions. Using 2.5 μM oligo (dT) primers and 10 U/μL SuperScript III Reverse Transcriptase (Invitrogen, Carlsbad, CA, USA), 500 ng RNA was reverse transcribed into cDNA in 20 μL final reaction volume for 5 min at 65°C. Quantitative PCR was performed on a StepOnePlus Real-Time PCR System (Applied Biosystems, Foster City, CA, USA) using 1/20 of the cDNA volume. mRNA levels of IFN-β and cGAS were measured in technical triplicate for each sample using the following primer pairs:

Mouse *Ifnb* (forward): TCCGAGCAGAGATCTTCAGGAA
Mouse *Ifnb* (reverse): TGCAACCACCACTCATTCTGAG
Mouse *Gapdh* (forward): GAAGGGCTCATGACCACAGT
Mouse *Gapdh* (reverse): GGATGCAGGGATGATGTTCT

Relative mRNA expression levels were calculated using the ΔΔCt method. Data are presented as the relative abundance of the indicated mRNA normalized to that of *Gapdh* expression.

Western Blot Analysis

For measurement of cGAS, IFN-β, caspase-3, caspase-9, and phosphorylated IRF3 (p-IRF3) by Western blotting, $1x10^6$ RAW 264.7 and AEP$^{-/-}$ RAW 264.7 cells were grown at 37°C in 36-mm plates in DMEM supplemented with 10% FBS and 2 mM L-glutamine. Cells were suspended in Laemmli sample buffer containing 5% β-mercaptoethanol (β-ME), followed by boiling for 5 min. Protein concentration was measured using a BCA Protein Assay Kit (Thermo Fisher Scientific, Waltham, MA, USA). Equal amounts of protein (50 μg) were run on 10% sodium dodecyl sulfate–polyacrylamide gel electrophoresis (SDS-PAGE), transferred onto nitrocellulose membranes, and blocked with 5% non-fat milk in Tris-buffered saline with Tween-20 (TBST) for 2 h at room temperature. Membranes were incubated overnight at 4°C with primary antibodies against GAPDH, cGAS, IFN-β, caspase-3, caspase-9, and p-IRF3, followed by incubation with the appropriate horseradish peroxidase (HRP)–conjugated secondary antibodies. Protein bands were visualized using enhanced chemiluminescence (ECL) substrate and imaged.

Assay for Caspase-3 and Caspase-9 Activities

Activities of caspase-3 and caspase-9 were measured colorimetrically using caspase-3 and caspase-9 Activity kits (Beyotime Biotechnology, Nanjing, China). A total of 1×10^6 cells were washed with cold PBS and lysed on ice, followed by centrifugation at 16,000–20,000 g for 15 min at 4°C. Caspase assays were performed in 96-well plates by incubating 50 µL supernatant per sample with 10 µL caspase substrate and 40 µL reaction buffer for 1.5 h at 37°C. Absorbance was read at 450 nm using a microplate reader (MK3, Thermo Fisher Scientific, Waltham, MA, USA).

Viral Plaque Assay

Viral plaque assay was performed as described by Khan et al. (18). Organs from control or virus-infected mice were homogenized, followed by three freeze-thaw cycles to release the virus. For VACV infectivity quantification, BS-C-1 cell monolayers were infected with virus culture medium containing 2% (wt/vol) methylcellulose. After 2 days, cells were stained with 0.1% crystal violet solution, plaques were counted, and average counts were multiplied by the dilution factor to determine the viral titer as PFU per mL.

Statistical Analysis

All data are presented as mean ± standard error of the mean (SEM) of at least three experiments. Statistical significance was determined using a two-tailed Student's t-test, with $p<0.05$ considered statistically significant. For mouse survival studies, Kaplan-Meier survival curves were generated using GraphPad Prism version 10.3 (GraphPad Software, Boston, MA, USA).

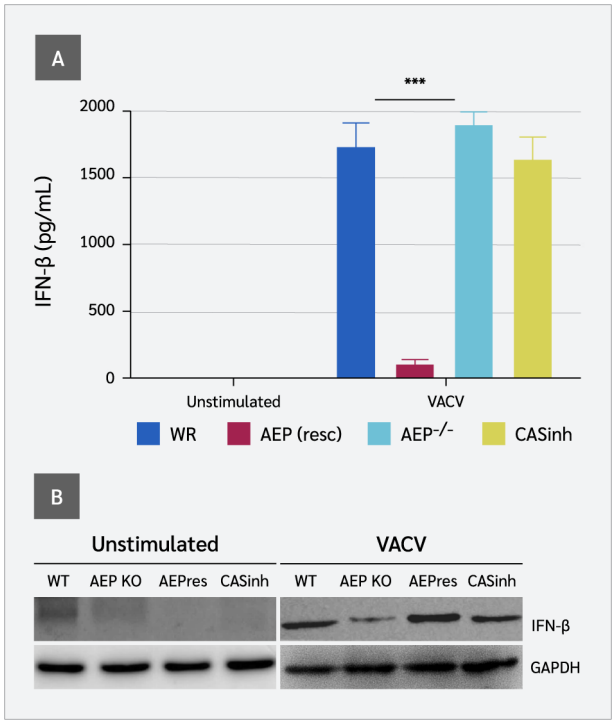

Figure 1. Effect of AEP on IFN-β expression.

Wild-type RAW 264.7, AEP$^{-/-}$, and AEP-reconstituted RAW 264.7 cells were cultured in 36-mm dishes in DMEM supplemented with 10% FBS and 2 mM L-glutamine. Following overnight incubation at 37°C, cells were infected with VACV and maintained at 37°C for 8 h. IFN-β levels in cell culture supernatants were measured by ELISA. For analysis of endogenous protein expression, cells were harvested after 8 h.

(A) IFN-β levels in cell culture supernatants. **(B)** Immunoblot analysis of IFN-β expression.

Data are presented as mean ± standard error of the mean from three independent experiments. *** represents p-value < 0.005

WT: Wild-type, **AEP:** Asparagine endopeptidase, **AEPresc:** AEP-reconstituted, **CASinh:** Caspase inhibitor–treated, **cGAS:** Cyclic GMP-AMP synthase, **AEP KO:** AEP knockout, **p-IRF3:** Phosphorylated interferon regulatory factor 3, **VACV:** Vaccinia virus, **GAPDH:** Glyceraldehyde-3-phosphate dehydrogenase.

Results

AEP$^{-/-}$ Cells Express Lower Levels of IFN-β

We first assessed the expression of IFN-β in WT and AEP$^{-/-}$ RAW 264.7 cells in response to VACV infection by measuring IFN-β in cell supernatants using an IFN-β bioassay. The ability of AEP-null cells to induce IFN-β was severely compromised. A significantly diminished level of IFN-β was detected in the supernatants from AEP-null cells in response to VACV infection ($p<0.005$) compared to WT cells (Figure 1A and 1B). Unlike cGAS-null cells, in which IFN levels were completely undetectable (19), IFN-β remained detectable at very low levels in the supernatants of AEP$^{-/-}$ RAW 264.7 cells following VACV infection. However, when AEP was rescued in AEP$^{-/-}$ cells, IFN-β levels were also restored. Interestingly, pharmacological inhibition of AEP$^{-/-}$ RAW 264.7 cells with z-VAD-fmk, a broad-spectrum inhibitor of caspases, enhanced IFN-β production following VACV infection.

AEP$^{-/-}$ Cells Express Low Levels of cGAS and p-IRF3

Because VACV induces type I IFNs via the cGAS-STING pathway, we hypothesized that the compromised production of IFN-β might result from disruption of the cGAS-STING pathway. Therefore, we examined the expression levels of key proteins in this pathway, i.e., cGAS and p-IRF3. Significantly lower levels of endogenous cGAS were detected in virally infected AEP-null cells, as shown by the

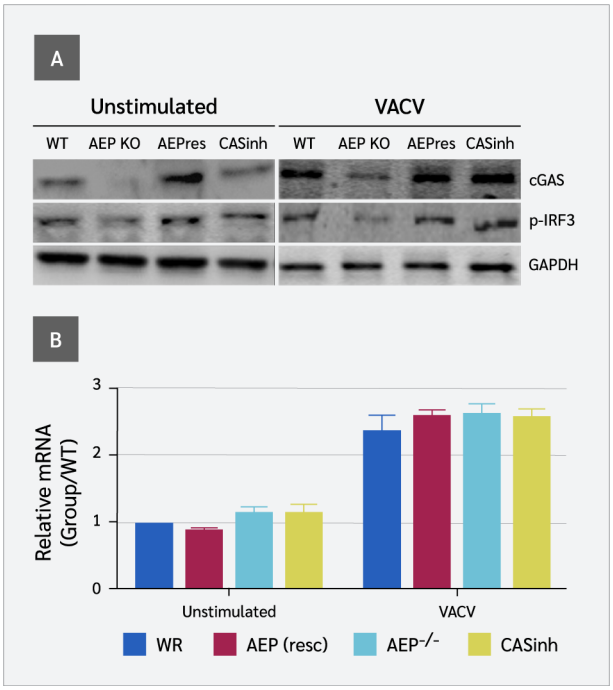

Figure 2. Effect of AEP on cGAS expression and p-IRF3 phosphorylation.

Wild-type RAW 264.7, AEP$^{-/-}$ RAW 264.7, and AEP-reconstituted RAW 264.7 cells were cultured in 36-mm dishes in DMEM supplemented with 10% FBS and 2 mM L-glutamine. Following overnight incubation at 37°C, cells were infected with VACV and maintained at 37°C for 8 h. For analysis of endogenous proteins and mRNA, cells were harvested after 8 h.

(A) Western blot analysis showing the expression of full-length cGAS and p-IRF3. **(B)** Relative cGas mRNA levels normalized to the unstimulated wild-type control, which was set to 1.

Data are presented as mean ± standard error of the mean from three independent experiments.

WT: Wild-type, **AEP:** Asparagine endopeptidase, **AEPresc:** AEP-reconstituted, **CASinh:** Caspase inhibitor–treated, **cGAS:** Cyclic GMP-AMP synthase, **AEP KO:** AEP knockout, **p-IRF3:** Phosphorylated interferon regulatory factor 3, **VACV:** Vaccinia virus, **GAPDH:** Glyceraldehyde-3-phosphate dehydrogenase.

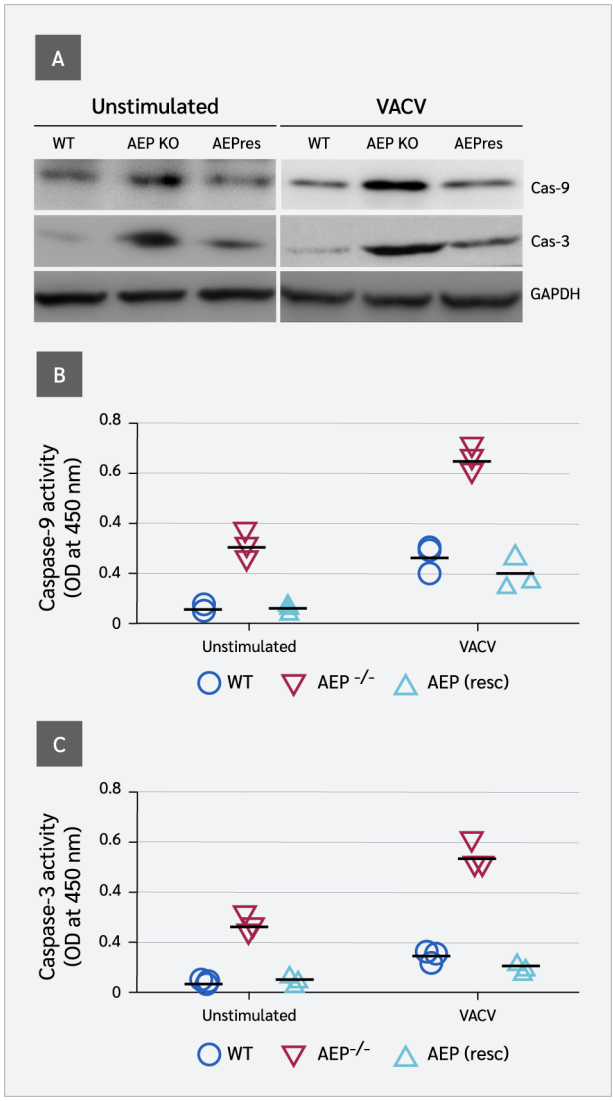

Figure 3. Effect of AEP on the expression and activity of caspase-9 and caspase-3.

Wild-type RAW 264.7, AEP$^{-/-}$ RAW 264.7, and AEP-reconstituted RAW 264.7 cells were cultured in 36-mm dishes in DMEM supplemented with 10% FBS and 2 mM L-glutamine. Following overnight incubation at 37°C, cells were infected with VACV and maintained at 37°C. For analysis of endogenous proteins, cells were harvested after 8 h.

(A) Western blot analysis showing the expression of caspase-9 and caspase-3. **(B)** Caspase-9 activity measured colorimetrically at 450 nm. (C) Caspase-3 activity measured colorimetrically at 450 nm.

Data are presented as mean ± standard error of the mean (SEM) from three independent experiments.

WT: Wild-type, **AEP:** Asparagine endopeptidase, **AEPresc:** AEP-reconstituted, **CASinh:** Caspase inhibitor–treated, **cGAS:** Cyclic GMP-AMP synthase, **AEP KO:** AEP knockout, **p-IRF3:** Phosphorylated interferon regulatory factor 3, **VACV:** Vaccinia virus, **GAPDH:** Glyceraldehyde-3-phosphate dehydrogenase.

loss of full-length cGAS protein (Figure 2A). However, qPCR results did not match well with the immunoblot results. At the mRNA level, we detected a small, non-significant decrease in cGAS expression in AEP-null cells (Figure 2B). These results imply that the reduction in cGAS did not occur at the expression level but rather at the protein level.

The decrease in cGAS was further assessed by its ability to catalyze the synthesis of cGAMP, which was assessed by measuring IRF3 dimerization (phosphorylation) using native gel electrophoresis. A significant decrease in IRF3 phosphorylation was observed in AEP-null cells in response to VACV infection, indicating reduced cGAMP production compared to WT cells. However, in AEP rescued cells, both cGAS and p-IRF3 levels were restored (Figure 2A). These results correlated with the presence or absence

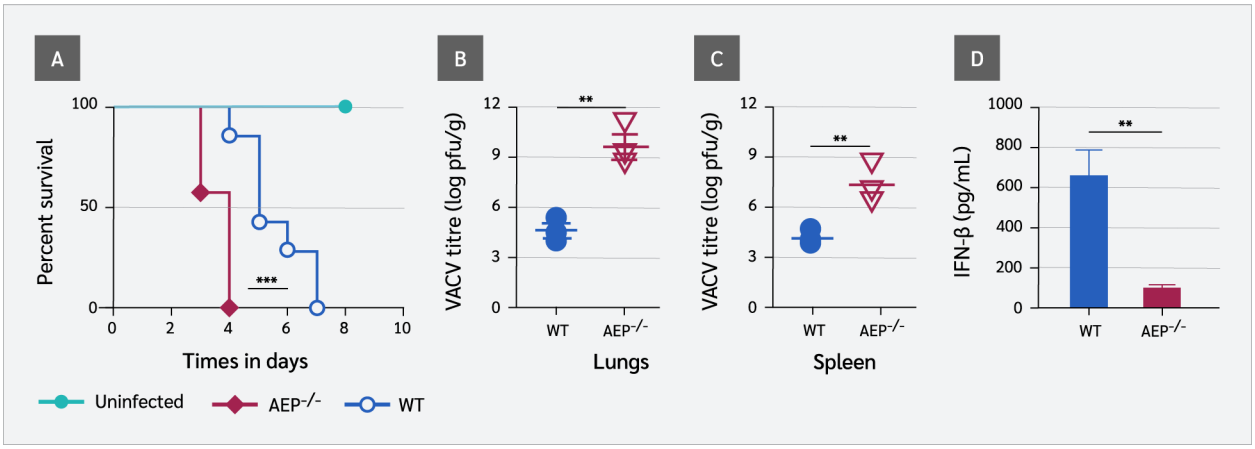

Figure 4. Characterization of the *in vivo* response to VACV infection in AEP-deficient mice.

Mice were infected by intranasal (i.n.) administration of VACV. Mice were euthanized at 5 h post infection for serum and tissue collection.
(A) Survival of WT and AEP$^{-/-}$ mice over a 10-day period (n=7) following intranasal infection with VACV (1 × 10^6 PFU/mouse). **(B)** VACV titers in the lungs and **(C)** Spleens of WT and AEP$^{-/-}$ mice (n=7). **(D)** IFN-β levels in lung tissues of WT and AEP$^{-/-}$ mice (n=7).

WT: Wild-type, **AEP:** Asparagine endopeptidase, **VACV:** Vaccinia virus.

Table 1. Summary of *in vivo* study results.

Assay/parameter	Uninfected	WT	AEP$^{-/-}$	*p*-value
Survival time (days post challenge)	10	7	4	0.0019
Lung viral titer (log PFU/g)	-	4.66	9.61	0.0042
Spleen viral titer (log PFU/g)	-	4.03	7.27	0.001
Lungs IFN-β (pg/mL)	ND	660	97	0.0018

AEP: Asparagine endopeptidase, **IFN-β:** Interferon beta, **PFU:** Plaque-forming unit, **WT:** Wild-type, **ND:** Not detected
(*) indicates *p*-value ≤ 0.05, (**) indicates *p*-value ≤ 0.01, (***) indicates P-value ≤ 0.001

of AEP and the level of IFN-β produced by WT and AEP-null cells. Together, these findings show a positive correlation between the presence of AEP and components of the cGAS-STING pathway involved in IFN-β induction.

AEP$^{-/-}$ Cells Show Enhanced Apoptotic Caspase Activity

Previous studies have shown that apoptotic caspases (caspase-9 and caspase-3) suppress type I IFN production by inactivating cGAS and IRF3 (2). We investigated the effect of AEP on the expression and activity of these caspases. AEP$^{-/-}$ cells displayed elevated levels of caspase-9 compared to WT cells (Figure 3A). Colorimetric results showed that caspase-9 activities were significantly higher in AEP-null cells than in WT cells. These results suggest that AEP suppresses the expression and activity of caspase-9. As caspase-3 acts downstream of caspase-9 and its activity is modulated by caspase-9, caspase-3 expression and activity were also significantly higher in AEP-null cells compared to WT cells. However, in AEP-reconstituted cells, the expression and activity of both caspases were repressed.

AEP Augments Host Resistance to Viral Infection

We first assessed the expression levels of cGAS, IRF3, caspase-9, and caspase-3 in BMDMs from WT and AEP-null mice. We detected significantly lower levels of cGAS and IRF3 and elevated levels of caspase-3 and caspase-9 (Figure 4E). To determine the contribution of AEP to the innate immune response against viral infection, we next evaluated *in vivo* evidence. Antiviral experiments

were performed in WT and AEP$^{-/-}$ mice. Wild-type and AEP$^{-/-}$ mice were infected with VACV (1×10^6 PFU/mouse), and lung inflammation was monitored on day 4 post-infection.

AEP-null mice are fertile and viable with no overt behavioral abnormality, although their body weights are reduced compared with WT littermates (20,21). We found that AEP-null mice were more susceptible to VACV infection, and all AEP-deficient mice (n=7) succumbed to VACV by day 4, whereas WT mice died on day 7 (Figure 4A). This was associated with higher viral loads in the lungs (p=0.0042) (Figure 4B) and the spleen (p=0.001) (Figure 4C) of AEP-null mice. This finding was consistent with the significantly lower IFN-β level (p=0.0018) in the sera of AEP-null mice (Figure 4D). A summary of the results from *in vivo* studies is presented in Table 1.

Discussion

Interferons are vital for host defense against viral infection and are constitutively expressed at low levels in cells (22). Such steady state IFN production is important for innate immune homeostasis in the absence of infection (22). However, aberrant interferon production leads to immunopathology or increased susceptibility to infections (15). Therefore, tight regulation of IFNs is critical for initiating effective immunity while avoiding inflammation. Our study revealed that AEP suppresses the expression and activity of apoptotic caspase-3 and caspase-9 and provides molecular insight into the coordination between AEP and antiviral innate immune activation.

Ning et al. (2) showed that apoptotic caspases (caspase-9 and caspase-3) negatively regulate virus-induced cytokine production by mediating cGAS and IRF3 cleavage to prevent excessive type I IFN induction and the resulting innate immune activation. However, uncontrolled or excessive cleavage of these proteins would be detrimental to the host. This necessitates a mechanism to prevent caspase-mediated excessive inactivation of cGAS and IRF3 while ensuring steady-state IFN production. Asparagine endopeptidase represents a simple but efficient way to fulfill this role. We showed that the activities of these caspases are under the control of AEP. Asparagine endopeptidase suppresses apoptotic caspase activity and thereby regulates type I IFN expression via the cGAS-STING pathway to establish an antiviral state. The results of the study by Sun et al. (23) support our findings, demonstrating that AEP suppresses caspase-3 and caspase-9 activity.

Our *in vitro* results show that in AEP-deficient RAW 264.7 cells, the expression and activity of caspase-3 and caspase-9 were significantly elevated. Based on the findings of Ning et al. (2), this increase would be expected to result in diminished levels of IFN-β, cGAS, and IRF3. Consistent with this expectation, the ability of AEP$^{-/-}$ RAW 264.7 cells to induce IFN-β was severely compromised. Similarly, the ability of these cells to express cGAS and to induce IRF3 phosphorylation was also markedly reduced. These findings were correlated with the elevated expression and activity of caspase-3 and caspase-9.

In vivo results further support our conclusion that AEP suppresses and regulates apoptotic caspase activity to establish an antiviral state. We found that AEP-null mice were more susceptible to VACV infection, and all AEP-deficient mice succumbed to infection by day 4, whereas WT mice died on day 7, which was associated with higher viral loads in the lungs and spleen of AEP-null mice. This was consistent with the significantly lower levels of cGAS and IRF3 in the BMDMs from AEP-deficient mice and reduced IFN-β levels in the sera. These findings are supported by Maschalidi et al. (13), who reported that AEP-deficient mice are unable to generate a strong antiviral response.

Our findings support the conclusion that AEP promotes type I IFN expression in mice via the cGAS-STING pathway by suppressing apoptotic caspase activity. This mechanism helps to maintain basal type I IFN production. However, the direct translation of murine experimental data to human physiology and pathological conditions is not straightforward due to important differences between mice and humans in immune defense strategies and pathogen responses. Liu et al. reported that cGAS activation mechanisms differ between mice and humans (24). Nevertheless, because the core components of this pathway—AEP, apoptotic caspases, and cGAS-STING—are highly conserved, these findings remain biologically relevant to human physiology. Further validation will require experimental confirmation.

Conclusion

We conclude that AEP suppresses the expression and activity of apoptotic caspase-3 and caspase-9, thereby

protecting cGAS and IRF3 from excessive cleavage and ensuring basal type I IFN production. These findings suggest that AEP plays an important role in maintaining finely tuned innate immune homeostasis during microbial infection.

Ethical Approval: The study was approved by the Shanghai Jiaotong University Institutional Animal Care and Use Committee (IACUC), on December 20, 2020, with the decision number A 2017054.

Informed Consent: N.A.

Peer-review: Externally peer-reviewed

Author Contributions: Concept – I.U.K., F.G.; Design – I.U.K., F.G.; Supervision – F.G.; Fundings – F.G.; Materials – I.U.K., A.S.S., Y.Z.; Data Collection and/or Processing – I.U.K., G.B., Y.Z.; Analysis and/or Interpretation – I.U.K., Y.Z., A.S.S; Literature Review – F.G., I.U.K.; Writer – I.U.K., G.B.; Critical Reviews – F.G., A.S.S., G.B.

Conflict of Interest: The authors declare no conflict of interest.

Financial Disclosure: The authors declared that this study has received no financial support.

Acknowledgment: The authors thank Shanghai Sorrento Medical Technology Co., Ltd. for technical support for this study.

References

1 Choubey D, Moudgil KD. Interferons in autoimmune and inflammatory diseases: regulation and roles. J Interferon Cytokine Res. 2011;31(12):857–65. [CrossRef]

2 Ning X, Wang Y, Jing M, Sha M, Lv M, Gao P, et al. Apoptotic caspases suppress type I interferon production via the cleavage of cGAS, MAVS, and IRF3. Mol Cell. 2019;74(1):19–31. e7. [CrossRef]

3 Baccala R, Hoebe K, Kono DH, Beutler B, Theofilopoulos AN. TLR-dependent and TLR-independent pathways of type I interferon induction in systemic autoimmunity. Nat Med. 2007;13(5):543–51. [CrossRef]

4 Marshak-Rothstein A. Toll-like receptors in systemic autoimmune disease. Nat Rev Immunol. 2006;6(11):823–35. [CrossRef]

5 Zhang Z, Xie M, Ye K. Asparagine endopeptidase is an innovative therapeutic target for neurodegenerative diseases. Expert Opin Ther Targets. 2016;20(10):1237–45. [CrossRef]

6 Chen H, Ning X, Jiang Z. Caspases control antiviral innate immunity. Cell Mol Immunol. 2017;14(9):736–47. [CrossRef]

7 Ishikawa H, Ma Z, Barber GN. STING regulates intracellular DNA-mediated, type I interferon-dependent innate immunity. Nature. 2009;461(7265):788–92. [CrossRef]

8 Sun L, Wu J, Du F, Chen X, Chen ZJ. Cyclic GMP-AMP synthase is a cytosolic DNA sensor that activates the type I interferon pathway. Science. 2013;339(6121):786–91. [CrossRef]

9 Anghelina D, Lam E, Falck-Pedersen E. Diminished innate antiviral response to adenovirus vectors in cGAS/STING-deficient mice minimally impacts adaptive immunity. J Virol. 2016;90(13):5915–27. [CrossRef]

10 Song M. The asparaginyl endopeptidase legumain: an emerging therapeutic target and potential biomarker for Alzheimer's disease. Int J Mol Sci. 2022;23(18):10223. [CrossRef]

11 Miller G, Matthews SP, Reinheckel T, Fleming S, Watts C. Asparagine endopeptidase is required for normal kidney physiology and homeostasis. FASEB J. 2011;25(5):1606–17. [CrossRef]

12 Zhao L, Hua T, Crowley C, Ru H, Ni X, Shaw N, et al. Structural analysis of asparaginyl endopeptidase reveals the activation mechanism and a reversible intermediate maturation stage. Cell Res. 2014;24(3):344–58. [CrossRef]

13 Maschalidi S, Hässler S, Blanc F, Sepulveda FE, Tohme M, Chignard M, et al. Asparagine endopeptidase controls anti-influenza virus immune responses through TLR7 activation. PLoS Pathog. 2012;8(8):e1002841. [CrossRef]

14 Freeley S, Cardone J, Günther SC, West EE, Reinheckel T, Watts C, et al. Asparaginyl endopeptidase (legumain) supports human Th1 induction via cathepsin l-mediated intracellular C3 activation. Front Immunol. 2018;9:2449. [CrossRef]

15 Khan IU, Brooks G, Guo NN, Chen J, Guo F. Fever-range hyperthermia promotes cGAS-STING pathway and synergizes DMXAA-induced antiviral immunity. Int J Hyperthermia. 2021;38(1):30–7. [CrossRef]

16 Khan IU, Ahmad F, Zhang S, Lu P, Wang J, Xie J, et al. Respiratory syncytial virus F and G protein core fragments fused to HBsAg-binding protein (SBP) induce a Th1-dominant immune response without vaccine-enhanced disease. Int Immunol. 2019;31(4):199–209. [CrossRef]

17 Bailey JD, Shaw A, McNeill E, Nicol T, Diotallevi M, Chuaiphichai S, et al. Isolation and culture of murine bone marrow-derived macrophages for nitric oxide and redox biology. Nitric Oxide. 2020;100–101:17–29. [CrossRef]

18 Khan IU, Huang J, Li X, Xie J, Zhu N. Nasal immunization with RSV F and G protein fragments conjugated to an M cell-targeting ligand induces an enhanced immune response and protection against RSV infection. Antiviral Res.

2018;159:95–103. [CrossRef]

19 Li XD, Wu J, Gao D, Wang H, Sun L, Chen ZJ. Pivotal roles of cGAS-cGAMP signaling in antiviral defense and immune adjuvant effects. Science. 2013;341(6152):1390–4. [CrossRef]

20 Manoury B, Hewitt EW, Morrice N, Dando PM, Barrett AJ, Watts C. An asparaginyl endopeptidase processes a microbial antigen for class II MHC presentation. Nature. 1998;396(6712):695–9. [CrossRef]

21 Manoury B, Mazzeo D, Fugger L, Viner N, Ponsford M, Streeter H, et al. Destructive processing by asparagine endopeptidase limits presentation of a dominant T cell epitope in MBP. Nat Immunol. 2002;3(2):169–74. [CrossRef]

22 Gough DJ, Messina NL, Clarke CJ, Johnstone RW, Levy DE. Constitutive type I interferon modulates homeostatic balance through tonic signaling. Immunity. 2012;36(2):166–74. [CrossRef]

23 Sun W, Lin Y, Chen L, Ma R, Cao J, Yao J, et al. Legumain suppresses OxLDL-induced macrophage apoptosis through enhancement of the autophagy pathway. Gene. 2018;652:16–24. [CrossRef]

24 Liu D, Zhang H, Huang YP, Gao YQ. Investigating the activation mechanism differences between human and mouse cGAS by molecular dynamics simulations. J Phys Chem B. 2023;127(22):5034–45. [CrossRef]

ORIGINAL RESEARCH

Turkish Journal of Immunology, 14(1):24–34

A Preliminary Study on Soluble Immune Checkpoint Proteins in Systemic Lupus Erythematosus and Sjögren's Syndrome Patients

Ege Gürlü[1], Başak Aru[2], Müge Bıçakçıgil Kalaycı[3], Gülderen Yanıkkaya Demirel[2,4]

[1]Yeditepe University Faculty of Medicine, İstanbul, Türkiye; [2]Yeditepe University Faculty of Medicine, Department of Immunology, İstanbul, Türkiye; [3]Yeditepe University Faculty of Medicine, Department of Internal Medicine, Division of Rheumatology, İstanbul, Türkiye; [4]Yeditepe University Training and Research Hospital, Stem Cell Laboratory, İstanbul, Türkiye

Abstract

Objective: The aim of this study was to assess serum levels of soluble immune checkpoint proteins (sICPs) in patients with systemic lupus erythematosus (SLE) and Sjögren's syndrome (SS) and to explore their association with disease activity.

Materials and Methods: This preliminary cross-sectional study included 27 patients with SLE, 23 patients with SS, and 23 healthy controls. Serum concentrations of sCD25 (soluble interleukin-2 receptor alpha [IL-2Rα; CD25]), 4-1BB (tumor necrosis factor receptor superfamily member 9 [TNFRSF9; CD137]), B7.2 (CD86; cluster of differentiation 86), transforming growth factor beta 1 (TGF-β1), cytotoxic T-lymphocyte-associated protein 4 (CTLA-4), programmed cell death protein 1 (PD-1), programmed death-ligand 1 (PD-L1), T-cell immunoglobulin and mucin-domain containing-3 (TIM-3), lymphocyte activation gene 3 (LAG-3), and Galectin-9 (Gal-9) were measured using a multiplex bead-based flow cytometric assay. Disease activity was evaluated using standard indices (Systemic Lupus Erythematosus Disease Activity Index [SLEDAI] for SLE; EULAR Sjögren's Syndrome Disease Activity Index [ESSDAI] for SS). Group differences were analyzed, and correlations between sICP levels and clinical indices were assessed.

Results: Compared with healthy controls, SLE patients had significantly elevated levels of soluble TIM-3 (sTIM-3) ($p<0.0001$), sLAG-3 ($p<0.0001$), and Gal-9 ($p<0.001$). A strong positive correlation was observed between sGal-9 and sTIM-3 levels ($r=0.79$, $p<0.0001$), and a moderate correlation was observed between sGal-9 and sLAG-3 levels ($r=0.55$, $p=0.002$). In SS, sICP levels did not differ significantly from controls; however, sPD-1 correlated with sPD-L1 ($r=0.56$, $p=0.004$), and sGal-9 with sTIM-3 ($r=0.54$, $p=0.007$). ESSDAI scores in SS correlated with sCD25 ($r=0.65$, $p=0.0007$), sTIM-3 ($r=0.49$, $p=0.01$), and sGal-9 ($r=0.41$, $p=0.04$).

Conclusion: Our findings suggest the potential use of sICPs as biomarkers in SLE and SS. However, larger studies are needed to validate the diagnostic and prognostic roles of these soluble checkpoints.

Keywords: Systemic lupus erythematosus, Sjögren's syndrome, soluble immune checkpoint proteins, flow cytometry

Correspondence
Gülderen Yanıkkaya Demirel

E-mail
gulderen.ydemirel@yeditepe.edu.tr

Received
January 20, 2026

Accepted
March 30, 2026

Published
April 30, 2026

Suggested Citation
Gürlü E, Aru B, Bıçakcıgil Kalaycı M, Yanıkkaya Demirel G. A preliminary study on soluble immune checkpoint proteins in systemic lupus erythematosus and Sjögren's syndrome patients. Turk J Immunol. 2026;14(1):24–34.

DOI
10.36519/tji.2026.947

Introduction

Immune checkpoint proteins (ICPs) regulate mechanisms that are critical for maintaining immune tolerance. The first ICP was discovered in the early 1990s, and over the past two decades, extensive research has underscored the importance of ICPs in regulating immune responses and preventing autoimmunity (1). To date, several ICPs have been characterized, including programmed cell death protein-1 (PD-1), cytotoxic T-lymphocyte-associated protein 4 (CTLA-4), B- and T-cell lymphocyte attenuator (BTLA), T-cell immunoglobulin and mucin-domain-containing protein 3 (TIM-3), T-cell immunoglobulin and immunoreceptor tyrosine-based inhibitory motif (ITIM) domain (TIGIT), V-domain Ig suppressor of T-cell activation (VISTA), lymphocyte activation gene 3 (LAG-3), and CD200 (2). The role of ICPs is critical not only for maintaining self-tolerance but also for preventing autoimmune diseases (3).

Systemic lupus erythematosus (SLE) and Sjögren's syndrome (SS) are chronic autoimmune diseases with complex and often overlapping features. Systemic lupus erythematosus is a multisystem disorder with a relapsing and remitting course that primarily affects women of childbearing age, with a striking female predominance of 9:1 (4). Systemic lupus erythematosus is particularly characterized by the presence of antibodies against nuclear and cytoplasmic antigens, as well as other autoantibodies such as anti-Scl-70, anti-La, anti-Ro, anti-cardiolipin, and antiphospholipid antibodies (5), suggesting an association between SLE and other autoimmune diseases. Similarly, SS is a systemic autoimmune disease of unclear etiology that primarily targets the salivary and lacrimal glands, leading to xerostomia and xerophthalmia (6). Sjögren's syndrome is a systemic disease with multisystem involvement and diverse clinical manifestations, commonly associated with fatigue, mood disorders, and reduced physical performance that markedly impair quality of life (7). It is classified as primary or secondary when occurring alone or in association with other autoimmune diseases, and its health-related quality-of-life burden is comparable to that of SLE and rheumatoid arthritis (RA) (8). Autoimmune diseases often require long-term or even lifelong medication, and some can be life-threatening and severely impair the quality of life (9).

A key feature of autoimmune diseases is the production of autoantibodies, which serve as important serologic markers for most of these diseases. However, they have limited sensitivity and specificity, requiring a more comprehensive diagnostic approach that incorporates clinical and demographic factors alongside laboratory findings (10). Recent research has highlighted the role of ICPs in regulating immune tolerance, and therapies targeting ICPs have shown promising results in the treatment of autoimmune diseases (3). Taken together, ICP expression could help to unravel disease mechanisms and identify new therapeutic targets. In the context of the association between soluble ICPs (sICPs) and autoimmune pathogenesis, this study aimed to assess the levels of 10 sICPs in serum samples from patients with SLE and SS compared with healthy controls, and to evaluate correlations among sICP levels to assess their potential as biomarkers.

Materials and Methods

Sample Collection

Inclusion criteria for patients were age ≥18 years and a diagnosis of either SLE (n=27) or SS (n=23) for this cross-sectional study. All participants were patients of the Rheumatology Department of Yeditepe University Hospital. A control group consisting of age-matched individuals without any evidence of autoimmune disease (n=23, mean age=53.9 ± 9.8; 20 [87.0%] female and 3 [13.0%] male) was also included. Ethical approval was granted by the Yeditepe University Clinical Research Ethics Committee with approval number 1631 dated July 7, 2022, and informed consent was obtained from all participants.

Disease activity was assessed using the SLE Disease Activity Index (SLEDAI) for SLE patients and the EULAR Sjögren's Syndrome Disease Activity Index (ESSDAI) for SS patients (11,12). Participants' age, gender, systemic involvement, and autoantibody profiles were recorded. The analysis of patients' serum autoantibodies was conducted in the HLA typing laboratory at Yeditepe University Hospital for clinical evaluation.

For the evaluation of serum soluble ICP levels, 5 mL of whole blood samples were drawn from subjects into serum tubes containing clot activator (BD Vacutainer® Serum Separation [SST™] tubes; Becton, Dickinson and Company, Franklin Lakes, NJ, USA; Catalog No: 367986), and the tubes were centrifuged at 400 × g for 20 minutes. Serum samples were aliquoted and stored at -80°C in an ultrafreezer for further analysis.

Measurement of Serum Soluble Immune Checkpoint Proteins

Serum concentrations of soluble ICPs— sCD25 (soluble interleukin-2 receptor alpha [IL-2Rα; CD25]), 4-1BB (tumor necrosis factor receptor superfamily member 9 [TNFRSF9; CD137]), B7.2 (CD86; cluster of differentiation 86), transforming growth factor beta 1 (TGF-β1; free active form), cytotoxic T-lymphocyte-associated protein 4 (CTLA-4), programmed death-ligand 1 (PD-L1), programmed cell death protein 1 (PD-1), T-cell immunoglobulin and mucin-domain-containing protein 3 (TIM-3), lymphocyte activation gene 3 (LAG-3), and Galectin-9 (Gal-9)— were quantified using the LEGENDplex™ HU Immune Checkpoint Panel 1 (10-plex) (BioLegend , San Diego, CA, USA; Catalog No: 740962). Laboratory analyses were conducted at the HLA Typing Laboratory of Yeditepe University Hospital.

For this purpose, aliquoted serum samples stored at -80°C were thawed immediately, diluted, and the assay was performed according to the manufacturer's instructions. Samples were acquired using a Beckman Coulter DxFLEX flow cytometry system (Beckman Coulter, Brea, CA, USA). Data were analyzed using the LEGENDplex Data Analysis Software Suite (BioLegend, San Diego, CA, USA). Performance data and patient positivity for the respective analytes are presented in Table 1.

Statistical Analysis

All statistical analyses were performed using GraphPad Prism software version 8 (GraphPad Software, San Diego, CA, USA). The Shapiro-Wilk test was used to assess the normality of the data. Comparisons between groups were performed using one-way analysis of variance (ANOVA) for parametric data or the Kruskal-Wallis test for non-parametric data. Correlations between sICPs were assessed using Pearson's correlation for normally distributed data and Spearman's rank correlation for non-normally distributed data. *P* values <0.05 were considered statistically significant.

Results

Patients' Demographic Characteristics

A total of 27 patients with SLE were enrolled in this study, of whom 26 (96.2%) were female, and 1 (3.7%) was male. The mean age of the subjects was 43.1 ± 10.9 years, and their mean SLEDAI score was 3.7 ± 3.9. Among all SLE patients, 5 (18.5%) had hematologic involvement, 4 (14.8%) had neurologic involvement, 3 (11.1%) had nephrologic involvement, and 1 (3.7%) had both hematologic and nephrologic involvement, while 14 (52.8%) patients had no systemic involvement.

Table 1. Performance characteristics of the assay and distribution of analyte positivity across study groups, presented as number (percentage).

Target	IC_{50}	R^2	LOD	LOQ	SLE, n (%)	SS, n (%)	Control, n (%)
sCD25	4894.466	0.987949	1.220703	1.220703	27 (100.00)	23 (100.00)	23 (100.00)
4-1BB	3921.525	0.991143	1.418207	293.046	2 (7.40)	6 (26.09)	4 (17.39)
B7.2	2213.927	0.997842	0.488281	0.488281	27 (100.00)	23 (100.00)	23 (100.00)
TGF-β1	2541.1	0.971964	0.488281	26.32961	4 (14.81)	5 (21.74)	6 (26.09)
CTLA-4	562.9534	0.95292	0.907904	74.37019	3 (11.11)	2 (8.70)	5 (21.74)
PD-L1	5520.906	0.982907	0.244141	18.0188	21 (77.77)	15 (65.22)	12 (52.17)
PD-1	826.0993	0.991235	0.244141	18.47389	9 (33.33)	7 (30.43)	3 (13.04)
TIM-3	12970.71	0.986893	1.220703	2.893706	27 (100.00)	23 (100.00)	23 (100.00)
LAG-3	21523.53	0.997092	4.882813	4.882813	22 (81.48)	12 (52.17)	5 (21.74)
Galectin-9	7689.858	0.994707	4.882813	294.0241	27 (100.00)	23 (100.00)	23 (100.00)

IC_{50}: Half maximal inhibitory concentration, ***R^2*:** Coefficient of determination, **LOD:** Limit of detection, **LOQ:** Limit of quantification, **SLE:** Systemic lupus erythematosus, **SS:** Sjögren's syndrome.

Three (11.1%) patients were anti-nuclear antibody (ANA) positive, and 15 (55.6%) were ANA negative, while ANA test results were not available for 9 (33.3%) patients. Eight (29.6%) patients were anti-double-stranded DNA (anti-dsDNA) positive, whereas 17 (62.7%) were anti-dsDNA negative; results were not available for 2 (7.4%) patients.

Among SLE patients, treatment information was unavailable for 1 (3.7%) patient. One (3.7%) patient was given a combination of prednisolone and methotrexate, while another was treated with methylprednisolone and mycophenolate mofetil. Two (7.4%) patients were administered mycophenolate mofetil monotherapy, and 8 (29.6%) patients received hydroxychloroquine alone. The remaining patients were treated with hydroxychloroquine in combination with other agents, including azathioprine, methylprednisolone, mycophenolate mofetil, hydrocortisone, colchicine, and methotrexate.

Among patients with SS, 22 (95.7%) were female, and 1 (4.3%) was male. The mean age of the subjects was 58.1 ± 14.9 years, while their mean ESSDAI score was 2.2 ± 2.3. When autoantibody status was evaluated, 14 (60.9%) patients were ANA-positive, 4 (17.4%) patients were ANA-negative, and results were unavailable for 5 (21.7%) patients. Regarding anti-SSA/Ro and anti-SSB/La antibodies, 3 (13%) patients were positive, 16 (69.6%) were negative, and results were not available for 4 (17.4%) patients.

Of the 23 patients with SS included in this study, 1 (4.3%) was under observation without medication, and 1 (4.3%) received a combination of prednisolone and methotrexate. The remaining 21 (91.3%) patients were administered hydroxychloroquine. Four (17.4%) patients received prednisolone in addition to hydroxychloroquine; 2 (8.7%) received sulfasalazine; and colchicine, methotrexate, and azathioprine were administered to 2 (8.7%), 1 (4.3%), and 1 (4.3%) patient, respectively.

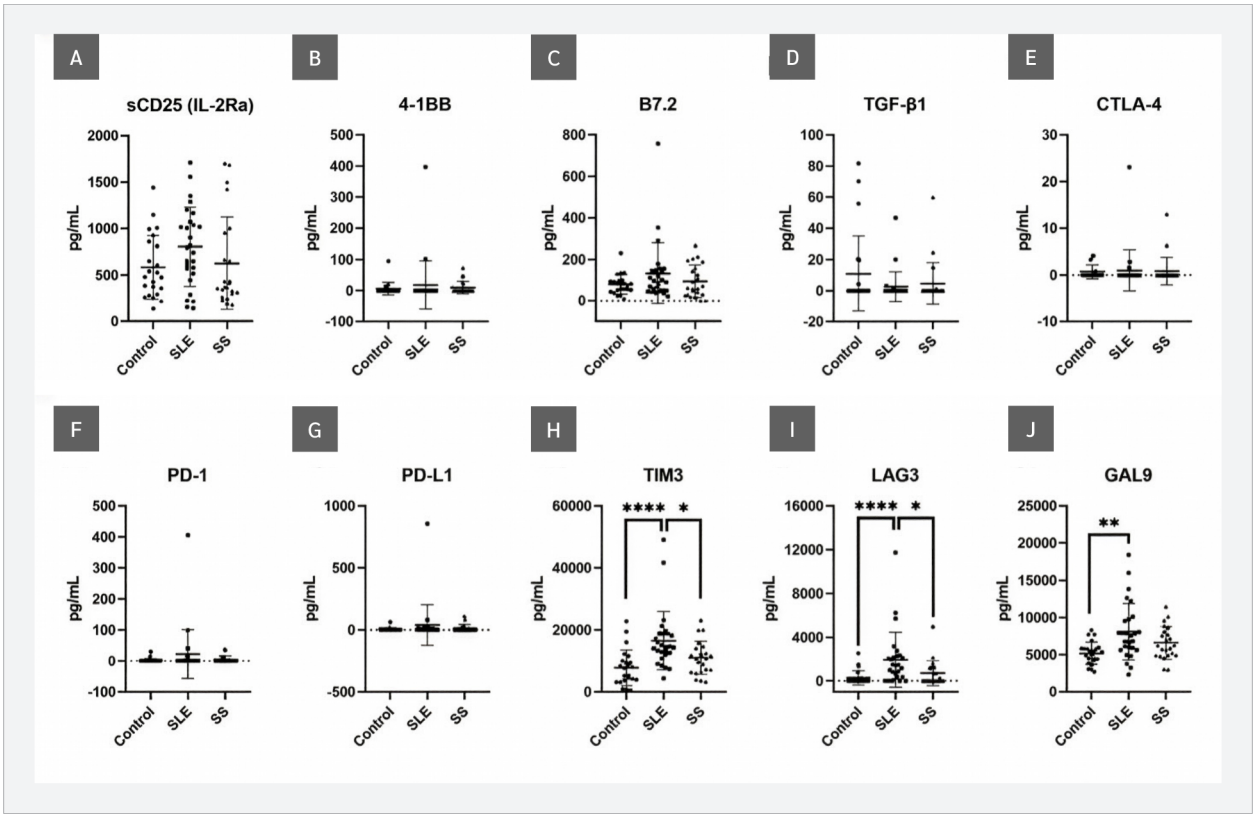

Figure 1. Statistical comparisons of soluble ICP levels among SLE, SS, and healthy controls. **(A)** sCD25, **(B)** 4-1BB, **(C)** B7.2, **(D)** TGF-β1, **(E)** CTLA-4, **(F)** PD-1, **(G)** PD-L1, ***(H)*** TIM-3, **(I)** LAG-3, **(J)** Galectin-9. Comparisons were performed using the Kruskal-Wallis test followed by Dunn's multiple comparisons test.

*p=0.0485 (TIM3, SLE vs. SS), * p =0.0273 (LAG-3, SLE vs. SS) ** p =0.0018, **** p <0.0001.

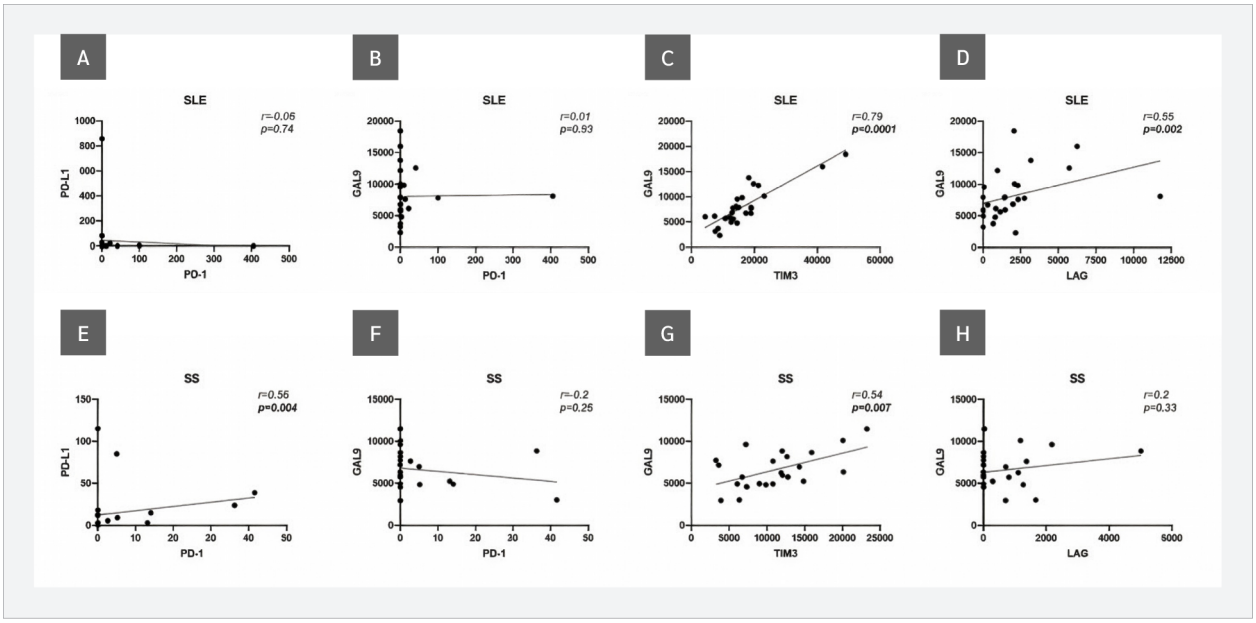

Figure 2. Correlation between sICP levels in patients with SLE and SS. **(A)** No correlation between PD-1 and PD-L1 levels was observed in SLE patients. **(B)** No correlation between Galectin-9 and PD-1 levels was observed in SLE patients. **(C)** A strong positive correlation between Galectin-9 and TIM-3 levels was observed in SLE patients. **(D)** A moderate positive correlation between Galectin-9 and LAG-3 levels was observed in SLE patients. **(E)** A moderate positive correlation between PD-1 and PD-L1 levels was observed in SS patients. **(F)** No correlation between Galectin-9 and PD-1 levels was observed in SS patients. **(G)** A moderate positive correlation between Galectin-9 and TIM-3 levels was observed in SS patients. **(H)** No correlation between Galectin-9 and LAG-3 levels was observed in SS patients.

When sICP levels were evaluated, significant increases in TIM-3 ($p<0.0001$), LAG-3 ($p<0.0001$), and Gal-9 ($p=0.018$) were observed in SLE patients compared with the control group. No significant differences were detected in sCD25, 4-1BB, B7.2, TGF-β1, CTLA-4, PD-1, or PD-L1 levels ($p>0.05$). In addition to the comparison with the control group, TIM-3 and LAG-3 levels were significantly higher in the SLE group than in the SS group ($p=0.0273$) (Figure 1).

Investigations of correlations between sICP levels revealed that, in SLE patients, Gal-9 and TIM-3 showed a strong positive correlation ($r=0.79$, $p<0.0001$), and a moderate positive correlation was observed between Gal-9 and LAG-3 ($r=0.55$, $p=0.002$). Similarly, in SS patients, Gal-9 and TIM-3 levels showed a moderate positive correlation ($r=0.54$, $p=0.007$), in addition to sPD-1 and sPD-L1 ($r=0.56$, $p=0.004$) (Figure 2).

Next, the correlations between serum sICP levels and SLEDAI scores in SLE patients and ESSDAI scores in SS patients were evaluated. No correlations were observed between sICP levels and SLEDAI scores (Figure 3). However, when ESSDAI scores and sICP levels were analyzed, a strong positive correlation with sCD25 ($r=0.65$, $p=0.0007$) and weak but statistically significant positive correlations with TIM-3 ($r=0.49$, $p=0.01$) and Gal-9 ($r=0.41$, $p=0.04$) were observed. In addition, the relationship between the ESSDAI score and B7.2 levels was close to statistical significance ($r=0.38$, $p=0.06$) (Figure 4).

CTLA-4 and free active TGF-β1 were not included in the evaluation of correlations with disease activity scores because their concentrations were accurately measured in only 3 (11%) patients with SLE and in only 2 (8%) and 4 (17%) patients with SS, respectively.

Discussion

Relevant ligand-receptor pairs were evaluated when investigating correlations between sICPs. Programmed cell death protein 1 (PD-1) plays a critical role in regulating immune responses and maintaining self-tolerance by modulating T-cell activity. One of its ligands, PD-L1, is a transmembrane protein that acts as a key co-inhibitory molecule in the immune system. By binding to PD-1, PD-L1 suppresses the proliferation of PD-1-positive cells, reduces their cytokine production, and induces their apoptosis, effectively dampening the immune response (13).

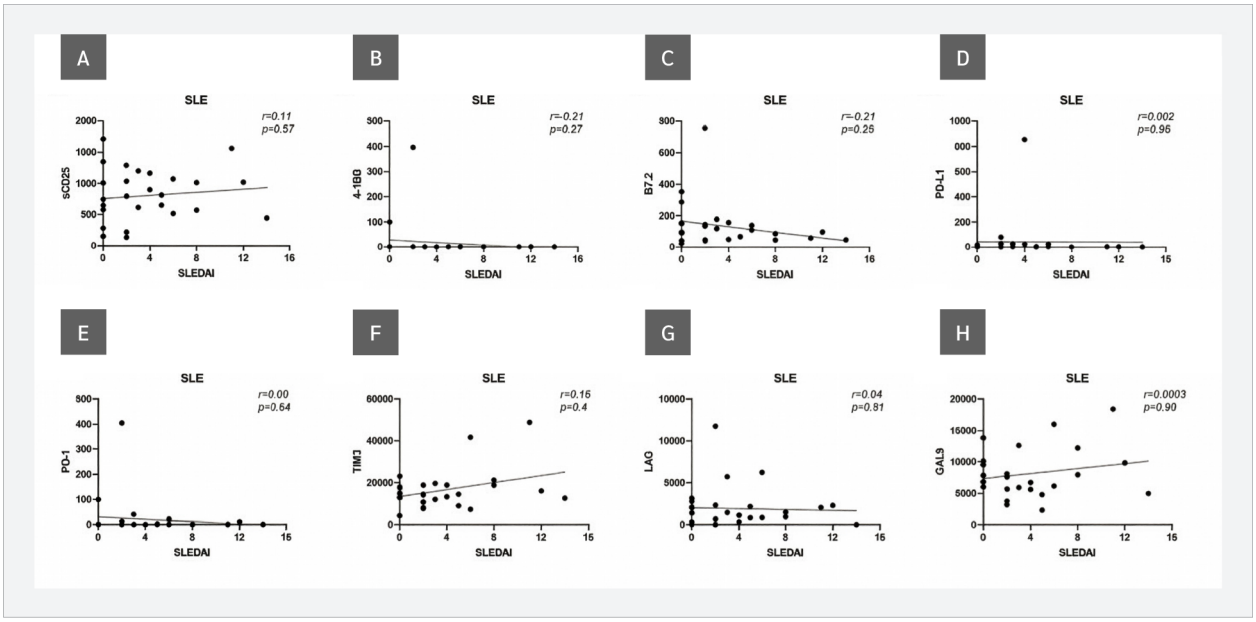

Figure 3. Correlations between serum sICP levels and SLEDAI scores in patients with SLE.

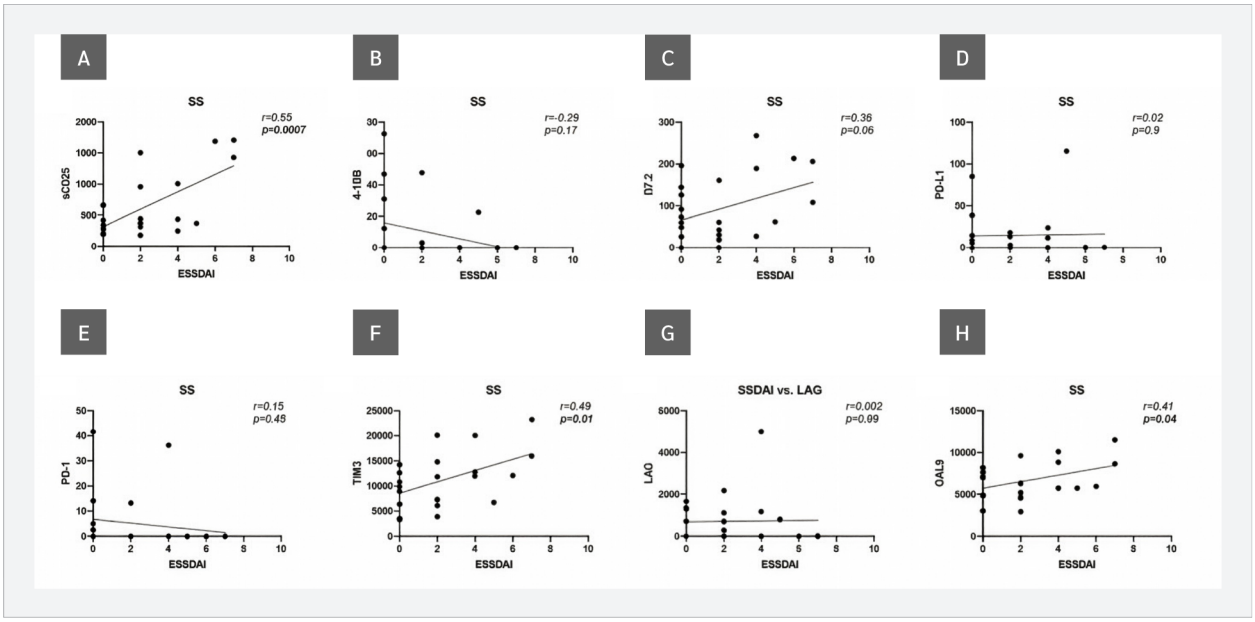

Figure 4. Correlations between serum sICP levels and ESSDAI scores in patients with SS.

Gal-9, a member of the galectin family with a tandem repeat structure, serves as a ligand for TIM-3, which is expressed on exhausted T cells (14). In addition to interacting with Gal-9, TIM-3 has been reported to bind PD-1 (15). Although no interaction between Gal-9 and LAG-3 has been reported, their co-expression has been described under certain conditions (16).

Autoimmune diseases result from a breakdown of immune tolerance and are multifactorial, with both genetic and environmental factors playing critical roles in their development (17). Although autoimmunity has a genetic component, incomplete concordance rates in monozygotic twins suggest that other factors contribute to disease onset (18). Environmental influences, such as

lifestyle, infections, and diet, are supported by variations in the incidence of autoimmune diseases across different ethnic groups and geographic regions. Although autoimmune diseases rarely cause mortality, they have a significant impact on quality of life (19). Their classification remains challenging, highlighting the complexity of these conditions (20). Furthermore, the frequent coexistence of autoimmune diseases suggests shared pathogenic mechanisms, as individuals with one autoimmune disease often have an increased risk of developing another (17). To date, more than 100 autoimmune diseases have been identified, and several other conditions exhibit autoimmune-related features. It has been reported that autoimmune diseases affect approximately 5.6% to 9.4% of the global population, with their incidence and prevalence increasing significantly over the past 30 years, particularly among younger individuals (21). Because of their widespread impact, autoimmune diseases have been identified by the World Health Organization (WHO) as the third greatest threat to human health (22).

Systemic lupus erythematosus is a complex autoimmune disease that affects multiple organ systems and is characterized by the presence of autoantibodies against nuclear antigens, the accumulation of immune complexes, and chronic inflammation in key organs, including the skin, joints, and kidneys. The disease course is unpredictable, and persistent inflammation carries the risk of progressive organ damage, which may lead to serious health complications and an increased risk of premature mortality in severe cases (23). Systemic lupus erythematosus is estimated to affect more than 3.4 million people worldwide. However, determining its true global incidence and prevalence remains challenging due to variations in case definitions used in epidemiological studies and the lack of comprehensive data from many regions. The disease predominantly affects women, with a ratio of approximately 9:1 (female:male). Although the disease can occur at any age, it most commonly develops in women of childbearing age, typically between 15 and 44 years. Childhood-onset SLE, defined as disease onset before the age of 18, has been reported to be associated with a more severe disease course (23).

Sjögren's syndrome is a systemic disease characterized by multiple manifestations resulting in exocrine gland dysfunction or damage. The diagnosis of SS involves several steps, including assessment of oral and ocular dryness, detection of anti-SSA/Ro and anti-SSB/La antibodies, and performing a gland biopsy (24).

According to a meta-analysis, the incidence of SS has been estimated at 6.92 cases per 100,000 person-years, with a prevalence of 60.82 cases per 100,000 individuals (approximately 1 in 1644 people) (25). The disease is most commonly diagnosed around the ages of 40–67 years and has shown a significantly higher prevalence in women over the past 15 years (26).

The most prominent and common clinical symptom is dryness of the eyes and mouth, caused by impaired function of the salivary and lacrimal glands. In addition to dryness, patients with SS frequently suffer from chronic and debilitating symptoms, including persistent pain, dental caries, vaginal dryness, and joint pain (arthralgia), all of which contribute to a significant reduction in quality of life (27).

Immune checkpoint proteins are ligand-receptor pairs that regulate immune responses by either enhancing or suppressing immune activity (28). These molecules are primarily expressed on cells of both the adaptive immune system, particularly T cells, and the innate immune system. They play a critical role in maintaining self-tolerance and controlling the duration and intensity of immune responses in various tissues, thereby helping to prevent excessive tissue damage. By modulating effector cell activity, immune checkpoints ensure that immune responses remain balanced (28).

Stimulatory immune checkpoints include molecules such as CD137, CD137L, OX40, OX40L, CD28, CD80, B7.2, inducible T cell costimulator (ICOS), B7-related protein 1 (B7RP1), CD27 and CD70 (29). These molecules promote T cell activation and proliferation. In contrast, inhibitory checkpoints play a role in dampening immune responses to prevent overactivation and autoimmunity (30). Key inhibitory molecules include PD-1 and its ligands PD-L1 and PD-L2, as well as cytotoxic T-lymphocyte-associated protein 4 (CTLA4), CD80, B7.2, TIM-3, Gal-9, LAG-3, B and T lymphocyte attenuator (BTLA), herpesvirus entry mediator (HVEM), TIGIT, B7-H3, and B7-H4(31). Together, these stimulatory and inhibitory pathways play an essential role in fine-tuning immune responses (32). The roles of ICPs, both in membrane-bound and soluble forms, are now well documented in cancer (2,33–35). However, their involvement in autoimmune diseases remains less well understood.

TIM-3 is a member of the TIM family of immunoregulatory proteins (36). Its soluble form, which can be released

from the cell surface through cleavage by membrane-associated proteases, suggests that TIM-3 also functions as a cell-free ligand (37). Through interaction with its ligand Galectin-9, TIM-3 plays an important role in the onset and progression of chronic autoimmune diseases and has therefore been proposed as a potential target for novel therapeutic strategies, including in SLE. Song et al. (38) demonstrated that increased TIM-3 expression on peripheral T-lymphocyte subsets in SLE patients is associated with higher disease activity. Similarly, Zhao et al. (39) reported that, in its soluble form, plasma TIM-3 levels positively correlate with anti-dsDNA positivity and SLEDAI scores, suggesting that soluble TIM-3 (sTIM-3) may serve as a biomarker of disease activity in SLE. In line with these studies, TIM-3 levels were significantly higher in SLE patients compared with both the control and SS groups in our study.

In addition to TIM-3, the significant increase in its ligand Gal-9 compared with the control group, as well as the strong positive correlation between sTIM-3 and Gal-9 in SLE patients, further supports activation of this pathway in SLE (40-42). On the other hand, no relationship was observed between SLEDAI scores and TIM-3 levels in our study. This finding might be attributed to the fact that the patients included in our study were not newly diagnosed and had already been receiving treatment, which may have reduced disease activity scores, as reported in previous studies (43,44). Besides its interaction with TIM-3, Gal-9 has also been shown to bind PD-1 (12), although no correlation between these two ICPs was observed in SLE patients in our study. Interestingly, serum LAG-3 levels were also significantly higher in SLE patients. LAG-3 has recently been recognized as a promising target for inhibitory drug development. Experimental studies have shown that the absence of LAG-3 does not induce autoimmune responses *in vivo* and that modulation of LAG-3-expressing T cells may reduce autoimmune symptoms (45). Therefore, LAG-3 has been proposed as a potential therapeutic target in SLE (45,46) and our findings further support this hypothesis. Moreover, a positive correlation between Gal-9 and LAG-3 levels was observed, which is consistent with previous reports (41).

Compared with SLE, relatively few studies have investigated the role of ICPs in SS. In its membrane-bound form, the role of PD-1 in SS remains controversial. Kobayashi et al. (47) reported increased PD-1 expression on infiltrating lymphocytes in the salivary glands of SS patients, whereas Zhai et al. (48) identified PD-1-expressing $CD8^{+}CXCR5^{+}$ cells in patients with primary SS, particularly in those with lung involvement. However, immunotherapies targeting the PD-1/PD-L1 axis have been reported to induce SS (49-51). Similar to PD-1, increased PD-L1 and CTLA-4 expression in the salivary glands of SS patients has also been reported (52). In our study, although serum levels of sPD-1 and sPD-L1 did not differ significantly between the SS and control groups, a moderate positive correlation between these two ICPs was observed which may support their involvement in SS. In contrast, a recent study suggested that TIM-3 expression is downregulated in T cells of SS patients (53). As a ligand of TIM-3, Gal-9 has been proposed as a biomarker for several autoimmune diseases, including SS (54). In our study, Gal-9 levels did not differ significantly between SS patients and controls, although a moderate positive correlation between Gal-9 and sTIM-3 was observed. In a study by van den Hoogen et al. (55), Gal-9 levels were reported to be elevated in primary Sjögren's disease compared with non-Sjögren sicca and showed a positive correlation with ESSDAI scores. The ESSDAI was introduced by EULAR to standardize the assessment of disease activity in SS and is widely used in both clinical trials and routine practice (56). In our study, a strong correlation between ESSDAI scores and serum sCD25 levels was detected. This finding is consistent with previous studies suggesting the involvement of sCD25 in autoimmune diseases, including primary SS (57, 58). In addition, weak but statistically significant positive correlations were observed between ESSDAI scores and both Gal-9 and sTIM-3. Nevertheless, the absence of significant increases in sICP levels between SS patients and healthy controls in our study highlights the need for studies including larger patient cohorts.

Overall, the significant increase in TIM-3, LAG-3, and Gal-9 levels in the SLE group is consistent with previous reports. However, no significant correlations were observed between these markers and disease activity parameters. In contrast, although no significant differences in sICP levels were detected between the SS group and healthy controls, sCD25, TIM-3, and Gal-9 plasma levels showed positive correlations with disease activity scores. Considering the relatively low mean disease activity in our cohort and the fact that the participants were receiving treatment at the time of sampling, these correlations should be interpreted cautiously and require further validation in treatment-naïve patients and larger study populations.

Conclusion

The results of our study are consistent with previous reports and suggest that sICPs may serve as potential biomarkers in SLE and SS. Among the 10 sICPs evaluated, TIM-3, Gal-9 and LAG-3 levels were significantly higher in SLE patients, and Gal-9 levels showed positive correlations with TIM-3 and LAG-3. However, no association was observed between SLEDAI scores and sICP levels. In SS patients, sICP levels were not significantly altered compared with those of controls and SLE patients, although PD-1/PD-L1 and TIM-3/Gal-9 levels showed a positive correlation. In addition, ESSDAI scores were positively correlated with TIM-3 and Gal-9 levels.

Our findings indicate that even in treated SLE patients, sICP levels remain significantly higher than those observed in healthy controls. Further studies including treatment-naïve patients and individuals with higher disease activity are needed to confirm the potential of sICPs as biomarkers for SLE and SS and to clarify their relationship with disease severity.

Ethical Approval: The study was approved by the Yeditepe University Clinical Research Ethics Committee on July 07, 2022, with the decision number 1631.

Informed Consent: Informed consent was obtained from all participants

Peer-review: Externally peer-reviewed

Author Contributions: Concept – M.B.K., G.Y.D.; Design – E.G., G.Y.D.; Supervision – M.B.K., G.Y.D.; Fundings – E.G., G.Y.D.; Materials – E.G., B.A., BMK, G.Y.D.; Data Collection and/or Processing – E.G., B.A., BMK, G.Y.D.; Analysis and/or Interpretation – B.A., M.B.K., G.Y.D.; Literature Review – E.G., B.A.; Writer – E.G., B.A., G.Y.D.; Critical Reviews – M.B.K., G.Y.D.

Conflict of Interest: The authors declare no conflict of interest.

Financial Disclosure: This study was supported by the Scientific and Technological Research Council of Türkiye (TÜBİTAK) under the 2209-A Research Funding Program for University Students (2021).

AI Statement: Anthropic's Claude AI was used to check the grammar of selected paragraphs.

Scientific Presentation: This study was presented as a poster at the 7th European Congress of Immunology (ECI), held in Dublin, Ireland, from September 1 to 4, 2024.

References

1 Linsley PS, Greene JL, Brady W, Bajorath J, Ledbetter JA, Peach R. Human B7-1 (CD80) and B7-2 (CD86) bind with similar avidities but distinct kinetics to CD28 and CTLA-4 receptors. Immunity. 1994;1(9):793–801. Erratum in: Immunity 1995;2(2):following 203. [CrossRef]

2 Gaikwad S, Agrawal MY, Kaushik I, Ramachandran S, Srivastava SK. Immune checkpoint proteins: Signaling mechanisms and molecular interactions in cancer immunotherapy. Semin Cancer Biol. 2022;86(Pt 3):137–50. [CrossRef]

3 Zhai Y, Moosavi R, Chen M. Immune checkpoints, a novel class of therapeutic targets for autoimmune diseases. Front Immunol. 2021;12:645699. [CrossRef]

4 Ameer MA, Chaudhry H, Mushtaq J, Khan OS, Babar M, Hashim T, et al. An overview of systemic lupus erythematosus (SLE) pathogenesis, classification, and management. Cureus. 2022;14(10):e30330. [CrossRef]

5 Didier K, Bolko L, Giusti D, Toquet S, Robbins A, Antonicelli F, et al. Autoantibodies associated with connective tissue diseases: what meaning for clinicians? Front Immunol. 2018;9:541. [CrossRef]

6 Negrini S, Emmi G, Greco M, Borro M, Sardanelli F, Murdaca G, Indiveri F, Puppo F. Sjögren's syndrome: a systemic autoimmune disease. Clin Exp Med. 2022;22(1):9–25. [CrossRef]

7 Segal BM, Pogatchnik B, Holker E, Liu H, Sloan J, Rhodus N, et al. Primary Sjogren's syndrome: cognitive symptoms, mood, and cognitive performance. Acta Neurol Scand. 2012;125(4):272–8. [CrossRef]

8 McCoy SS, Bartels CM, Saldanha IJ, Bunya VY, Akpek EK, Makara MA, et al. National Sjögren's Foundation Survey: Burden of oral and systemic involvement on quality of life. J Rheumatol. 2021;48(7):1029–36. [CrossRef]

9 Pisetsky DS. Pathogenesis of autoimmune disease. Nat Rev Nephrol. 2023;19(8):509–24. [CrossRef]

10 Sciascia S, Bizzaro N, Meroni PL, Dimitrios B, Borghi MO, Bossuyt X, et al. Autoantibodies testing in autoimmunity: Diagnostic, prognostic and classification value. Autoimmun Rev. 2023;22(7):103356. [CrossRef]

11 Touma Z, Urowitz MB, Gladman DD. Systemic lupus erythematosus disease activity index 2000 responder index-50 website. J Rheumatol. 2013;40(5):733. [CrossRef]

12 Seror R, Bootsma H, Saraux A, Bowman SJ, Theander E, Brun JG, et al; EULAR Sjögren's Task Force. Defining disease activity states and clinically meaningful improvement in primary Sjögren's syndrome with EULAR primary Sjögren's syndrome disease activity (ESSDAI) and patient-reported indexes (ESSPRI). Ann Rheum Dis. 2016;75(2):382–9. [CrossRef]

13 Han Y, Liu D, Li L. PD-1/PD-L1 pathway: current researches in cancer. Am J Cancer Res. 2020;10(3):727–42.

14 Elahi S, Niki T, Hirashima M, Horton H. Galectin-9 binding to Tim-3 renders activated human CD4+ T cells less susceptible to HIV-1 infection. Blood. 2012;119(18):4192–204. [CrossRef]

15 Yang R, Sun L, Li CF, Wang YH, Yao J, Li H, et al. Galectin-9 interacts with PD-1 and TIM-3 to regulate T cell death and is a target for cancer immunotherapy. Nat Commun. 2021;12(1):832. [CrossRef]

16 Okoye I, Xu L, Motamedi M, Parashar P, Walker JW, Elahi S. Galectin-9 expression defines exhausted T cells and impaired cytotoxic NK cells in patients with virus-associated solid tumors. J Immunother Cancer. 2020;8(2):e001849. [CrossRef]

17 Samuels H, Malov M, Saha Detroja T, Ben Zaken K, Bloch N, Gal-Tanamy M, et al. Autoimmune disease classification based on PubMed text mining. J Clin Med. 2022;11(15):4345. [CrossRef]

18 Generali E, Ceribelli A, Stazi MA, Selmi C. Lessons learned from twins in autoimmune and chronic inflammatory diseases. J Autoimmun. 2017;83:51-61. [CrossRef]

19 Shiha MG, Chetcuti Zammit S, Elli L, Sanders DS, Sidhu R. Updates in the diagnosis and management of coeliac disease. Best Pract Res Clin Gastroenterol. 2023;64-65:101843. [CrossRef]

20 Casal Moura M, Merkel PA, Jayne D, Cid MC, Basu N, Hellmich B, et al. Challenges in the diagnosis, classification and prognosis of ANCA-associated vasculitis. Nat Rev Rheumatol. 2025;21(12):719–36. [CrossRef]

21 Ohta A, Nagai M, Nishina M, Tomimitsu H, Kohsaka H. Age at onset and gender distribution of systemic lupus erythematosus, polymyositis/dermatomyositis, and systemic sclerosis in Japan. Mod Rheumatol. 2013;23(4):759–64. [CrossRef]

22 Yuan L, Wang Y, Shen X, Ma F, Wang J, Yan F. Soluble form of immune checkpoints in autoimmune diseases. J Autoimmun. 2024;147:103278. [CrossRef]

23 Hoi A, Igel T, Mok CC, Arnaud L. Systemic lupus erythematosus. Lancet. 2024;403(10441):2326-2338. Erratum in: Lancet. 2024;403(10441):2292. [CrossRef]

24 Zhan Q, Zhang J, Lin Y, Chen W, Fan X, Zhang D. Pathogenesis and treatment of Sjogren's syndrome: Review and update. Front Immunol. 2023;14:1127417. [CrossRef]

25 Qin B, Wang J, Yang Z, Yang M, Ma N, Huang F, Zhong R. Epidemiology of primary Sjögren's syndrome: a systematic review and meta-analysis. Ann Rheum Dis. 2015 Nov;74(11):1983–9. [CrossRef]

26 Thurtle E, Grosjean A, Steenackers M, Strege K, Barcelos G, Goswami P. Epidemiology of Sjögren's: a systematic literature review. Rheumatol Ther. 2024;11(1):1–17. [CrossRef]

27 Cornec D, Devauchelle-Pensec V, Mariette X, Jousse-Joulin S, Berthelot JM, Perdriger A, et al. Severe health-related quality of life impairment in active primary Sjögren's syndrome and patient-reported outcomes: data from a large therapeutic trial. Arthritis Care Res (Hoboken). 2017;69(4):528–35. [CrossRef]

28 Zhang Y, Zheng J. Functions of immune checkpoint molecules beyond immune evasion. Adv Exp Med Biol. 2020;1248:201–26. [CrossRef]

29 Marin-Acevedo JA, Kimbrough EO, Manochakian R, Zhao Y, Lou Y. Immunotherapies targeting stimulatory pathways and beyond. J Hematol Oncol. 2021;14(1):78. [CrossRef]

30 Funes SC, Manrique de Lara A, Altamirano-Lagos MJ, Mackern-Oberti JP, Escobar-Vera J, Kalergis AM. Immune checkpoints and the regulation of tolerogenicity in dendritic cells: Implications for autoimmunity and immunotherapy. Autoimmun Rev. 2019;18(4):359–68. [CrossRef]

31 Pardoll DM. The blockade of immune checkpoints in cancer immunotherapy. Nat Rev Cancer. 2012;12(4):252–64. [CrossRef]

32 Pitts SC, Schlom J, Donahue RN. Soluble immune checkpoints: implications for cancer prognosis and response to immune checkpoint therapy and conventional therapies. J Exp Clin Cancer Res. 2024;43(1):155. [CrossRef]

33 He X, Xu C. Immune checkpoint signaling and cancer immunotherapy. Cell Res. 2020 Aug;30(8):660–9. [CrossRef]

34 Alturki NA. Review of the immune checkpoint inhibitors in the context of cancer treatment. J Clin Med. 2023;12(13):4301. [CrossRef]

35 Chen L, Chao Y, Li W, Wu Z, Wang Q. Soluble immune checkpoint molecules in cancer risk, outcomes prediction, and therapeutic applications. Biomark Res. 2024;12(1):95. [CrossRef]

36 Wolf Y, Anderson AC, Kuchroo VK. TIM3 comes of age as an inhibitory receptor. Nat Rev Immunol. 2020;20(3):173–85. [CrossRef]

37 Gorman JV, Colgan JD. Regulation of T cell responses by the receptor molecule Tim-3. Immunol Res. 2014;59(1-3):56–65. [CrossRef]

38 Song LJ, Wang X, Wang XP, Li D, Ding F, Liu HX, et al. Increased Tim-3 expression on peripheral T lymphocyte subsets and association with higher disease activity in systemic lupus erythematosus. Diagn Pathol. 2015;10:71. [CrossRef]

39 Zhao D, Li C, Yang X, Yan W, Zhang Y. Elevated soluble Tim-3 correlates with disease activity of systemic lupus erythematosus. Autoimmunity. 2021;54(2):97–103. [CrossRef]

40 Zeggar S, Watanabe KS, Teshigawara S, Hiramatsu S, Katsuyama T, Katsuyama E, et al. Role of Lgals9 deficiency in attenuating nephritis and arthritis in BALB/c mice in a pristane-induced lupus model. Arthritis Rheumatol. 2018;70(7):1089–101. [CrossRef]

41 Yuksel K, Sag E, Demir S, Özdel S, Kaya UA, Atalay E, et al. Plasma checkpoint protein levels and galectin-9 in juvenile systemic lupus erythematosus. Lupus. 2021;30(6):998–1004. [CrossRef]

42 Matsuoka N, Fujita Y, Temmoku J, Furuya MY, Asano T, Sato S, et al. Galectin-9 as a biomarker for disease activity in systemic lupus erythematosus. PLoS One. 2020;15(1):e0227069. [CrossRef]

43 Li M, Liang J, Pan W, Liu L, Wu M, Ding F, et al. Predictors of improvement in disease activity in first hospitalized patients with systemic lupus erythematosus: a multicenter

retrospective study of a Chinese cohort. Clin Rheumatol. 2022;41(11):3355–62. [CrossRef]

44 Kamanamool N, Ingsathit A, Rattanasiri S, Ngamjanyaporn P, Kasitanont N, Chawanasuntorapoj R, et al. Comparison of disease activity between tacrolimus and mycophenolate mofetil in lupus nephritis: a randomized controlled trial. Lupus. 2018;27(4):647–56. [CrossRef]

45 Wang B, Zhang B, Wu M, Xu T. Unlocking therapeutic potential: Targeting lymphocyte activation Gene-3 (LAG-3) with fibrinogen-like protein 1 (FGL1) in systemic lupus erythematosus. J Transl Autoimmun. 2024;9:100249. [CrossRef]

46 Chen K, Li X, Shang Y, Chen D, Qu S, Shu J, et al. FGL1-LAG3 axis impairs IL-10-Producing regulatory T cells associated with Systemic lupus erythematosus disease activity. Heliyon. 2023;9(10):e20806. [CrossRef]

47 Kobayashi M, Kawano S, Hatachi S, Kurimoto C, Okazaki T, Iwai Y, et al. Enhanced expression of programmed death-1 (PD-1)/PD-L1 in salivary glands of patients with Sjögren's syndrome. J Rheumatol. 2005;32(11):2156–63.

48 Zhai X, Wang Y, Guo H, Liang Z, Feng M, Wu Y, Qin Y, Zhao X, Gao C, Luo J. Altered levels of circulating $CD8^{+}CXCR5^{+}PD\text{-}1^{+}$T follicular cytotoxic cells in primary Sjögren's syndrome. Clin Rheumatol. 2022;41(6):1697–708. [CrossRef]

49 Caeyman A, Vandekerckhove O, Pat K, Wynants J, Weytjens K, de Wergifosse I, et al. Sjögren's syndrome caused by PD-1 inhibition in a lung cancer patient. Case Rep Oncol. 2023;16(1):1095–9. [CrossRef]

50 Ramos-Casals M, Maria A, Suárez-Almazor ME, Lambotte O, Fisher BA, Hernández-Molina G, et al; ICIR. Sicca/Sjögren's syndrome triggered by PD-1/PD-L1 checkpoint inhibitors. Data from the International ImmunoCancer Registry (ICIR). Clin Exp Rheumatol. 2019;37 Suppl 118(3):114–22.

51 Pellegrino C, D'Antonio C, Ierinò D, Onesti CE, Aschelter AM, Santini D, et al. Sjögren syndrome induced by anti PDL-1 treatment for TNBC: case report and review of literature. Front Immunol. 2024;15:1417444. [CrossRef]

52 An Q, Zhao J, Zhu X, Yang B, Wu Z, Su Y, et al. Exploiting the role of T cells in the pathogenesis of Sjögren's syndrome for therapeutic treatment. Front Immunol. 2022;13:995895. [CrossRef]

53 Sun T, Liu S, Yang G, Zhu R, Li Z, Yao G, et al. Mesenchymal stem cell transplantation alleviates Sjögren's syndrome symptoms by modulating Tim-3 expression. Int Immunopharmacol. 2022;111:109152. [CrossRef]

54 Moar P, Tandon R. Galectin-9 as a biomarker of disease severity. Cell Immunol. 2021;361:104287. [CrossRef]

55 van den Hoogen LL, van der Heijden EHM, Hillen MR, Mertens JS, Fritsch-Stork RDE, Radstake TRDJ, et al. Galectin-9 reflects the interferon signature and correlates with disease activity in systemic autoimmune diseases. Response to: 'Biomarkers: to be or not to be' by Yavuz and Rönnblom. Ann Rheum Dis. 2020;79(1):e9. [CrossRef]

56 Seror R, Bowman SJ, Brito-Zeron P, Theander E, Bootsma H, Tzioufas A, et al. EULAR Sjögren's syndrome disease activity index (ESSDAI): a user guide. RMD Open. 2015;1(1):e000022. [CrossRef]

57 Cao S, Liu X, Li Y, Yang Y, Cai X, Cong S, et al. Serum sCD25 is an indicator for rheumatoid arthritis-associated interstitial lung disease. Clin Exp Rheumatol. 2024;42(3):633–41. [CrossRef]

58 Chen J, Jin Y, Li C, Gan Y, Li J, Chen S, Sun X, He J, Li Z. Evaluation of soluble CD25 as a clinical and autoimmune biomarker in primary Sjögren's syndrome. Clin Exp Rheumatol. 2020;38 Suppl 126(4):142–9.

ORIGINAL RESEARCH

Turkish Journal of Immunology, 14(1):35–44

The Correlation Between the Onset of Autoinflammatory Response and Gouty Arthritis

Rojan G.M.AL-Allaff[1], Enass Waad AL- Hadidi[1], Hiyam Adil Altaii[1]

[1]*University of Mosul, College of Sciences, Biology Department, Mosul, Iraq*

Abstract

Objective: This study aimed to determine the concentration of anti-type II collagen (anti-CII) and interleukin-1 beta (IL-1β) in patients with hyperuricemia and to evaluate their relationship with uric acid and other hematological parameters.

Materials and Methods: This case-control study included patients with chronic hyperuricemia and healthy controls. Serum uric acid levels, complete blood counts, and quantitative levels of IL-1β and anti-CII antibodies were measured using an enzyme-linked immunosorbent assay (ELISA).

Results: A total of 80 patients with chronic hyperuricemia and 40 healthy controls were included in the study. Data analysis showed that uric acid (8.20 ± 1.06 mg/dL vs 4.99 ± 1.20 mg/dL; $p<0.001$), MID cells (627.48 ± 283.84 cells/μL vs 375.29 ± 173.43 cells/μL; $p=0.001$), anti-CII (9.67 ± 7.30 ng/mL vs 5.58 ± 1.35 ng/mL; $p=0.027$), and IL-1β (2.21 ± 2.18 pg/mL vs 0.94 ± 0.81 pg/mL; $p=0.024$) were significantly higher in patients than in controls. Regression analysis revealed a significant negative correlation between MID cells and hemoglobin (Hb) levels ($R^2=0.30$; $p=0.049$). Notably, IL-1β was the only variable that showed a statistically significant effect on anti-CII levels (β=0.578, $p=0.014$).

Conclusion: The study concludes that the anti-CII-mediated autoimmune response in gout occurs through an IL-1β-mediated production axis rather than as a direct consequence of elevated uric acid levels. Moreover, the negative correlation between MID cells and Hb suggests that chronic gout may exert a systemic suppressive effect on erythropoiesis.

Keywords: Gouty arthritis, autoimmunity, anti-CII, IL-1β, hyperuricemia, MID

Correspondence
Rojan G.M.AL-Allaff

E-mail
rojsbio57@uomosul.edu.iq

Received
February 16, 2026

Accepted
April 15, 2026

Published
April 30, 2026

Suggested Citation
G.M.AL-Allaff R, AL- Hadidi EW, Altaii HA. The correlation between the onset of autoinflammatory response and gouty arthritis. Turk J Immunol. 2026;14(1):35–44.

DOI
10.36519/tji.2026.1051

Introduction

Gouty arthritis is a complex inflammatory condition associated with metabolic derangements and an enhanced innate immune response. Gout is caused by the accumulation of monosodium urate (MSU) crystals in the synovial fluid and joint tissues. However, the transition from asymptomatic hyperuricemia to an acute, self-limiting attack is regulated by a complex network of immunological signals. At the heart of this network is the activation of the NLR family pyrin domain-containing 3 (NLRP3; formerly NOD-, LRR- and pyrin domain-containing protein 3) inflammasome and the ensuing release of interleukin-1 beta (IL-1β), a key proinflammatory cytokine that coordinates neutrophil recruitment and activation (1). However, MSU crystals and their associated cytokines do not solely determine the immune landscape of gout. The articular environment, particularly the extracellular matrix, which is mainly composed of type II collagen (CII), also modulates the inflammatory response (2). Recent research has shown that injury to articular cartilage and the release of CII fragments act as immunological modifiers that influence the structural properties of MSU crystals and enhance macrophage activation (3).

This phenomenon creates a harmful feedback loop in which IL-1β-driven inflammation stimulates the production of matrix-degrading enzymes, releasing collagen fragments and thereby perpetuating the inflammatory response (4). Understanding this relationship requires an in-depth assessment of the molecular interplay between MSU crystals, IL-1β signaling, and the cartilage matrix (5).

Gouty arthritis begins with hyperuricemia, which occurs when blood uric acid levels exceed the physiological saturation point of approximately 6.8 mg/dL. In humans, purine metabolism ultimately produces uric acid, which is largely eliminated via the kidneys and intestines (6). When the concentration of urate ions ($C_5H_3N_4O_3^-$) in the synovial fluid becomes supersaturated, needle-like MSU crystals begin to form. Crystal formation is not determined by concentration alone; the local microenvironment, including pH, electrolyte levels, and matrix components such as proteoglycans and collagen, also plays a crucial role (7). Elevated uric acid levels are often considered a risk factor for metabolic and inflammatory conditions. However, their systemic effects on immune markers and the hematological profile remain unclear. It is therefore important to investigate the relationship between high uric acid concentrations, the autoimmune marker anti-type II collagen (Anti-CII), and the pro-inflammatory cytokine IL-1β.

Furthermore, it is unclear how these markers vary across demographic variables such as age and sex or whether there are significant changes in hematological parameters, including white blood cell (WBC) counts, neutrophil counts, and hemoglobin (Hb) levels. To better understand the autoinflammatory response induced by uric acid, this study aimed to investigate these relationships. Therefore, this study aimed to investigate the relationship between uric acid levels, anti-CII antibodies, and IL-1β concentrations in patients with hyperuricemia and to evaluate their association with hematological parameters (Figure 1).

Materials and Methods

Patient Recruitment and Sample Collection

Samples were collected from patients with persistently elevated blood uric acid levels. Participants were recruited from Al-Salam Teaching Hospital, Ibn Sina Hospital, and several outpatient clinics. Sample collection took place between January and September 2025. Ethical approval for the study was granted by the Scientific and Ethical Committee of the University of Mosul, Iraq, in collaboration with the Iraqi Ministry of Health.

Study Subjects

This study involved participants aged 25–65 years, including patients diagnosed with chronic hyperuricemia. The control group comprised healthy individuals with no history of elevated serum uric acid (SUA) levels. Patients were diagnosed with gouty arthritis by specialist rheumatologists according to the 2015 American College of Rheumatology (ACR)/European Alliance of Associations for Rheumatology (EULAR) classification criteria for gout. Diagnosis required a combination of clinical presentation (history of acute inflammatory arthritis episodes), laboratory findings (SUA levels > 6.8 mg/dL), and the presence of tophi. Individuals with asymptomatic hyperuricemia alone were excluded from the patient cohort to ensure that the evaluated inflammatory markers accurately represented the active disease state. Exclusion criteria for all participants included active bacterial or viral infections, autoimmune diseases, and the use of pharmacological therapies or antibiotics.

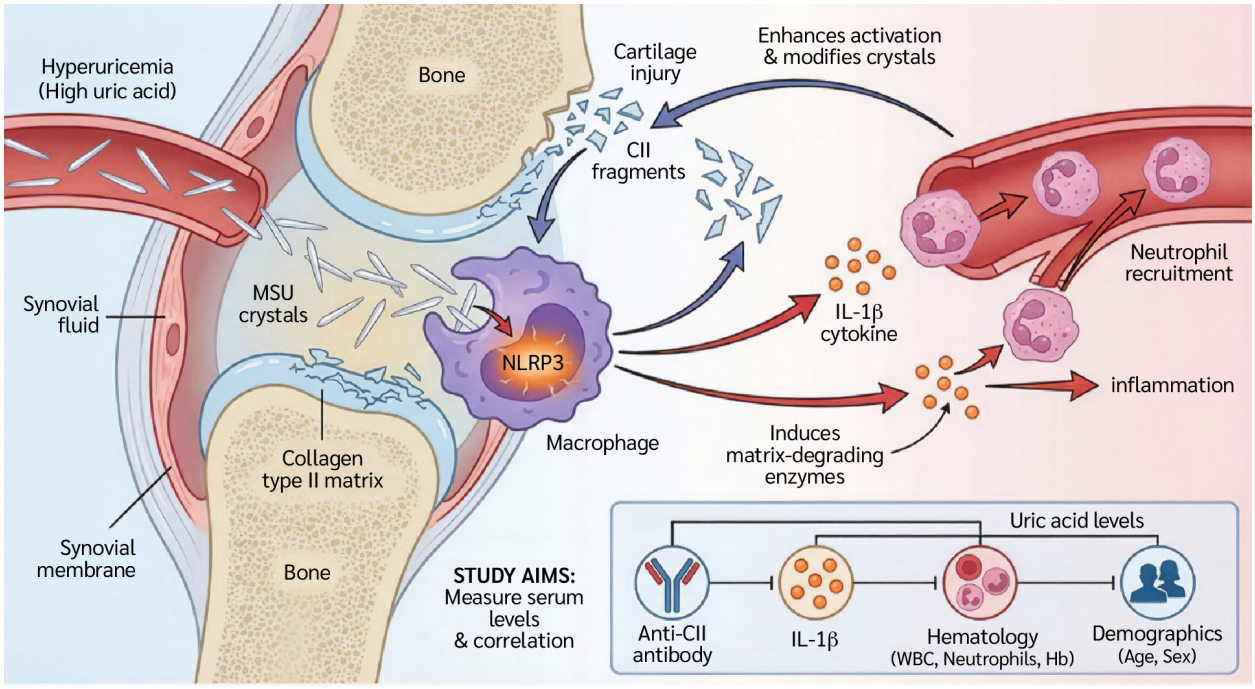

Figure 1. Conceptual framework of gout-associated inflammation linking hyperuricemia, monosodium urate crystal deposition, IL-1β signaling, cartilage damage, and study variables.

Serum Collection

Three milliliters of venous blood were collected from each participant and divided into two tubes: one containing ethylenediaminetetraacetic acid (EDTA) for complete blood count analysis and the other containing a serum separator gel. The gel tubes were centrifuged at 5000 rpm for 10 minutes to obtain serum. Aliquots of serum were then transferred to Eppendorf tubes and stored at -20°C until further analysis (8).

Estimation of Serum Uric Acid

Principle

This reaction produces allantoin and hydrogen peroxide (H_2O_2). The generated hydrogen peroxide then reacts with 4-aminoantipyrine and a phenolic compound (such as dichlorophenol sulfonate) in the presence of peroxidase (POD) to form a colored quinonimine complex. The intensity of the resulting red-pink color is directly proportional to the uric acid concentration in the sample (9).

Complete Blood Count (CBC)

An automated Mythic™ 18 hematology analyzer (Orphée SA, Geneva, Switzerland) was used to measure 18 hematological parameters (10).

Human IL-1β (Interleukin-1 Beta) ELISA Kit

Principle

The Human IL-1β ELISA Kit (Catalog No. RE1074H; Reed Biotech Ltd, Shanghai, China) was used according to the manufacturer's instructions. The assay utilizes a microplate pre-coated with a monoclonal antibody specific for human IL-1β. Samples and standards were added to the wells and incubated, allowing the target protein to bind to the immobilized antibody. Subsequently, a biotinylated detection antibody specific for IL-1β was added, followed by an additional incubation step.

After removal of unbound components, an avidin-horseradish peroxidase (HRP) conjugate was added to the wells and incubated again.

Following a final wash to eliminate excess conjugate, a substrate solution was added, producing a blue color whose intensity was proportional to the amount of bound IL-1β. The reaction was stopped using a stop solution, causing the color to change from blue to yellow. The optical density (OD) was measured spectrophotometrically at 450 nm, and IL-1β concentrations in the samples were calculated by interpolation from a standard curve generated using standards of known concentrations (11,12).

Procedure

- Microplate strips were removed from the frame, and the remaining strips were returned to the aluminum foil bag containing desiccants and sealed for storage.
- Standard, blank, and sample wells were designated. A volume of 100 µL of diluted standards, blank solution, and sample dilutions was added to the appropriate wells. The plate was sealed with the kit sealer and incubated at 37°C for 90 minutes. Solutions were added carefully to the bottom of the wells without touching the well walls to avoid foaming.
- The plate was aspirated and cleaned three times. Immediately afterward, 100 µL of biotinylated detection antibody working solution was added to each well. A new sealer was applied, and the plate incubated at 37°C for 1 hour.
- After decanting the solution, 300 µL of wash buffer was added to each well. After 0.5 minutes, the solution was aspirated or decanted, and the plate was patted dry on clean absorbent paper. The washing procedure was repeated three times. Test strips were used immediately after washing, and wells were not allowed to dry.
- A volume of 100 µL of HRP conjugate working solution was added to each well. A new sealer was applied, and the plate was incubated at 37°C for 30 minutes.
- After decanting the solution from each well, the washing procedure described in step 4 was repeated three times.
- A volume of 100 µL of substrate reagent was added to each well. The plate was covered with a new sealer and incubated at 37°C for 15 minutes in the dark. Optical density was measured after a 15-minute microplate preheating and reading step.
- A volume of 50 µL of stop solution was added to each well in the same sequence as the substrate solution.
- The OD at 450 nm of each well was measured immediately using a microplate reader.

Human Anti-Type II Collagen Antibody (Anti-CIIAb) Enzyme-Linked Immunosorbent Assay (ELISA) Kit

Principle

The Human Anti-Type II Collagen Antibody (Anti-CIIAb) ELISA Kit (Catalogue No. EH5105; FineTest, Wuhan Fine Biotech Co., Ltd, Wuhan, China) was used according to the manufacturer's instructions. The assay utilizes an indirect ELISA method in which specific antigens are pre-coated onto a 96-well microplate. Detection is achieved using a biotin-conjugated antibody system.

Standards and samples were added to the wells and incubated. After the initial incubation, unbound components were removed by washing, and a biotinylated detection antibody was added.

Following additional washing to remove unbound material, HRP-conjugated streptavidin was applied. The enzymatic activity of HRP was visualized by adding 3,3′,5,5′-tetramethylbenzidine (TMB) substrate, producing a blue color that turned yellow after the addition of an acidic stop solution.

The OD was measured at 450 nm using a microplate reader. The concentration of the target antibody in the samples was directly proportional to the OD450 values and was calculated using a standard curve (13).

Procedure

- Preparation and loading of samples: The pre-coated microplate was prepared by designating appropriate wells for standards, samples, and blank controls. All measurements were performed in triplicate to minimize experimental error. A volume of 100 µL of each standard solution was added to the designated standard wells. A volume of 100 µL of sample dilution buffer was added to the blank control wells, whereas 100 µL of diluted serum samples was added to the sample wells. The plate was sealed and incubated at 37°C for 90 minutes. Solutions were carefully dispensed into the bottom of the wells without touching the well walls to avoid foaming.
- Initial washing and antibody incubation: After incubation, the liquid was aspirated, and the plate was gently blotted on absorbent paper. The wells were washed twice with 350 µL of wash buffer without soaking. Subsequently, 100 µL of biotin-conjugated antibody working solution was added to each well. The plate was sealed and incubated statically at 37°C for 60 minutes. Following incubation, the plate was washed three times by immersing the wells in 350 µL of wash buffer for 1 min and discarding the liquid.
- SABC conjugation and chromogenic development: A volume of 100 µL of the HRP-streptavidin-biotin complex (SABC) working solution was added to each well and incubated at 37°C for 30 minutes. The TMB

substrate solution was equilibrated to 37°C before use.

- The plate then underwent five washing cycles using the previously described immersion washing procedure. Subsequently, 90 µL of TMB substrate was added to each well. The plate was sealed and incubated in the dark at 37°C for 10–20 minutes. Color development was monitored visually, and the incubation time did not exceed 30 minutes. A clear color gradient was observed in the standard wells.
- Stopping the reaction and measuring: The enzymatic reaction was terminated by adding the stop solution in the same sequence as the TMB substrate was added. After the stop solution was added, the color in each well immediately changed to yellow. Optical density was measured immediately at 450 nm using a microplate reader. To correct background interference, wavelength correction was performed using reference readings at either 570 nm or 630 nm before calculating the final OD450 values.

Statistical Analysis

Data were analyzed using IBM SPSS Statistics for Windows, version 26.0 (IBM Corp., Armonk, NY, USA). Descriptive statistics were expressed as mean ± standard deviation (SD). Differences between hyperuricemic patients and healthy controls were evaluated using the independent-samples *t*-test. Associations between hematological parameters and inflammatory markers were examined using simple linear regression analysis. Additionally, a multiple linear regression analysis was performed to identify independent predictors of anti-CII levels. Statistical significance was set as $p<0.05$.

Results

This study involved a total 120 participants, including 80 patients with chronic hyperuricemia and 40 healthy controls with no history of elevated SUA levels.

Statistical Implications of the Current Study Groups

The differences between the study variables are presented in Table 1. Statistical analysis demonstrated that serum uric acid levels were significantly higher in the patient group (8.20 ± 1.06 mg/dL) compared with the control group (4.99 ± 1.20 mg/dL; $t=9.992$, $p<0.001$). Similarly, MID cell counts were significantly elevated in patients ($p=0.001$).

Regarding immunological markers, both anti-CII and IL-1β levels were significantly higher in the patient group compared with controls ($p=0.027$ and $p=0.024$, respectively). In contrast, no statistically significant differences were observed between the two groups in Hb levels ($p=0.110$), WBC ($p=0.863$), neutrophil count ($p=0.268$), or lymphocyte count ($p=0.158$).

Simple Linear Regression Analyses

Association Between MID Cell Count and Hemoglobin

A simple linear regression analysis was performed to evaluate the relationship between MID cell count and Hb levels (Table 2). The analysis demonstrated a statistically significant negative association between MID cell count and Hb levels (β=-31.231, $t=-1.970$, $p=0.049$). The coefficient of determination indicated that MID cell count explained 30% of the variance in Hb levels ($R^2=0.30$). These findings suggest that higher MID cell counts are associated with lower Hb levels.

Association Between Neutrophil Count and Hemoglobin

A simple linear regression analysis was conducted to examine the relationship between neutrophil count (cells/µL) and Hb levels (g/dL) (Table 3). The results revealed a statistically significant negative association between neutrophil count and Hb levels (β=-0.001, $t=-2.173$, $p=0.036$). The coefficient of determination (R^2) *was* 0.11.

Multiple Linear Regression Analysis

A multiple linear regression model was constructed to evaluate the effects of uric acid (mg/dL), MID cell count (cells/µL), Hb levels (g/dL), and IL-1β (pg/mL) on anti-CII levels (ng/mL) (Table 4).

The analysis showed that:

- Uric acid was not significantly associated with anti-CII levels ($p=0.534$).
- MID cell count was not significantly associated with anti-CII levels ($p=0.969$).
- Hemoglobin levels were not significantly associated with anti-CII levels ($p=0.286$).
- IL-1β showed a significant positive association with anti-CII levels ($p=0.014$).
- The regression coefficient (β=0.578) indicated that each 1-unit increase in IL-1β was associated with an increase of 0.578 ng/mL in anti-CII levels.
- The coefficient of determination showed that 47% of the variance in IL-1β levels was explained by the

Table 1. Comparison of inflammatory markers, hematological parameters, and uric acid levels between patients with gouty arthritis and healthy controls.

Variable	Type	n	Mean ±SD	*t*	df	*p-value*
Uric acid, mg/dL	Patient	80	8.20 ± 1.06	9.992	118	**0.001**
	Control	40	4.99 ± 1.20			
Hb, g/dL	Patient	80	13.82 ± 2.41	-1.623	118	0.110
	Control	40	14.85 ± 1.60			
WBC, cell/µL	Patient	80	7401 ± 1852.02	0.174	118	0.863
	Control	40	7305.88 ± 1991.06			
Neutrophils, cell/µL	Patient	80	4124.18 ± 1377.53	-1.118	118	0.268
	Control	40	4567.65 ± 1350.17			
Lymphocytes, cell/µL	Patient	80	2649.30 ± 668.51	1.432	118	0.158
	Control	40	2360 ± 763.82			
MID cells, cell/µL	Patient	80	627.48 ± 283.84	3.394	118	**0.001**
	Control	40	375.29 ± 173.43			
Anti-CII, ng/mL	Patient	80	9.67 ± 7.30	2.279	118	**0.027**
	Control	40	5.58 ± 1.35			
IL-1β, pg/mL	Patient	80	2.21 ± 2.18	2.330	118	**0.024**
	Control	40	0.94 ± 0.81			

SD: Standard deviation

variables included in the model, while the remaining 53% may be attributable to other factors not included in the analysis.

Discussion

The present study demonstrates clear biochemical and immunological differences between patients with gouty arthritis and healthy controls. The most prominent finding was the significantly elevated SUA levels in the patient group compared with controls. These values exceed the physiological saturation threshold for MSU, thereby promoting crystallization within joint tissues. This observation aligns with the treat-to-target approach in gout management, which recommends maintaining SUA levels below 6.0 mg/dL to prevent crystal formation and recurrent flares (14).

In addition to hyperuricemia, patients exhibited a significant increase in MID cell counts, likely reflecting enhanced monocyte activity. Recent immunological studies have shown that hyperuricemia induces a form of trained immunity in monocytes. Once recruited to the synovium, these cells phagocytose MSU crystals and activate the NLRP3 inflammasome (15). This intracellular mechanism likely explains the concurrent significant rise in IL-1β observed in our patient cohort. IL-1β is the key cytokine in gouty inflammation, responsible for neutrophil recruitment and the intense pain characteristic of acute flares.

Another important finding of this study is the significant elevation of anti-CII antibodies in patients with gout. Although anti-CII antibodies are traditionally associated with rheumatoid arthritis, emerging evidence indicates that chronic crystal-induced inflammation can lead to citrullination of proteins in the joint environment, triggering an autoantibody response. These findings support the growing theory that chronic gout may involve an autoimmune reactivity driven by persistent tissue damage (16,17).

Regression analysis revealed a significant negative relationship between MID cell counts and Hb levels. This

Table 2. Simple linear regression analysis of the association between MID cell counts and hemoglobin levels.

Independent variable	Dependent variable	β	SE (β)	Std. β	R^2	*t*	*p*-value*
Constant	Hb, g/dL	1037.223	223.138	-	0.30	4.648	0.000
MID cells, cell/µL		-31.231	15.855	-0.308		-1.970	0.049

β: Regression coefficient, **SE:** Standard error, **Std. β:** Standardized regression coefficient, **R²:** Coefficient of determination, **Hb:** Hemoglobin, **MID:** Mid-sized cells (monocytes, eosinophils, basophils).
*$p<0.05$ was considered statistically significant.

Table 3. Simple linear regression analysis of the effect of neutrophils on Hb levels.

Independent variable	Dependent variable	β	SE (β)	Std. β	R^2	*t*	*p*-value*
Constant	Hb, g/dL	16.273	1.166	-	0.11	13.955	0.000
Neutrophils, cell/µl		-0.001	0.000	-0.336		-2.173	0.036

β: Regression coefficient, **SE:** Standard error, **Std. β:** Standardized regression coefficient, **R²:** Coefficient of determination, **Hb:** Hemoglobin.
*$p<0.05$ was considered statistically significant.

Table 4. Multiple linear regression analysis of predictors for anti-CII levels.

Independent variable	Dependent variable	β	SE (β)	Std. β	R^2	*t*	*p*-value*
Constant	Anti-Cll, ng/ml	7.921	5.139	--	0.47	1.541	0.133
Uric acid-mg/dL		0.290	0.461	0.099		0.629	0.534
MID, cell/µL		-8.300×10^{-5}	0.002	-0.007		-0.039	0.969
Hb, g/dL		0.0230	0.212	-0.178		-1.084	0.286
IL-1 Beta, pg/mL		0.578	0.224	0.408		2.577	0.014

β: Regression coefficient, **SE:** Standard error, **Std. β:** Standardized regression coefficient, **R²:** Coefficient of determination, **Anti-CII:** Anti-type II collagen antibody, **Hb:** Hemoglobin, **MID:** Mid-sized cells (monocytes, eosinophils, basophils), **IL-1β:** Interleukin-1 beta.
*$p<0.05$ was considered statistically significant.

association may reflect the systemic inflammatory burden in gouty arthritis. Activated monocytes and macrophages produce cytokines such as IL-1β and tumor necrosis factor alpha (TNF-α) (18). Recent studies indicate that chronic inflammatory signaling induces hepcidin, a liver-derived hormone that sequesters iron, thereby disrupting iron metabolism and reducing its availability for erythropoiesis (19). This mechanism underlies the anemia of chronic disease (ACD), also called anemia of inflammation, explaining the lower Hb levels in patients with elevated inflammatory markers (higher MID) (20). The significance level in our regression analysis suggests that immune activation in gout extends beyond the joints, potentially exerting a suppressive effect on erythropoiesis and contributing to subclinical anemia in chronic gout patients.

Additionally, neutrophil counts demonstrated a statistically significant negative correlation with Hb levels. However, the low regression coefficient indicated that neutrophils have a measurable negative impact on Hb levels in this population. Neutrophils are major effector cells in gouty inflammation, releasing a cascade of pro-inflammatory cytokines upon activation, most notably IL-1β and IL-6. Elevated neutrophil activity in gouty arthritis patients may therefore reflect a broader systemic inflammatory state rather than a purely localized joint response (21). Our findings indicate that as this

inflammatory burden increases (as reflected in elevated neutrophil counts), a corresponding decline in Hb levels may occur.

The inverse correlation can be explained by ACD mechanism. Recent studies (22) show that chronic inflammation induces hepatic production of hepcidin, the key regulator of iron homeostasis. Elevated IL-6, driven by neutrophil activity, stimulates hepcidin, which inhibits ferroportin, leading to iron sequestration within macrophages and reduced intestinal absorption (23). In addition, TNF-α and other neutrophil-derived factors can directly suppress erythroid progenitor cells in the bone marrow and diminish the biological activity of erythropoietin (EPO).

It has been shown that approximately 11% of the variation in Hb levels is explained by neutrophil count. While this confirms that neutrophils are an independent predictor, the remaining 89% of the variance is likely attributable to multifactorial causes common in gout patients, including renal impairment and chronic kidney disease, which affect EPO production; pharmacological factors, such as long-term use of nonsteroidal anti-inflammatory drugs (NSAIDs) leading to subclinical gastrointestinal blood loss; and nutritional status, including diet-related iron or vitamin deficiencies.

Nevertheless, the statistically significant difference demonstrates that the neutrophil-Hb axis may represent an important component of the systemic inflammatory burden in gout. Recent studies have suggested that the neutrophil-to-Hb ratio may serve as a potential biomarker for monitoring disease activity in inflammatory arthropathies (24).

The multiple linear regression analysis revealed that IL-1β was the only significant predictor of anti-CII levels. The positive and significant correlation between IL-1β and anti-CII can be explained through the inflammasome-cartilage damage axis. In gouty arthritis, the deposition of MSU crystals activates the NLRP3 inflammasome in macrophages, provoking a robust release of IL-1β (25). This proinflammatory cytokine stimulates the production of matrix metalloproteinases, which directly degrade type II collagen in the articular cartilage. As collagen fragments are released into the joint space, immune tolerance may be disrupted, leading to the production of anti-CII autoantibodies (26).

Interestingly, the initial hypothesis proposed a direct relationship between SUA and anti-CII; however, statistical analysis did not support this. This divergence may be explained by the "crystallization paradox." Serum hyperuricemia represents a systemic metabolic state, whereas pathologic cartilage destruction is a local inflammatory event (27). Clinical evidence suggests that elevated SUA does not necessarily indicate active crystal deposition or acute inflammation, as seen in asymptomatic hyperuricemia (28). Therefore, the local inflammatory process mediated by IL-1β appears to be more strongly associated with the autoimmune response rather than circulating uric acid levels (29,30).

Taken together, these findings suggest that gouty arthritis involves complex interactions between metabolic disturbances, innate immune activation, and potential autoimmune responses. Beyond the classical role of uric acid, inflammatory mediators such as IL-1β may represent key drivers linking crystal deposition, cartilage damage, and systemic inflammatory effects.

Conclusion

This study highlights the complex interplay between hyperuricemia, systemic inflammation, and potential autoimmune responses in patients with gouty arthritis. While elevated uric acid levels remain central to disease pathogenesis, our findings suggest that IL-1β-mediated inflammation may play a pivotal role in linking crystal deposition with cartilage damage and anti-CII antibody production. Additionally, the observed associations between inflammatory cell counts and hemoglobin levels indicate that the systemic inflammatory burden of gout may influence erythropoiesis. These results underscore the importance of therapeutic strategies targeting not only urate reduction, but also inflammatory pathways involved in disease progression.

Ethical Approval: Ethical approval for the study was granted by the Scientific and Ethics Committee of the University of Mosul, Iraq, in collaboration with the Iraqi Ministry of Health on March 28, 2024 with decision no. 4s/34.

Informed Consent: Written informed consent was obtained from each participant, confirming their understanding of the voluntary nature of participation and their right to withdraw at any time without penalty.

Peer-review: Externally peer-reviewed

Author Contributions: Concept – R.G.M.A., E.W.A., H.A.A.; Design – R.G.M.A., H.A.A.; Supervision – R.G.M.A.; Fundings – R.G.M.A., E.W.A.; Materials – R.G.M.A., E.W.A.; Data Collection and/or Processing – R.G.M.A., E.W.A.; Analysis and/or Interpretation – R.G.M.A., E.W.A., H.A.A.; Literature Review – R.G.M.A.; Writer – R.G.M.A.; Critical Reviews – R.G.M.A.

Conflict of Interest: The authors declare no conflict of interest.

Financial Disclosure: The authors declared that this study has no financial support.

Acknowledgement: The authors would like to thank the Department of Biology, College of Science, University of Mosul, for their contribution and support in completing this manuscript.

AI Statement: The authors used Grammarly to improve the language and readability of the manuscript. After using this tool, the authors reviewed and edited the content as needed and took full responsibility for the final version of the manuscript.

References

1 Zhao J, Wei K, Jiang P, Chang C, Xu L, Xu L, et al. Inflammatory response to regulated cell death in gout and its functional implications. Front Immunol. 2022;13:888306. [CrossRef]

2 Sandoval-Plata G, Morgan KM, Doherty M, Abhishek A. Inter-critical gout, not hyperuricemia or asymptomatic urate crystal deposition, is associated with systemic inflammation. Gout Urate Crystal Depos Dis. 2025;3(3):11. [CrossRef]

3 Xie X, Song Y, Chen W, Zhao H, Chu N, Wang F. Association between circulating inflammatory proteins and gout: A Mendelian randomization study. Medicine (Baltimore). 2025;104(20):e42379. [CrossRef]

4 Grant MP, Alad M, Yousef F, Epure LM, Antoniou J, Mwale F. Link N directly targets IL-1β to suppress inflammation and regulate sensory pain in intervertebral disc degeneration. Biomolecules. 2025;15(4):603. [CrossRef]

5 Wahi K, Kodar K, McConnell MJ, Harper JL, Timmer MSM, Stocker BL. MSU Crystals Enhance TDB-Mediated Inflammatory Macrophage IL-1β Secretion. Inflammation. 2019;42(3):1129–36. [CrossRef]

6 Roman YM. The role of uric acid in human health: insights from the *uricase* gene. J Pers Med. 2023;13(9):1409. [CrossRef]

7 Sansano-Muñoz E, López-González MC, Rodríguez-Alvear C, Calabuig I, Martínez-Sanchis A, Rodríguez-Navarro C, et al. Length of monosodium urate crystals in synovial fluid based on ultrasound articular deposits: advancements in crystallization process. Gout Urate Crystal Depos Dis. 2025;3(4):21. [CrossRef]

8 Kang T, Yun SG, Nam MH, Cho Y, Nam M. Comparative evaluation of serum separator V-Tube™, VQ-Tube™, and K2EDTA V-Tube™ with Becton Dickinson Tubes for chemistry, immunology, and hematology examinations. Diagnostics (Basel). 2025;15(14):1775. [CrossRef]

9 Rajamanikandan R, Ilanchelian M, Ju H. Highly selective uricase-based quantification of uric acid using hydrogen peroxide sensitive poly-(vinylpyrrolidone) templated copper nanoclusters as a fluorescence probe. Chemosensors. 2023;11(5):268. [CrossRef]

10 Al-Allaff RGM, Bakr Al-Sawaf TM. Correlation between a deficiency of D3 levels and the development of allergic rhinitis. Pak J Biol Sci. 2024;27(1):27–34. [CrossRef]

11 Tsai TC, Wang YW, Lee MS, Wu WN, Hsu W, Yao DJ, et al. Detection of interleukin-1 β (IL-1β) in single human blastocyst-conditioned medium using ultrasensitive bead-based digital microfluidic chip and its relationship with embryonic implantation potential. Int J Mol Sci. 2024;25(7):4006. [CrossRef]

12 Hiba A.M.AL-Heyali H, G.M.AL-Allaff R. Novelty in colorectal cancer biomarkers: the predictive value and clinical utility of the carcinoembryonic antigen and aldehyde dehydrogenase 1B1 autoantibodies for assessing tumour biology and the cancer stem cell burden. Asian Pac J Cancer Biol. 2025;10(4):905–13. [CrossRef]

13 Lewandowska K, Mikuła-Pietrasik J, Książek K, Tykarski A, Uruski P. Uric acid promotes human umbilical vein endothelial cell senescence *in vitro*. Metabolites. 2025;15(6):402. [CrossRef]

14 Moses A, Voshaar MO, Laar Mvd, Jansen TLT. Treat to target in gout management: a critical reappraisal of current strategies. Gout Urate Cryst Depos Dis. 2025;3(1):3. [CrossRef]

15 Yu Q, Sun Z, Wang Y, Du X, Huang J, Wang L. Hyperuricemia is accompanied by elevated peripheral $CD4^+$ T cells. Sci Rep. 2023;13(1):12537. [CrossRef]

16 Tilvawala R, Nguyen SH, Maurais AJ, Nemmara VV, Nagar M, Salinger AJ, et al. The rheumatoid arthritis-associated citrullinome. Cell Chem Biol. 2018;25(6):691–704.e6. [CrossRef]

17 Liu YR, Wang JQ, Li J. Role of NLRP3 in the pathogenesis and treatment of gout arthritis. Front Immunol. 2023;14:1137822. [CrossRef]

18 Gao L, Liu C, Ye G, Gao Y, Wang H. Advancing gouty arthritis research: the clinical value of complete blood cell count ratios and immune-inflammatory interactions. J Inflamm Res. 2025;18:16597–610. [CrossRef]

19 Quintana-Castanedo L, Maseda R, Pérez-Conde I, Butta N, Monzón-Manzano E, Acuña-Butta P, et al. Interplay between iron metabolism, inflammation, and EPO-ERFE-hepcidin axis in RDEB-associated chronic anemia. Blood Adv. 2025;9(9):2321–35. [CrossRef]

20 Cabău G, Crișan TO, Klück V, Popp RA, Joosten LAB. Urate-induced immune programming: Consequences for gouty arthritis and hyperuricemia. Immunol Rev. 2020;294(1):92–105. [CrossRef]

21 Li C, Wu C, Li F, Xu W, Zhang X, Huang Y, et al. Targeting neutrophil extracellular traps in gouty arthritis: insights into pathogenesis and therapeutic potential. J Inflamm Res. 2024;17:1735–63. [CrossRef]

22 Weiss G, Ganz T, Goodnough LT. Anemia of inflammation. Blood. 2019;133(1):40–50. [CrossRef]

23 Joosten LAB, Crişan TO, Bjornstad P, Johnson RJ. Asymptomatic hyperuricaemia: a silent activator of the innate immune system. Nat Rev Rheumatol. 2020;16(2):75–86. [CrossRef]

24 Zhang H, Liu J, Lin R, Xie D, Lin W, Zhang Q, et al. Neutrophil-to-lymphocyte ratio predicts inpatient gout recurrence: a large-scale multicenter retrospective cohort with machine-learning validation. Front Immunol. 2025;16:1688516. [CrossRef]

25 Wu M, Hu X, Lu T, Liu C, Lu H. Uric acid is independently associated with interleukin-1β levels in tear fluid of hyperuricemia and gout patients. Immun Inflamm Dis. 2023;11(3):e805. [CrossRef]

26 Li D, Yuan S, Deng Y, Wang X, Wu S, Chen X, et al. The dysregulation of immune cells induced by uric acid: mechanisms of inflammation associated with hyperuricemia and its complications. Front Immunol. 2023;14:1282890. [CrossRef]

27 Mdivnishvili M, Kharebashvili M, Chumburidze V, Nadaraia K, Gujejiani L, Virkovi K. The impact of hyperuricemia on the progression of atherosclerotic cardiovascular disease. Cureus. 2025;17(10):e94371. [CrossRef]

28 Deng H, Zhang X, Cheng N, Zhang J, Song C, Sun Y, et al. Asymptomatic hyperuricemia associated with increased risk of nephrolithiasis: a cross-sectional study. BMC Public Health. 2023;23(1):1525. [CrossRef]

29 Dinarello CA. How interleukin-1β induces gouty arthritis. Arthritis Rheum. 2010;62(11):3140–4. [CrossRef]

30 Ahn EY, So MW. The pathogenesis of gout. J Rheum Dis. 2025;32(1):8–16. [CrossRef]

ORIGINAL RESEARCH

Turkish Journal of Immunology, 14(1):45–58

Comparative Evaluation of Magnetic Cell Separation Systems Based on Cell Recovery and CD14 mRNA Enrichment

Arzuhan Büyüker[1,2], Hafize Emine Sönmez[3], Betül Sözeri[4], Aynur Karadenizli[2, 5]

[1]*Kocaeli University Institute of Gastroenterology and Hepatology, Department of Molecular Gastroenterology and Hepatology, Kocaeli, Türkiye;* [2]*Kocaeli University Faculty of Medicine, Medical Sciences Education and Research Center, Molecular Research and Antibody Laboratory, Kocaeli, Türkiye;* [3]*Kocaeli University Faculty of Medicine, Department of Pediatrics, Division of Pediatric Rheumatology, Kocaeli, Türkiye;* [4]*Ümraniye Training and Research Hospital, Department of Pediatric Rheumatology, Istanbul, Türkiye;* [5]*Kocaeli University Faculty of Medicine, Department of Medical Microbiology, Kocaeli, Türkiye*

Abstract

Objective: Efficient enrichment of CD14-expressing cell fractions is important for downstream applications such as *in vitro* differentiation and molecular analyses. However, selecting an optimal magnetic separation method can be challenging, particularly when both cell yield and enrichment efficiency must be considered. To address this challenge, we compared two magnetic separation platforms, MACS™ and MojoSort™, that use anti-CD14 antibody-conjugated beads for positive selection, focusing on cell recovery and *CD14* mRNA enrichment.

Materials and Methods: Peripheral blood mononuclear cells (PBMCs) were isolated from eight healthy pediatric donors using Ficoll gradient centrifugation. The performance of two immunomagnetic cell isolation methods utilizing antibody-conjugated magnetic particles, differing in separation format (column-based vs. column-free) was evaluated based on viable cell recovery and relative *CD14* gene expression levels measured by RT-qPCR across input and output fractions, including PBMCs, *CD14*-enriched fractions, and flow-through fractions.

Results: Column-based method demonstrated higher cell recovery and yielded fractions with significantly greater *CD14* mRNA expression compared to column-free system. Both systems produced fractions with increased CD14 transcript levels relative to input PBMCs and corresponding flow-through fractions. Cells derived from both methods exhibited comparable expression of macrophage-associated genes following *in vitro* differentiation.

Conclusion: Under the tested conditions, Column-based separation system provided higher cell recovery and stronger enrichment of *CD14* mRNA expression than the column-free system. These findings highlight differences in enrichment efficiency at the transcript level, while both systems generated cell fractions suitable for downstream molecular and functional applications.

Keywords: Magnetic cell separation, CD14 mRNA enrichment, column-free magnetic separation system, column-based magnetic separation system, RT-qPCR

Correspondence
Arzuhan Büyüker

E-mail
arzuhan.buyuker@kocaeli.edu.tr

Received
February 25, 2026

Accepted
April 23, 2026

Published
April 30, 2026

Suggested Citation
Büyüker A, Sönmez HE, Sözeri B, Karadenizli A. Comparative evaluation of magnetic cell separation systems based on cell recovery and CD14 mRNA enrichment. Turk J Immunol. 2026;14(1):45–58.

DOI
10.36519/tji.2026.1040

Introduction

Magnetic cell sorting is a rapid and reliable technique commonly used to isolate specific cell types from blood or tissue samples. Anti-CD14 magnetic beads are commonly employed in positive selection strategies, as CD14 is predominantly expressed in monocyte-lineage cells, including monocytes, macrophages, and certain dendritic cell subsets (1–5).

The choice of cell separation strategy can influence not only cell recovery but also downstream cellular behavior, including differentiation potential. Accordingly, obtaining viable and sufficiently enriched cell fractions is critical for applications such as *in vitro* differentiation and molecular analyses. However, achieving efficient enrichment can be particularly challenging in pediatric settings, where limited blood volume and low peripheral blood mononuclear cell (PBMC) counts often restrict the number of cells available for downstream applications. These limitations may result in insufficient recovery of CD14-expressing cell fractions for use in cell culture or nucleic acid–based analyses.

In addition, monocyte-lineage cells are relatively sensitive to handling, and the multi-step procedures required for PBMC isolation and subsequent magnetic separation can introduce variability in both yield and enrichment efficiency.

Several magnetic-bead-based cell separation systems are currently available, including column-based system, (MACS™; Miltenyi Biotec, Bergisch Gladbach, Germany) and column-free system (MojoSort™; BioLegend, San Diego, CA, USA). Among these, magnetic-activated cell column-based sorting system (MACS™) is one of the most widely used systems and relies on direct magnetic labeling with antibody-conjugated microbeads. In this system, labeled cells are retained within a magnetic column, while unlabeled cells are removed, followed by elution of the retained fraction (2,6).

In contrast, the column-free system (MojoSort™) system uses indirect magnetic labeling of cells prior to separation in a magnetic field, first with the primary antibody, then with magnetic streptavidin nanobeads (7–9). Although both approaches have been reported to be effective, differences in labeling strategy and workflow may influence cell recovery and enrichment efficiency.

In the present study, we compared two magnetic bead–based separation systems, focusing on post-separation cell viability and the enrichment of CD14 mRNA expression. Separation performance was assessed by measuring viable cell yield through cell counting and relative *CD14* transcript levels across input and output fractions using reverse transcription quantitative polymerase chain reaction (RT-qPCR).

In addition, the functional potential of the enriched fractions was assessed through *in vitro* macrophage differentiation assays. Overall, this study aimed to provide a practical and reproducible framework for optimizing magnetic separation workflows, particularly in settings where sample availability is limited, and evaluation is primarily based on transcript-level analyses.

Materials and Methods

Sample Collection

Peripheral blood samples were obtained from healthy pediatric donors (n=8) in accordance with an approved institutional ethics committee protocol and following informed consent from parents or legal guardians. All donors were clinically evaluated prior to inclusion, had no history of rheumatic or inflammatory diseases, and were not receiving any medication at the time of sampling.

In addition, inflammatory markers, including C-reactive protein (CRP) and erythrocyte sedimentation rate (ESR), were within normal reference ranges, confirming the absence of active systemic inflammation. Blood samples were collected into ethylenediaminetetraacetic acid (EDTA)-coated tubes (16 × 100 mm) under sterile conditions and processed on the same day to preserve cell integrity.

Peripheral blood samples were collected from each donor into two 8 mL EDTA tubes. For the EDTA comparison experiments, blood from one tube was divided into three equal portions, with approximately 2.5 mL allocated to each experimental condition. For the magnetic separation experiments, PBMCs isolated from the other 8 mL blood sample were divided into two equal fractions and subjected to MojoSort™ and MACS™ separation protocols, respectively.

All experimental procedures were conducted in accordance with relevant guidelines and regulations.

Demographic and clinical characteristics of the donors, including age, sex, body mass index (BMI), CRP, and ESR values, are provided in Table S1.

Isolation of Peripheral Blood Mononuclear Cells

Equal volumes of peripheral blood were mixed with Dulbecco's phosphate-buffered saline without calcium and magnesium, or with DPBS supplemented with 1–2 mM EDTA (0.5 M stock solution, pH 8.0, RNase-free; Thermo Scientific™, Waltham, MA, USA) in 15- or 50- mL Falcon tubes. The blood-DPBS mixture was layered onto the Ficoll-Paque™ Plus (density 1.077 g/mL; GE Healthcare, Chicago, IL, USA) by placing the pipette tip against the inner wall of the tube.

The samples were centrifuged at 400 × g for 40 minutes, with the brake off, at 18-20°C. The buffy coat layer, containing PBMCs, was drawn between the plasma and Ficoll-Paque layers and washed twice with three volumes of DPBS (with or without EDTA) by centrifugation at 450 × g for 10 minutes.

Cell counting was performed using a hemocytometer using 0.4% Gibco™ Trypan Blue Solution (Thermo Fisher Scientific, Waltham, MA, USA). All procedures involving cells were conducted in a biosafety level 2 (BSL-2) cell culture hood.

Technical challenges encountered during the experimental workflow, along with corresponding troubleshooting strategies, are summarized in Table S2. Peripheral blood mononuclear cells isolated from each donor were divided into equal fractions (5×10^6 input cells per condition) and subjected to two magnetic separation systems in parallel, allowing paired comparison within the same donor. Additionally, PBMCs isolated using DPBS without EDTA were subsequently used for magnetic sorting experiments.

Magnetic Cell Separation Using Miltenyi Biotec MACS™

Peripheral blood mononuclear cells from each sample were first passed through a 40-µm cell strainer (Corning, Corning, NY, USA) to obtain a single-cell suspension prior to magnetic labeling. Following cell counting, 1×10^7 PBMCs were divided into two aliquots, with 5×10^6 input cells allocated to each separation method, and centrifuged at 300 × g for 5 – 10 minutes at 4°C.

The supernatant was completely aspirated, and 80 µL ice-cold MACS buffer (prepared with 0.5% bovine serum albumin [BSA], 2 mM EDTA, and DPBS without Ca^{++} and Mg^{++}, and filtered using the Stericup® Quick Release Vacuum Filtration System; MilliporeSigma, Burlington, MA, USA) was added to the cell pellet. The suspension was then transferred into a 5-mL polypropylene round-bottom tube (Corning, Corning, NY, USA).

To minimize non-specific antibody binding, Human TruStain FcX™ Fc Receptor Blocking Solution (BioLegend, San Diego, CA, USA; cat. no. 422301) was added to the cell suspension. After 10 min of incubation at room temperature, 20 µL MACS™ CD14 MicroBeads (Miltenyi Biotec, Bergisch Gladbach, Germany; cat. no. 130-050-201) was added, and the mixture was incubated for 15 minutes on ice with shaking.

The volume was then adjusted to 3 mL with MACS buffer, and the cells were gently mixed and centrifuged at 300 × g for 5 minutes at 4°C. LS columns (Miltenyi Biotec; cat. no. 130-042-401) were rinsed with 3 mL MACS buffer, and the cell pellet was resuspended in 500 µL of MACS buffer.

The cell suspension was applied onto the column placed in a MidiMACS™ Separator (Miltenyi Biotec; cat. no. 130-042-302), and the flow-through containing unlabeled cells was collected. After all the cell mixture left the reservoir, the column was washed twice with 3 mL MACS buffer.

The column was then removed from the magnetic field, and the retained CD14-positive cells were immediately flushed out with 5 mL MACS buffer by forcefully pushing the plunger. Both fractions were spun at 300 × g for 10 minutes at 4°C.

Cell counting was performed using trypan blue solution, and the cells were separated for either nucleic acid isolation or *in vitro* macrophage differentiation.

Magnetic Cell Separation Using BioLegend MojoSort™

In parallel with the MACS™ protocol, 5×10^6 PBMCs were transferred into a 15-mL Falcon tube and centrifuged at 300 × g for 5–10 minutes at 4°C. The supernatant was completely aspirated, and 100 µL ice-cold MACS buffer was added to the cell pellet. The suspension was then transferred into a 5-mL polypropylene round-bottom tube.

To reduce non-specific antibody binding, 5 µL of Human TruStain FcX™ Fc Receptor Blocking Solution (BioLegend, San Diego, CA, USA; cat. no. 422301) was added, and the cells were incubated at room temperature for 10 minutes.

Subsequently, 10 µL of MojoSort™ Biotin Anti-Human CD14 Antibody (BioLegend; cat. no. 480048) was added, and the cells were incubated for 15 minutes. This was followed by the addition of 10 µL of MojoSort™ Streptavidin Nanobeads (BioLegend), with an additional 15 minutes of incubation on ice with shaking.

The total volume was then adjusted to 4 mL with MACS buffer, and the cells were centrifuged at 300 × g for 5 minutes at 4°C. The pellet was resuspended in 2.5 mL of MACS buffer, and the tube was placed in the MojoSort™ Magnet (BioLegend; cat. no. 480019) for 5 minutes at room temperature.

Without removing the tube from the magnetic separator, the supernatant containing the unlabeled cells (remaining in the middle of the tube) was carefully decanted into a clean tube. The magnetic separation step was repeated twice to improve purity.

After the final separation, the tube was removed from the magnet, and the collected putative monocyte-enriched fraction was resuspended in 3 mL MACS buffer. Both fractions were centrifuged at 300 × g for 10 minutes at 4°C, then counted using trypan blue solution.

The resulting cells were subsequently used for nucleic acid isolation or *in vitro* macrophage differentiation assays. Non-target fractions obtained from both methods were used as labeling controls.

Specifically, the number of PBMCs processed was standardized to 5 × 10^6 cells for each method, and bead volumes were applied according to the manufacturer's recommended ratios for this input cell number.

Assessment of Cell Viability and Separation Yield

For each donor, isolated PBMCs were split into two equal fractions and processed in parallel using the MACS™ and MojoSort™ separation kits. Peripheral blood mononuclear cells, magnetically selected fractions, and the corresponding flow-through cells were counted using trypan blue exclusion.

Cell viability and separation yield were calculated as follows:

Post-sort cell viability (%) = (Number of viable cells after sorting / Total number of recovered cells after sorting) × 100

Separation yield (%) = (Number of cells obtained in the magnetically selected CD14-enriched fraction after sorting / Input PBMCs) × 100

RNA Extraction and Quantitative PCR

Total RNA was extracted from equal numbers of cells derived from PBMCs, magnetically selected fractions, and corresponding flow-through cells using the PureLink™ RNA Mini Kit (Invitrogen™, Thermo Fisher Scientific, Waltham, MA, USA) according to the manufacturer's instructions.

RNA concentration and purity were assessed spectrophotometrically using the NanoDrop™ One Microvolume Ultraviolet-Visible (UV-Vis) Spectrophotometer (Thermo Scientific™, Thermo Fisher Scientific, Waltham, MA, USA).

Complementary DNA (cDNA) was synthesized from equal input amounts of total RNA (200 ng) using the OneScript Plus cDNA Synthesis Kit (Applied Biological Materials Inc., Richmond, BC, Canada) following the manufacturer's protocol.

RT-qPCR was performed using BlasTaq™ 2X qPCR MasterMix (Applied Biological Materials Inc., Richmond, BC, Canada) on a LightCycler® 480 Real-Time PCR System (Roche Diagnostics, Basel, Switzerland). Each reaction was performed in technical replicates using gene-specific primers (Table S3) and standardized amounts of cDNA.

Relative gene expression levels were calculated using the $2^{-}\Delta Ct$ method, after normalization to an internal housekeeping gene glyceraldehyde-3-phosphate dehydrogenase (*GAPDH*) (10).

In Vitro Macrophage Differentiation

Cells from the magnetically selected fraction were seeded at a density of 3 × 10^4 cells/cm^2 in 12-well tissue culture-treated plates containing RPMI-1640 medium (Gibco™, Thermo Fisher Scientific, Waltham, MA, USA; cat. no. 21875034) supplemented with 2 mM GlutaMAX™ (Gibco™, Thermo Fisher Scientific, Waltham, MA, USA),

10% heat-inactivated standardized commercial newborn calf serum (NBCS; Gibco™, Thermo Fisher Scientific, Waltham, MA, USA), 1% NEAA (Life Technologies), 1% sodium pyruvate (Gibco™, Thermo Fisher Scientific, Waltham, MA, USA), and 500 U/mL of penicillin-streptomycin (Gibco™, Thermo Fisher Scientific, Waltham, MA, USA).

To induce macrophage differentiation, the culture medium was further supplemented with 25 ng/mL recombinant human granulocyte-macrophage colony-stimulating factor (GM-CSF; R&D Systems, Minneapolis, MN, USA; cat. no. 215-GM-010) and 50 ng/mL macrophage colony-stimulating factor (M-CSF; R&D Systems, Minneapolis, MN, USA; cat. no. 216-MCC-010).

Cells were maintained under standard culture conditions (37°C, 5% CO_2) for 7 days, with partial medium replacement performed at regular intervals. At the end of the differentiation period, adherent macrophages were gently washed and either collected or directly used for downstream functional and molecular analyses.

Cell morphology was routinely examined using an inverted light microscope (Axio Vert.A1, ZEISS, Oberkochen, Germany).

Statistical Analysis

Statistical analysis was performed using IBM SPSS Statistics for Windows, version 29.0 (IBM Corp., Armonk, NY, USA). Data were shown as mean ± standard deviation (SD).

For comparisons between the two isolation methods, paired statistical tests were performed, as measurements obtained from the same eight donors constitute dependent (matched) quantitative data. All comparisons were conducted using paired samples derived from the same donor to eliminate inter-individual variability.

Normality of the paired differences was assessed using the Shapiro-Wilk test. When data were normally distributed, group comparisons were conducted using a paired t-test; otherwise, the Wilcoxon signed-rank test was applied.

A p-value < 0.05 was considered statistically significant.

Results

Optimizing the Working Conditions of PBMC Isolation

In this protocol comparison and optimization study, we first evaluated several critical parameters that can be decisive for efficient PBMC isolation. One key parameter examined was working temperature. Although standard protocols recommend maintaining all consumables used for PBMC isolation at room temperature (18–22°C),

Table 1. Comparison of PBMC yields obtained using DPBS supplemented with varying EDTA concentrations. The initial blood volume was standardized to 2.5 mL for each condition. PBMC yields are presented as cells/mL of blood.

Samples	Count of PBMC DPBS w/out EDTA / PS-PBMC yield	Count of PBMC DPBS w/ 1 mM EDTA / PS-PBMC yield	Count of PBMC DPBS w/ 2 mM EDTA / PS-PBMC yield
#1	3.5×10^6 / 1.40×10^6 cells/mL	3.8×10^6 / 1.52×10^6 cells/mL	4.1×10^6 / 1.64×10^6 cells/mL
#2	3.45×10^6 / 1.38×10^6 cells/mL	3.95×10^6 / 1.58×10^6 cells/mL	3.75×10^6 / 1.450×10^6 cells/mL
#4	3.8×10^6 / 1.52×10^6 cells/mL	3.75×10^6 / 1.50×10^6 cells/mL	3.65×10^6 / 1.46×10^6 cells/mL
#5	3.25×10^6 / 1.30×10^6 cells/mL	4.05×10^6 / 1.62×10^6 cells/mL	3.95×10^6 / 1.58×10^6 cells/mL
#6	3.4×10^6 / 1.36×10^6 cells/mL	3.95×10^6 / 1.58×10^6 cells/mL	3.9×10^6 / 1.56×10^6 cells/mL
#8	3.65×10^6 / 1.46×10^6 cells/mL	3.90×10^6 / 1.56×10^6 cells/mL	3.95×10^6 / 1.58×10^6 cells/mL
Mean ± SD	$3.51 \times 10^6 \pm 0.2 \times 10^6$ / $1.40 \times 10^6 \pm 0.08 \times 10^6$ cells/mL	$3.9 \times 10^6 \pm 0.11 \times 10^6$ / $1.56 \times 10^6 \pm 0.05 \times 10^6$ cells/mL	$3.88 \times 10^6 \pm 0.16 \times 10^6$ / $1.55 \times 10^6 \pm 0.06 \times 10^6$ cells/mL

PS: Post-sorting, **SD:** Standard deviation.

Table 2. Post-isolation viable cell counts, viability, and separation yield of magnetically selected and corresponding flow-through fractions obtained using different cell separation systems. Input cell numbers were standardized to 5 × 10^6 PBMCs for each method. Output cell counts were calculated as the sum of cells recovered in the magnetically selected fraction and the corresponding flow-through fraction.

Method	Samples	Viable cell counts in flow-through fraction	Viable cell counts in magnetically selected fraction†	Total output cell counts	PS cell viability (%)	Recovery yield (%)
Column-based system	#1	4.2×10^6	4.5×10^5	4.65×10^6	93.00	9.68
	#2	3.9×10^6	4.1×10^5	4.31×10^6	86.20	9.51
	#3	4×10^6	3.9×10^5	4.39×10^6	87.80	8.88
	#4	4.2×10^6	4.35×10^5	4.64×10^6	92.70	9.38
	#5	4.3×10^6	4.15×10^5	4.72×10^6	94.30	8.80
	#6	3.1×10^6	3.8×10^5	3.48×10^6	69.60	10.92
	#7	3.5×10^6	3.7×10^5	3.87×10^6	77.40	9.56
	#8	4×10^6	4.3×10^5	4.44×10^6	88.70	9.68
	Mean ± SD	$3.90 \times 10^6 \pm 0.41 \times 10^6$	$4.1 \times 10^5 \pm 0.3 \times 10^5$	$4.31 \times 10^6 \pm 0.43 \times 10^6$	86.21 ± 8.58	9.55 ± 0.62
Column-free system	#1	4.10×10^6	3.50×10^5	4.45×10^6	89.00	7.87
	#2	4.00×10^6	3.25×10^5	4.33×10^6	86.50	7.51
	#3	3.85×10^6	2.95×10^5	4.15×10^6	82.90	7.11
	#4	4.25×10^6	3.15×10^5	4.57×10^6	91.30	6.89
	#5	3.95×10^6	3.30×10^5	4.28×10^6	85.60	7.71
	#6	3.55×10^6	2.70×10^5	3.82×10^6	76.40	7.07
	#7	3.90×10^6	3.10×10^5	4.21×10^6	84.20	7.36
	#8	4.15×10^6	2.95×10^5	4.45×10^6	88.90	6.63
	Mean ± SD	$3.97 \times 10^6 \pm 0.22 \times 10^6$	$3.11 \times 10^5 \pm 0.25 \times 10^5$	$4.28 \times 10^6 \pm 0.23 \times 10^6$	85.6 ± 4.62	7.27 ± 0.40
	***p*-value**	N.S.	3.278E-06	NS	NS	7.94797E-07

† The selected fraction refers to the magnetically retained cell population obtained after separation, while the flow-through fraction represents the unbound cells. Enrichment was evaluated based on cell recovery and downstream molecular analyses and does not represent phenotypic purity or cellular composition.

Statistical comparisons were performed between the separation systems (Column-based system vs. column-free system).

FT: Flow-through, **Sel:** Selected fraction. **NS:** Non-significant. **PS:** Post-separation. **SD:** Standard deviation.

lower temperatures are often preferred to preserve cell viability during long isolation periods.

When cold DPBS was used, and centrifugation was performed at 4°C, the resulting buffy coat appeared clumpy (Figure S1a) and was difficult to dissociate into a single-cell suspension, although it was more readily visible and easier to collect (Figure S1b). In contrast, samples processed at room temperature consistently yielded homogeneous single-cell suspensions, facilitating accurate PBMC quantification and efficient downstream separation and differentiation. Therefore, we continued our experiments, including PBMC handling, at room temperature to ensure consistency across all processing steps.

Furthermore, previous studies have reported enhanced PBMC yield when DPBS is supplemented with EDTA (11,12). To evaluate this effect, each blood sample was divided into three equal aliquots: (i) DPBS alone, (ii) DPBS supplemented with 1 mM EDTA, and (iii) DPBS supplemented with 2 mM EDTA. Peripheral blood mononuclear cell yield was quantified at the end of isolation (n=6 per group).

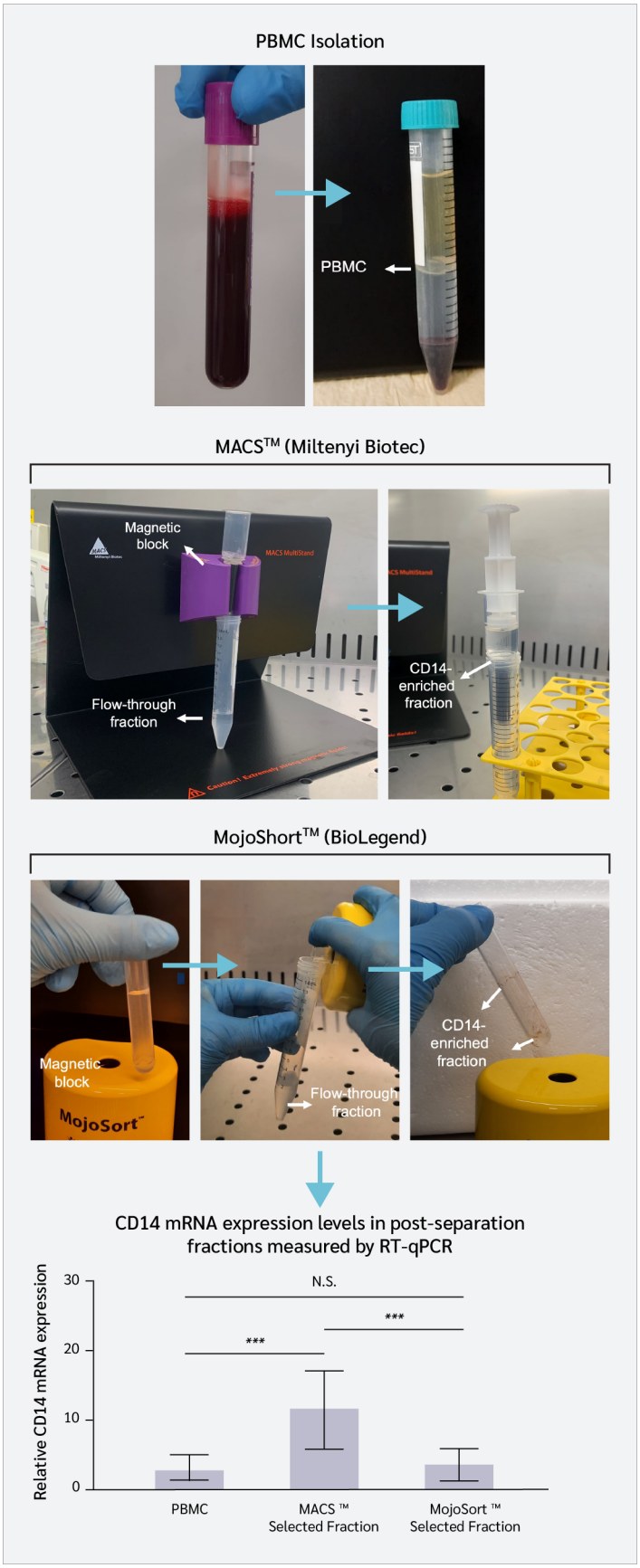

Supplementation with EDTA concentration significantly increased PBMC yield compared with DPBS alone. Specifically, PBMC counts and yields were $3.51 \times 10^6 \pm 0.2 \times 10^6$ cells / $1.40 \times 10^6 \pm 0.8 \times 10^6$ cells/mL for the DPBS without EDTA group, $3.9 \times 10^6 \pm 1.1 \times 10^6$ cells / $1.56 \times 10^6 \pm 0.44 \times 10^6$ cells/mL for DPBS with 1 mM EDTA group, and $3.88 \times 10^6 \pm 1.6 \times 10^6$ cells / $1.55 \times 10^6 \pm 0.64 \times 10^6$ cells/mL for DPBS with 2 mM EDTA group (Figure S1c, Table 1).

A statistically significant increase was observed only between the DPBS-alone group and the EDTA-supplemented groups (p=0.0015 and p=0.0044, respectively; Table 1). The higher EDTA concentration also increased PBMC counts; however, this difference was not statistically significant (p=0.8376; Table 1).

Comparison of Two Magnetic Bead-Based Cell Separation Platforms

We evaluated two magnetic bead–based cell separation platforms, by comparing standard outcome parameters, including post-separation cell viability and recovery yield. In addition, relative enrichment efficiency was assessed by downstream analysis of CD14 mRNA expression. All samples were processed using identical starting material (5×10^6 PBMCs per separation; n=8 per group).

Overall cell viability, calculated as the percentage of viable output cells relative to the input, was comparable between the two systems (column-based system: 86.21% ± 8.58; column-free system: 85.60% ± 4.62; $p > 0.05$; Table 2). The number of recovered cells in the magnetically selected fraction was significantly higher with column-based system ($4.1 \times 10^5 \pm 0.3 \times 10^5$) compared with column-free system ($3.11 \times 10^5 \pm 0.25 \times 10^5$), indicating a statistically significant increase in recovered

Figure 1. Schematic workflow of magnetic bead–based cell separation and assessment of *CD14* mRNA expression by reverse transcription quantitative polymerase chain reaction (RT-qPCR).

Relative enrichment of CD14 mRNA in magnetically selected fractions and corresponding flow-through fractions after separation using the column-based and column-free magnetic cell sorting systems. Results were normalized to glyceraldehyde-3-phosphate dehydrogenase (GAPDH). RT-qPCR reactions were performed in duplicate, and eight biological samples were analyzed. The graph was generated using Simplistats (https://simplistats.com). Cycle threshold (Ct) values for unbound flow-through cells were 35 or higher. p values were 6.234×10^{-6} for column-based vs column-free system, 9.695×10^{-7} for peripheral blood mononuclear cells (PBMCs) vs column-based system, and 0.417 for PBMCs vs column-free system.

NS: Nonsignificant.

cell numbers with the column-based system ($p < 0.001$, Table 2).

Accordingly, paired analyses demonstrated that recovery efficiency was significantly higher following column-based system (9.55 ± 0.62%) compared to column-free system (7.27% ± 0.40) ($p<0.001$, Table 2).

To further characterize the isolated fractions at the molecular level, *CD14* gene expression was analyzed by quantitative RT-PCR (Figure 1). Following normalization to *GAPDH*, CD14 mRNA expression showed a 2.74 ± 2.11-fold increase in PBMCs, an 11.46 ± 5.83-fold increase in column-based system-selected fractions, and a 3.39 ± 2.64-fold increase in column-free system-selected fractions (Figure 1).

Cells obtained using the column-based system exhibited significantly higher CD14 mRNA expression compared to PBMCs and to fractions obtained using the column-free platform ($p<0.001$; Figure 1).

At the individual donor level, *CD14* mRNA levels were consistently higher in fractions obtained using the column-based system than in those obtained using the column-free system, based on *GAPDH*-normalized values ($2^{-}\Delta Ct$; Figure 2a). Paired statistical analysis (n=8) confirmed this observation, demonstrating a significant difference between the two separation methods ($p=0.0105$; Figure 2b), independent of donor variability.

Microscopic observations during trypan blue–based cell counting revealed differences in cellular composition between the two systems. Column-based system-derived fractions appeared more uniform, whereas Column-free system-derived fractions contained a higher proportion of additional cellular elements, including platelets (Figure S1d, Figure S1e). These observations, however, were qualitative and not quantitatively assessed.

To evaluate functional potential, magnetically selected fractions were subjected to *in vitro* differentiation for 7 days. Cells derived from both platforms exhibited morphology consistent with macrophage-like cells (Figure 3a, Figure 3b).

Expression of the macrophage-associated markers *CD68* and colony-stimulating factor 1 receptor (*CSF1R*) was assessed by RT-qPCR. No statistically significant differences were observed between the two groups ($p>0.05$; Figure 3c, Figure 3d). *CD68* mRNA expression increased by 6.51 ± 1.8-fold in column-free system-derived cells and by 6.4 ± 0.97-fold in column-based system-derived cells relative to their respective undifferentiated counterparts (Figure 3c). Similarly, *CSF1R* mRNA expression increased by 17.08 ± 9.77-fold and 19.82 ± 6.3-fold in column-free and column-based system-derived cells, respectively (Figure 3d).

Discussion

This study aimed to comparatively evaluate the performance of two commercially available magnetic bead–based cell separation platforms, under standardized experimental conditions. The comparison focused on cell recovery, viability, and enrichment efficiency as assessed by *CD14* mRNA expression. Although *CD14* is commonly associated with monocyte-lineage cells, it is important to note that the present study evaluates enrichment at the transcript level rather than at the phenotypic level.

MACS™, as one of the earliest and most widely adopted magnetic separation technologies, has been extensively used in previous studies (2,6,13). In the present work, both MACS™ and MojoSort™ systems were evaluated in parallel using identical starting material and processed by the same operator to minimize technical variability and ensure an unbiased comparison. In addition, we present practical optimization strategies for PBMC isolation and magnetic separation that may improve cell recovery and viability, particularly in settings with limited sample availability (Table S2).

Pre-analytical variables were found to play a critical role in downstream outcomes. The use of EDTA-containing blood collection tubes is recommended for RNA-based applications, as heparin may inhibit reverse transcriptase and DNA polymerase activity (14,15). However, EDTA may not be suitable for all cell types and applications (16), and its use should be considered in the context of the intended downstream analysis. Consistent with previous reports, the inclusion of EDTA in washing buffers reduced cell aggregation and improved recovery (12). Although Efthymiou et al. (12) reported no significant difference in PBMC counts between washing buffer with or without EDTA, flow cytometry analysis revealed higher frequencies of $CD4^{+}$ and $CD8^{+}$ T cells in the EDTA-supplemented group. In our experiments, phosphate-buffered saline

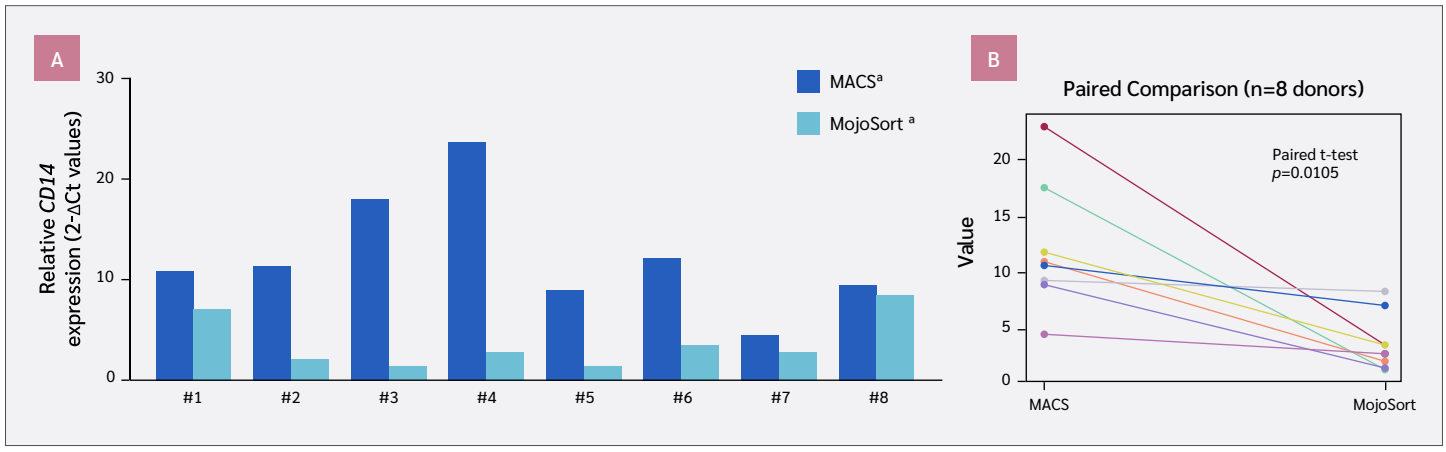

Figure 2. Paired comparison of *CD14* expression between two isolation methods.

(A) Relative *CD14* mRNA expression levels ($2^{-\Delta Ct}$) of the samples. ΔCt values of *CD14* were normalized to *GAPDH*. **(B)** Paired comparison of *CD14* mRNA expression levels ($2^{-\Delta Ct}$) between the two isolation methods. Each point represents an individual donor (n=8), and paired samples are connected by lines. Statistical analysis was performed using the Wilcoxon signed-rank test (p=0.0105).

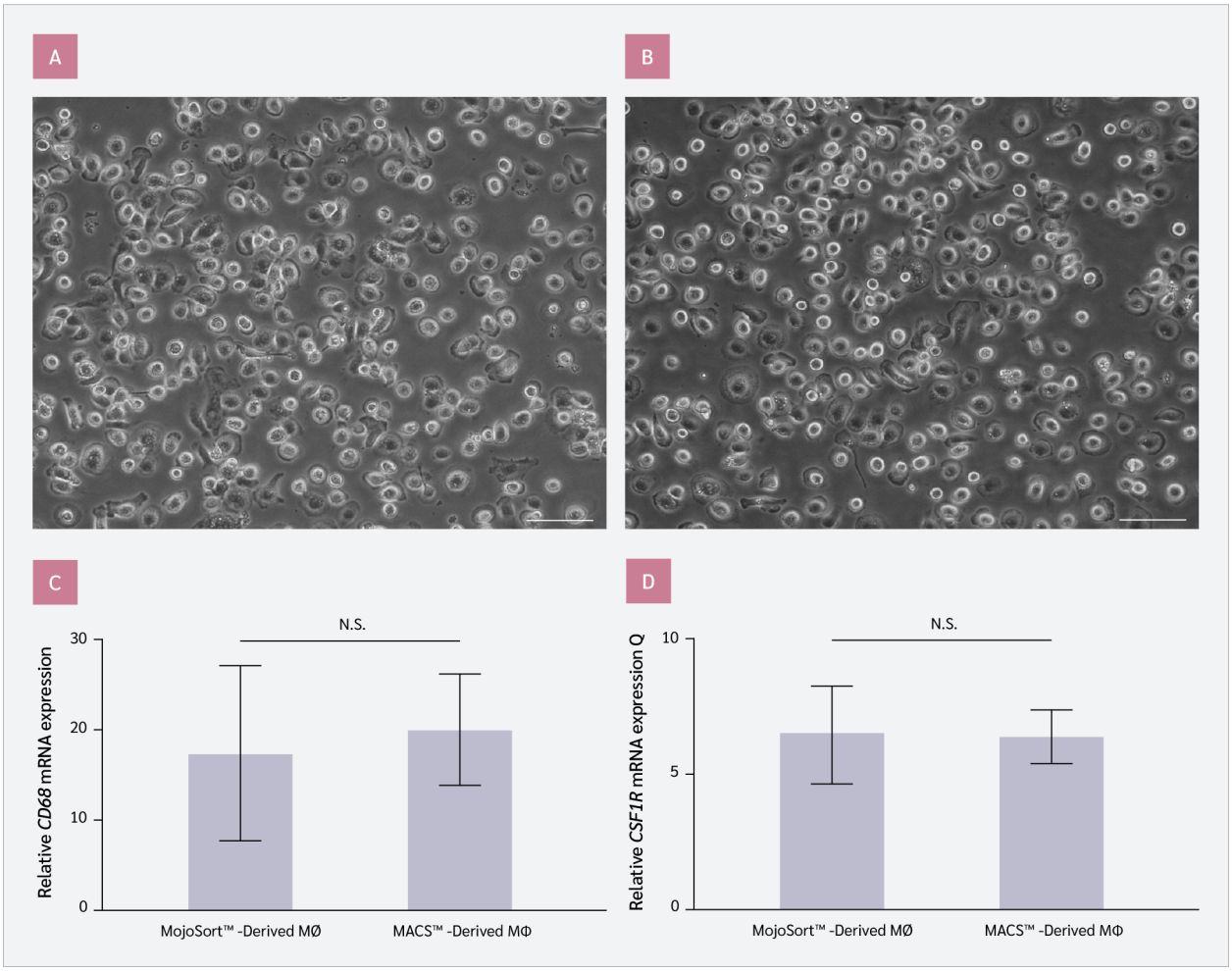

Figure 3. Comparison of macrophage differentiation efficiency in *CD14* mRNA-enriched cells isolated using two methods.

Representative inverted microscope images of macrophage (MΦ) cultures differentiated from **(A)** MojoSort™-sorted and **(B)** Column-based platform—sorted CD14-mRNA enriched cell fractions. Scale bar: 100 µm. Differential **(C)** *CD68* and **(D)** *CSF1R* mRNA expression levels of macrophages (p=0.576 and p=0.902, respectively). Results were normalized to *GAPDH*. RT-qPCR reactions were performed in duplicate, and n=8 biological samples were analyzed. Differences between conditions were analyzed using a paired Student's t-test.

(PBS) supplemented with EDTA increased PBMC yield by approximately 12%, which is particularly relevant when working with limited blood volumes (Table 1, Figure S1). Furthermore, timely processing of fresh blood samples and careful execution of density gradient centrifugation were essential for maintaining PBMC integrity and minimizing cell loss (17).

Magnetic separation workflows also require careful handling to ensure reproducibility. Preventing cell aggregation, optimizing column loading (for column-based system), and applying controlled washing steps were critical factors influencing recovery efficiency (1,2,7–9). The inclusion of BSA in separation buffers contributed to improved cell stability and reduced nonspecific binding, consistent with its known protective and blocking properties (18,19).

Post-separation viability is a key determinant of downstream usability. In the present study, both platforms demonstrated comparable viability (approximately 86%), with no statistically significant difference between systems. Although magnetic separation is generally associated with lower cell loss than fluorescence-activated cell sorting, some cell loss is expected due to mechanical handling and processing steps. Maintaining high viability after PBMC isolation and magnetic separation is critical for downstream applications, as mechanical stress and dead cells can promote nonspecific microbead binding. Although magnetic sorting is associated with approximately 10% cell loss (compared with approximately 70% for FACS) (20), our platforms showed similar overall losses with comparable post-sorting viability. Notably, although both systems showed similar overall recovery profiles, Column-based system yielded a significantly higher cell count in the magnetically selected fraction.

At the molecular level, *CD14* mRNA expression assessed by RT-qPCR was used as an indirect indicator of enrichment efficiency in this study. Importantly, studies evaluating magnetic separation methods often report outcomes in terms of cell purity and phenotypic identity. However, when characterization is based solely on gene expression analysis, such as RT-qPCR, the results reflect transcript-level enrichment rather than direct evidence of protein expression or cellular composition. Therefore, careful interpretation of enrichment data is required, particularly in the absence of protein-level validation methods such as flow cytometry. In our study, column-based system achieved significantly higher *CD14* mRNA-enriched cell yield, which aligns more closely with the expected ~10% monocyte fraction in peripheral blood (21). Importantly, these results reflect relative enrichment of *CD14* mRNA expression rather than direct quantification of CD14 protein-positive cells. Therefore, interpretations regarding cell identity should be made with caution. The consistency of increased *CD14* mRNA expression across all donors suggests that the observed differences are method-dependent rather than driven by inter-individual variability.

Functional assessment demonstrated that cells derived from both separation methods could undergo *in vitro* differentiation into macrophage-like cells, as evidenced by morphology and increased expression of macrophage-associated genes, including *CD68* and *CSF1R* (Figure 3). No significant differences were observed between the two systems for these differentiation-associated markers, suggesting that both platforms generate cell fractions suitable for downstream functional applications. These findings are consistent with previous reports indicating that magnetic separation methods do not adversely affect subsequent differentiation capacity (21).

Qualitative microscopic observations revealed differences in cellular composition between fractions obtained with the two systems, with column-based system-derived fractions appearing more uniform, whereas column-free system-derived fractions contained additional cellular elements, such as platelets (Figure S1). However, these observations were not quantitatively assessed and should be interpreted cautiously, as no phenotypic validation was performed.

Both positive selection–based magnetic separation systems present inherent advantages and limitations. The column-based system employs a direct labeling strategy and column-based separation, which may contribute to higher retention efficiency of labeled cells. In contrast, the column-free system relies on indirect labeling and column-free separation, which may result in partial loss of labeled cells during handling steps. Moreover, negatively selected CD14-positive monocytes have been reported to be highly contaminated with platelets (3), whereas positive selection may be time-consuming (2). In our experimental setting, column-based system demonstrated higher recovery and stronger enrichment of *CD14* mRNA expression, along with a shorter processing time. However, factors such as cost, required equipment, and

workflow preferences may influence the choice of system in different laboratory settings.

A key limitation of this study is the absence of protein-level validation of the isolated cell fractions. *CD14* expression was assessed exclusively at the mRNA level using RT-qPCR, and no flow cytometric or immunophenotypic analysis was performed. Consequently, the proportion of CD14 protein-positive cells within the isolated fractions and the precise cellular composition remain undetermined. The results should therefore be interpreted as measures of relative enrichment rather than phenotypic purity or definitive identification of monocytes. Future studies incorporating multiparametric flow cytometry and additional lineage markers will be necessary to confirm cellular identity and quantify population composition.

Despite the relatively small sample size, the use of a paired donor-matched design strengthened the statistical power and reduced the impact of inter-individual variability. All samples were processed in parallel under identical conditions, supporting the robustness and reproducibility of the comparative analysis. Nevertheless, validation in larger and independent cohorts will be important to confirm the generalizability of these findings.

Conclusion

This study provides a systematic comparison of two magnetic bead–based separation systems under controlled conditions and highlights key procedural factors that influence experimental outcomes. Both magnetic-bead cell sorting systems yielded viable cell fractions suitable for downstream molecular and functional analyses. However, column-based system demonstrated higher cell recovery and stronger enrichment of *CD14* mRNA expression under the conditions tested. These findings support the use of column-based system as an efficient approach for generating *CD14* mRNA-enriched cell fractions, while emphasizing that conclusions are limited to transcript-level enrichment in the absence of phenotypic validation.

Ethical Approval: The study was approved by the Kocaeli University Human Research Ethics Committee on July 18, 2024, with decision no. GOKAEK-2024/11.37.

Informed Consent: Written informed consent was obtained from parents or legal guardians of all participants.

Peer-review: Externally peer-reviewed

Author Contributions: Concept – A.B.; Design – A.B; Supervision – H.E.S, A.K.; Fundings – H.E.S., A.K.; Materials – A.B.; Data Collection and/or Processing – A.B., B.S., A.K.; Analysis and/or Interpretation – A.B.; Literature Review – A.B., B.S.; Writer – A.B., H.E.S., B.S.; Critical Reviews – A.K.

Conflict of Interest: The authors declare no conflict of interest.

Financial Disclosure: This study was supported by The Scientific and Technological Research Council of Türkiye under the Scientific and Technological Research Projects Funding Program (Grant No. 124R020).

AI Statement: During the preparation of this manuscript, the authors used OpenAI's ChatGPT to improve text flow and Grammarly to enhance grammatical clarity. The authors critically reviewed and edited the content and take full responsibility for the accuracy and integrity of the manuscript.

Acknowledgment: We sincerely thank Prof. Esra Çağavi for generously providing partial support for the MACS™ system consumables used in this study and Assist. Prof. Hüseyin Uzuner and Sena Nur Bütünay for their valuable technical and experimental assistance.

References

1 Koc A, Akdeniz C, Cagavi E. Human macrophages directly modulate iPSC-derived cardiomyocytes at healthy state and congenital arrhythmia model in vitro. Pflugers Arch. 2022;474(12):1295–310. [CrossRef]

2 Mayer A, Lee S, Lendlein A, Jung F, Hiebl B. Efficacy of $CD14^+$ blood monocytes/macrophages isolation: positive versus negative MACS protocol. Clin Hemorheol Microcirc. 2011;48(1):57–63. [CrossRef]

3 Nielsen MC, Andersen MN, Møller HJ. Monocyte isolation techniques significantly impact the phenotype of both isolated monocytes and derived macrophages in vitro. Immunology. 2020;159(1):63–74. [CrossRef]

4 Ohradanova-Repic A, Machacek C, Fischer MB, Stockinger H. Differentiation of human monocytes and derived subsets of macrophages and dendritic cells by the HLDA10 monoclonal antibody panel. Clin Transl Immunology. 2016;5(1):e55. [CrossRef]

5 Zarif JC, Hernandez JR, Verdone JE, Campbell SP, Drake CG, Pienta KJ. A phased strategy to differentiate human CD14+-monocytes into classically and alternatively activated macrophages and dendritic cells. Biotechniques. 2016;61(1):33–41. [CrossRef]

6 Schmitz B, Radbruch A, Kümmel T, Wickenhauser C, Korb H, Hansmann ML, et al. Magnetic activated cell sorting (MACS)--a new immunomagnetic method for megakaryocytic cell isolation: comparison of different separation techniques. Eur J Haematol. 1994;52(5):267–75. [CrossRef]

7 Kalinina O, Minter LM, Sperling AI, Hollinger MK, Le P, Osborne BA, et al. Exopolysaccharide-treated dendritic cells effectively ameliorate acute graft-versus-host disease. Transplant Cell Ther. 2024;30(1):79.e1–e10. [CrossRef]

8 Damara A, Wegner J, Trzeciak ER, Kolb A, Nastaranpour M, Khatri R, et al. LL37/self-DNA complexes mediate monocyte reprogramming. Clin Immunol. 2024;265:110287. [CrossRef]

9 Xiao R, Zeng J, Bressler EM, Lu W, Grinstaff MW. Synthesis of bioactive (1→6)-β-glucose branched poly-amido-saccharides that stimulate and induce M1 polarization in macrophages. Nat Commun. 2022;13(1):4661. [CrossRef]

10 Livak KJ, Schmittgen TD. Analysis of relative gene expression data using real-time quantitative PCR and the 2(-Delta Delta C(T)) Method. Methods. 2001;25(4):402–8. [CrossRef]

11 Dinh B, Hoeksema MA, Spann NJ, Rendler J, Cobo I, Glass CK, et al. Isolation and cryopreservation of highly viable human peripheral blood mononuclear cells from whole blood: a guide for beginners. J Vis Exp. 2024;(212). [CrossRef]

12 Efthymiou A, Mureanu N, Pemberton R, Tai-MacArthur S, Mastronicola D, Scottà C, et al. Isolation and freezing of human peripheral blood mononuclear cells from pregnant patients. STAR Protoc. 2022;3(1):101204. [CrossRef]

13 Miltenyi S, Müller W, Weichel W, Radbruch A. High gradient magnetic cell separation with MACS. Cytometry. 1990;11(2):231–8. [CrossRef]

14 Ding M, Bullotta A, Caruso L, Gupta P, Rinaldo CR, Chen Y. An optimized sensitive method for quantitation of DNA/RNA viruses in heparinized and cryopreserved plasma. J Virol Methods. 2011;176(1-2):1–8. [CrossRef]

15 Marteau JB, Mohr S, Pfister M, Visvikis-Siest S. Collection and storage of human blood cells for mRNA expression profiling: a 15-month stability study. Clin Chem. 2005;51(7):1250–2. [CrossRef]

16 Betsou F, Gaignaux A, Ammerlaan W, Norris PJ, Stone M. Biospecimen science of blood for peripheral blood mononuclear cell (PBMC) functional applications. Curr Pathobiol Rep. 2019;7(2):17–27. [CrossRef]

17 Lehle S, Völkl S, Seitz K, Goossens C, Emons J, Ruebner M, et al. Effect of delayed isolation of peripheral blood mononuclear cells on cell viability and functionality. BMC Immunol. 2025;26(1):21. [CrossRef]

18 Mahmoud NN, Hammad AS, Al Kaabi AS, Alawi HH, Khatoon S, Al-Asmakh M. Evaluating the effects of BSA-coated gold nanorods on cell migration potential and inflammatory mediators in human dermal fibroblasts. J Funct Biomater. 2024;15(10):284. [CrossRef]

19 Hermanson GT. Homobifunctional crosslinkers. In: Hermanson GT, editor. Bioconjugate techniques. 3rd ed. Amsterdam: Elsevier; 2013. p. 275–98. [CrossRef]

20 Sutermaster BA, Darling EM. Considerations for high-yield, high-throughput cell enrichment: fluorescence versus magnetic sorting. Sci Rep. 2019;9(1):227. [CrossRef]

21 Weiss R, Gerdes W, Leonhardt F, Berthold R, Sack U, Grahnert A. A comparative study of two separation methods to isolate monocytes. Cytometry A. 2019;95(2):234–41. [CrossRef]